



## Durham E-Theses

---

### *The preparation and properties of pyrolytic graphite*

Morant, Ruth A.

#### How to cite:

---

Morant, Ruth A. (1971) *The preparation and properties of pyrolytic graphite*, Durham theses, Durham University. Available at Durham E-Theses Online: <http://etheses.dur.ac.uk/10256/>

#### Use policy

---

The full-text may be used and/or reproduced, and given to third parties in any format or medium, without prior permission or charge, for personal research or study, educational, or not-for-profit purposes provided that:

- a full bibliographic reference is made to the original source
- a [link](#) is made to the metadata record in Durham E-Theses
- the full-text is not changed in any way

The full-text must not be sold in any format or medium without the formal permission of the copyright holders.

Please consult the [full Durham E-Theses policy](#) for further details.

THE PREPARATION AND PROPERTIES OF PYROLYTIC GRAPHITE

by

Ruth A. Morant, B.Sc.

A thesis presented in candidature for the degree  
of Master of Science in the University of Durham

May 1971

### ACKNOWLEDGMENTS

The author would like to acknowledge the financial support given by the Department of Scientific and Industrial Research (now the Science Research Council) for the initial part of this work. The work was subsequently supported by the University of Durham. She would also like to thank Mr. R. Philips of the Geology Department for discussions and for the use of the microdensitometer. Particularly helpful discussions on the problems of x-ray work in graphite were held with Mr. H.P. Rooksby of the Hirst Research Centre, General Electric Co. Ltd., and with Dr. W.T. Eeles of the Central Electricity Generating Board, Berkeley Nuclear Laboratories. Professor D.A. Wright, who supervised this work provided constant encouragement during its course. Finally the author would like to thank her husband for his tolerance during the writing and preparation of this thesis.

## CONTENTS

Abstract

### CHAPTER 1

#### INTRODUCTION AND BACKGROUND

1.1	Introduction	1
1.2	The Etingshausen Effect	2
1.3	Material requirements	8
1.4	Description of the project	14
1.5	Summary of the results of the investigation by J.J. Mills of the thermomagnetic effects in pyrolytic graphite	
1.5.1	Experimental results	15
1.5.2	Theoretical results	17

### CHAPTER 2

#### MATERIAL PREPARATION

2.1	Introduction	20
2.2	Description of apparatus	
2.2.1	General	25
2.2.2	The furnace and vacuum equipment	25
2.2.3	Gas Handling	27
2.2.4	Electrode design	29
2.2.5	Power supplies and control	31
2.3	The growth and assessment of the pyrolytic graphite	34

2.4	Details of the growth of bar 22	41
2.5	Estimation of the temperature profile across the deposit	43
2.6	Comparison of the estimated temperatures with annealing studies	46

## CHAPTER 3

### PREFERRED ORIENTATION

3.1	Introduction	50
3.2	Qualitative description of the preferred orientation	
3.2.1	Optical examination	50
3.2.2	X-ray examination	52
3.3	Measurement of the preferred orientation	54
3.4	Experimental results	58
3.5	Discussion	61

## CHAPTER 4

### MEASUREMENT OF THE THERMAL CONDUCTIVITY

4.1	Introduction	64
4.2	Description of apparatus	
4.2.1	The cryostat	65
4.2.2	The vacuum system	68
4.2.3	Temperature measurement	68
4.2.4	Sample mounting, contacts and the heater	70
4.2.5	Supplies and measuring equipment	72

4.3	Experimental results	
4.3.1	Thermal conductivity	75
4.3.2	Thermoelectric power	77
4.4	Estimation of the crystallite size	80
4.5	Discussion	86

## CHAPTER 5

### MEASUREMENT OF THE CRYSTALLITE SIZE

5.1	Introduction	91
5.2	Crystallite size determination from x-ray line broadening	91
5.3	Line broadening in graphite	99
5.4	Practical considerations	
5.4.1	Choice of Debye-Scherrer camera or diffractometer	105
5.4.2	Choice of standard	109
5.4.3	Sample preparation	109
5.4.4	Choice of lines for analysis	112
5.4.5	Film measurement	114
5.5	Method of analysis	116
5.6	Experimental results	119
5.6.1	Layer thickness	120
5.6.2	Stacking factor	121
5.6.3	The a-direction layer size	122
5.6.4	Accuracy	123
5.7	Discussion	124

## CHAPTER 6

### GENERAL DISCUSSION

6.1	Ettingshausen Cooling	127
6.1.1	Extrapolation to liquid helium temperatures	128
6.1.2	Phonon drag	132
6.1.3	Prospects for improving the figure of merit	133
6.2	Structure and properties	137
6.2.1	Preferred orientation	137
6.2.2	Crystallite growth	142
6.2.3	Prospects for obtaining improved quality graphite	147
6.3	Conclusions	150

### APPENDIX I

Published papers on work in this thesis	152
---	-----

### APPENDIX II

More recent published work on graphite	153
--	-----

### REFERENCES

156
-----

## ABSTRACT

The use of the Etingshausen effect as an alternative to thermoelectric effects for the production of useful cooling at low temperatures is discussed, and the reasons leading to the investigation of pyrolytic graphite as a possible material for Etingshausen cooling are given.

The Brown and Watt method for the deposition of pyrolytic graphite was successfully developed to enable good quality deposits with consistent properties to be obtained using surface deposition temperatures of  $2200^{\circ}\text{C}$  and propane as the hydrocarbon gas. The work showed the importance of the temperature gradient developed across the deposit in this method of growth. The temperature profile was estimated and the properties of the material showed good agreement with the values obtained in other workers' annealing studies. One particular bar of pyrolytic graphite was cleaved into a number of sections and its properties studied as a function of the effective formation temperature.

Measurements were made of the a-direction thermal conductivity in the temperature range 70 to  $300^{\circ}\text{K}$  and of the crystallite preferred orientation. The thermal conductivity results were used to estimate the crystallite sizes and the values obtained agreed well with those obtained from the saturation of the mobility. The crystallite size was also measured directly by x-ray line broadening. A variance method was used to separate

the strain component of the broadening. X-ray determinations of the crystallite size have always in the past yielded low values, but the use of the proper correction for stacking faults gave good agreement with the indirect estimates. A thermal activation energy of 5.9 eV was obtained for crystallite growth.

The graphitisation process is discussed and it is suggested that better quality material than any produced so far could be obtained by annealing highly oriented soot-free deposits at high temperatures. An upper limit of 100  $\mu\text{m}$  is set for the crystallite size of such material produced at 3500°C.

It is concluded that in the absence of phonon drag effects graphite is unlikely to be a suitable material for Etingshausen cooling.

## CHAPTER 1

### INTRODUCTION AND BACKGROUND

#### 1.1 Introduction

At the time work on this project was started many laboratories were actively engaged in trying to develop suitable materials to enable the Peltier effect to be used in cooling devices, and it was the optimistic hope that eventually many of the cumbersome compressor and expansion machines might be replaced by simple electrical devices with no moving parts. Even if the devices could not be made competitive with conventional machinery in the ordinary commercial range of refrigeration, there would be applications in which these compact and ruggedly simple devices could be used and conventional machinery could not. In scientific research, particularly, where there is much interest in low temperature measurements, temperatures around  $80^{\circ}\text{K}$  can be attained easily because of the ready and cheap availability of liquid nitrogen, but below this the need to use liquid helium as a refrigerant makes low temperature experiments extremely costly. A simple electrical device that would cool from liquid nitrogen temperature down towards the liquid helium range would have obvious advantages, and if the devices could be made sufficiently cheaply would be of enormous technological importance since in many electronic applications much improved performance could be obtained by

operating at low temperatures.

In practice it has proved difficult to develop a material for Peltier cooling that is any more efficient than bismuth telluride. Cooling elements of this material are now commercially available, and a 3-stage cooler using bismuth telluride can reach a temperature of  $-100^{\circ}\text{C}$ . Solar batteries using the inverse effect are a common part of space research. For Peltier devices it must be possible to obtain the material in both n- and p-type forms with similar properties. In materials like bismuth telluride the cooling effect falls off below room temperature, and as a result the possibility of using materials such as the Bi-Sb alloys was investigated. However it is not possible to obtain a p-type form of the material. Because of the difficulties encountered with Peltier cooling below room temperature attention was turned to the less well known Etingshausen effect. If a suitable material could be found, this effect might give a more efficient device for low temperature cooling than is possible with thermoelectric materials, and has the advantage that the device does not require the use of two types of material. This thesis is concerned with the preparation and evaluation of one possible material for Etingshausen cooling.

## 1.2 The Etingshausen effect

The Etingshausen effect is one of several thermomagnetic

effects (see for example Putley<sup>1</sup>), and the geometry of the effect is shown in figure 1.1(a). A bar of suitable material has an electrical current flowing along its length in the x-direction and is placed in a magnetic field B which acts in the z-direction, and because of the Ettingshausen effect a temperature gradient  $\partial T/\partial y$  is set up in the y-direction. The Ettingshausen coefficient, P, can be defined as

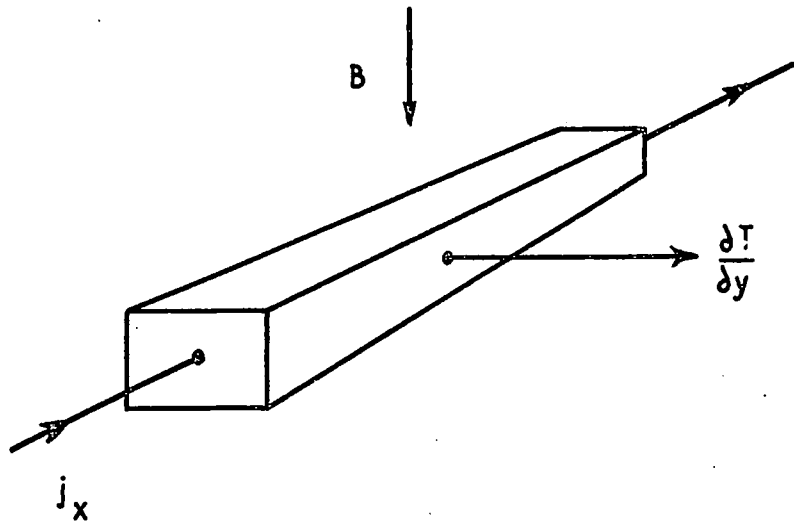
$$\frac{\partial T}{\partial y} = P j_x B$$

where  $j_x$  is the electrical current density in the x-direction. It is assumed that there is no temperature gradient in the x-direction and no heat flow or electrical current flowing in the y-direction. In most materials the Ettingshausen coefficient is very small and its effect is usually only encountered as an almost negligible correction in some determinations of the Hall coefficient.

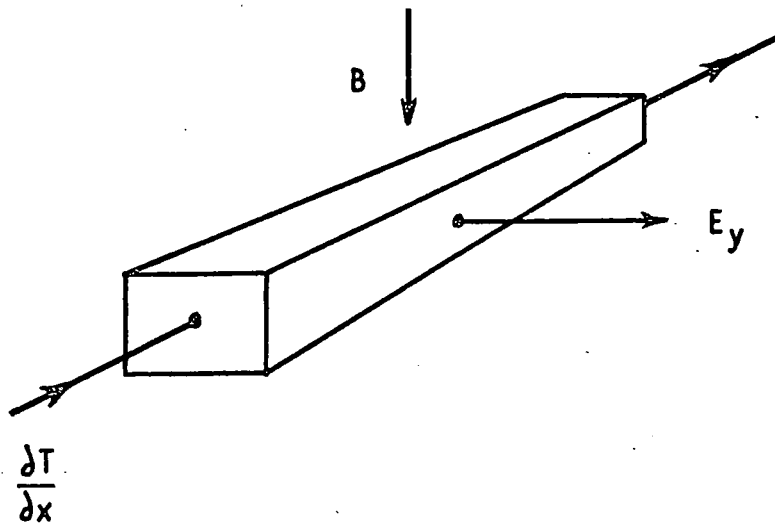
A related thermomagnetic effect is the Nernst effect. The geometry of this effect is shown in figure 1.1(b). In this case a temperature gradient is established in the x-direction with the magnetic field again in the z-direction, and because of the Nernst effect an electrical field  $E_y$  appears in the y-direction. The auxiliary conditions are that no electrical currents should flow in either x- or z-directions and also in most experimental conditions that there is no heat flow in the y-direction. The Nernst coefficient, Q, is

FIGURE 1.1

(a) The Ettingshausen Effect



(b) The Nernst Effect



defined by

$$E_y = -QB \frac{\partial T}{\partial x}$$

In practice, because it involves the measurement of an electrical field rather than a small temperature difference, the Nernst coefficient is easier to obtain than the Etingshausen coefficient. The two coefficients are related through the Bridgman relation which states that

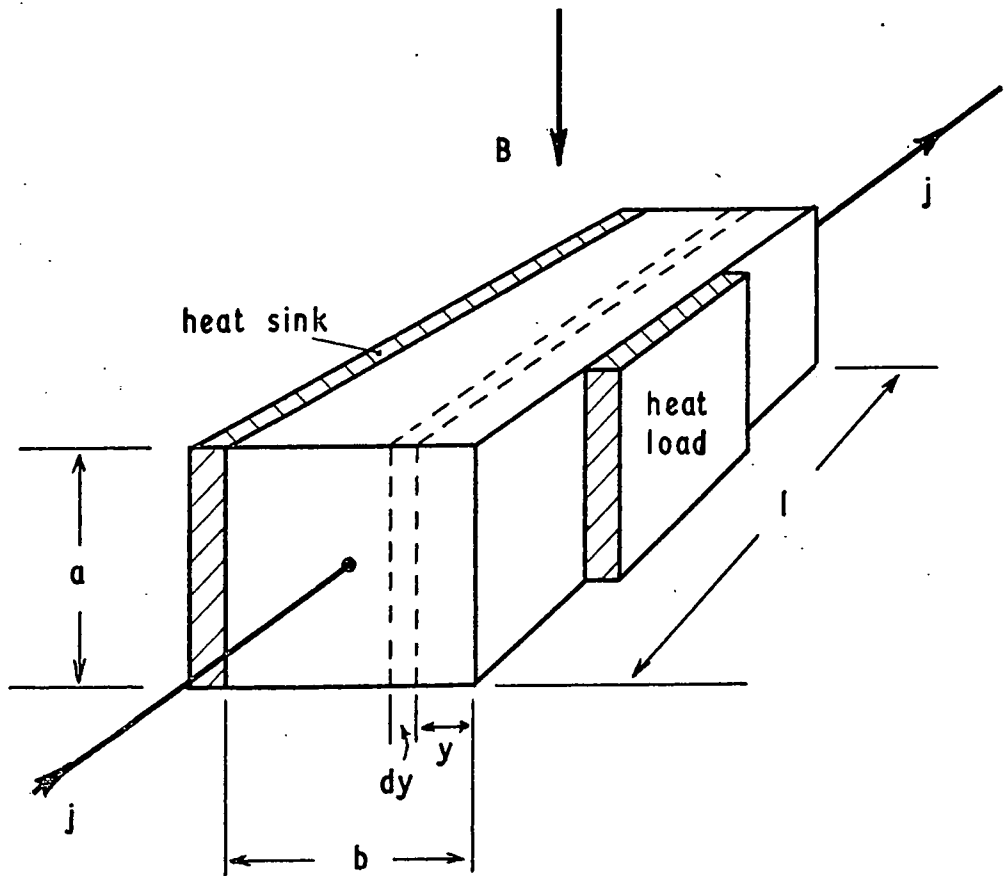
$$PK = QT$$

where K is the total thermal conductivity of the material and T the absolute temperature.

Following the method used for thermoelectric materials a figure of merit, Z, for a material operating in a device can be obtained. In the simple device shown schematically in figure 1.2, a rectangular rod of dimensions a, b and  $l$  is placed in a magnetic field B and a current of density j is passed along its length. The object to be cooled is placed in good thermal contact with the cold face of the bar and the hot face is in good thermal contact with a suitable heat sink. All the other faces of the bar and the heat load are thermally isolated so that the heat flow is limited to transfer from the cold face to the heat sink. Consider a thin slice of thickness  $dy$  and at a distance y from the cold face as shown in the diagram. The temperature gradient developed across the slice as a result of the Etingshausen effect will be reduced due to the flow of

FIGURE 1.2

An Etingshausen Cooling Device



heat across it both from the heat load  $W$  and from the Joule heat generated in that part of the bar between the cold face and the slice. If  $K$  is the thermal conductivity of the material in the direction of the heat flow and  $\sigma$  is the electrical conductivity in the direction of the current flow, this may be written

$$\begin{aligned}\frac{\partial T}{\partial y} &= PjB - \frac{1}{Kla} \left[ W + \int_0^y j^2 \frac{al}{\sigma} dy \right] \\ &= PjB - \frac{1}{Kla} \left[ W + \frac{1}{2} j^2 \frac{al}{\sigma} y \right]\end{aligned}$$

The total temperature difference,  $\Delta T$ , across the bar is then

$$\begin{aligned}\Delta T &= \int_0^b \left\{ PjB - \frac{1}{Kla} \left[ W + \frac{1}{2} j^2 \frac{al}{\sigma} y \right] \right\} dy \\ &= PjBb - \frac{1}{Kla} \left[ Wb + \frac{1}{2} j^2 \frac{alb^2}{\sigma} \right] \\ &= PjBb - \frac{Wb}{Kla} - \frac{j^2 b^2}{2K\sigma}\end{aligned}$$

The value of the current density,  $j$ , can be optimised to give the maximum possible temperature difference. To do this the above expression is differentiated with respect to  $j$  and the differential set equal to zero.

$$\frac{d(\Delta T)}{dj} = PBb - \frac{b^2 j}{K\sigma}$$

so that

$$j_{\max} \Delta T = \frac{PBK\sigma}{b}$$

The maximum temperature difference,  $\Delta T_{\max}$  is obtained when there is no heat load and this current density is flowing

$$\begin{aligned}\Delta T_{\max} &= PBbj_{\max} \Delta T - \frac{b^2}{2K\sigma} j_{\max}^2 \Delta T \\ &= \frac{1}{2}P^2B^2K\sigma\end{aligned}$$

The figure of merit  $Z$  is defined by the expression

$$\Delta T_{\max} = \frac{1}{2}ZT^2$$

so that 
$$Z = \frac{P^2B^2K\sigma}{T^2}$$

Since it is the Nernst coefficient,  $Q$ , that is usually measured the Bridgman relation can be used to write  $Z$  in terms of  $Q$ ,

giving 
$$Z = \frac{Q^2B^2\sigma}{K}$$

This expression was first derived for Etingshausen cooling under no load conditions by O'Brian and Wallace<sup>2</sup>. They also showed that the Etingshausen equivalent of cascading Peltier devices is obtained by giving the cooling element a defined exponential profile. Later El-Saden<sup>3</sup> showed that the same result is obtained if the effect of a heat load is included.

Following this simple early work, and in advance of obtaining a suitable material, a great deal of work has been put into elaborating the theory of the operating characteristics of Etingshausen devices (see, for example, references 4, 5 and 6), and the optimisation of the various operating parameters has been considered for devices used with isotropic and anisotropic materials, and in different geometrical arrangements<sup>7,8</sup>.

Some confusion has arisen because of differing results from the

various authors, but Delves<sup>9</sup> has shown that all the results are equivalent if account is taken of the varying definitions of the coefficients used by the authors. The definitions of the coefficients can differ in the auxiliary conditions specified. Putley<sup>1</sup>, for example, divides the coefficients into two groups, adiabatic and isothermal, depending on whether there is or is not a temperature gradient in the y-direction. With this grouping the Etingshausen coefficient is always adiabatic since there must be a temperature difference in the y-direction. The Nernst coefficient as defined earlier in this section is also adiabatic, but an isothermal Nernst coefficient can be obtained when the third auxiliary condition is changed from no heat flow in the y-direction to no temperature gradient in the y-direction. The two coefficients are related through the Seebeck and Righi-Leduc coefficients. A different set of related coefficients is obtained if the electrical auxiliary conditions specify no electrical field rather than no electrical current. The various authors divide into two groups. The authors of references 4, 5, 6, 7 and 8 fall into one group which finds effectively that their figure of merit  $Z_E^*$  is related to  $\Delta T_{\max}$  through

$$\Delta T_{\max} = \frac{1}{2} Z_E^* T_h^2$$

where  $T_h$  is the temperature of the hot face.

The authors of references 2, 3, 10, 13 and 23 find that their figure of merit  $Z_E$  is related to  $\Delta T_{\max}$  by

$$\Delta T_{\max} = \frac{1}{2} Z_E T_c^2$$

where  $T_c$  is the temperature of the cold face.

Delves<sup>9</sup> showed that

$$Z_E^* = \frac{Z_E}{1 + Z_E T}$$

If this, and particularly the different definitions used for thermal conductivity are taken into account the different authors' results are in agreement.

### 1.3 Material requirements

The Etingshausen effect in materials with non-degenerate statistics will be considered first and later in the section the effects of degeneracy will be included. An extrinsic non-degenerate semiconductor with acoustic mode lattice scattering has an Etingshausen coefficient given by

$$P = - \frac{3}{16} \frac{kT\mu}{eK}$$

where  $\mu$  is the mobility of the carriers,  $k$  is the Boltzman constant and  $K$  is the total thermal conductivity. It is not sufficient just to choose a material with high  $P$  since it is the value of  $Z$  which must be maximised.  $Z$  will increase with increasing magnetic field  $B$ , but Delves<sup>10</sup> points out that in this case  $Z$  will reach a maximum value near  $\mu B = 1$  and will fall to zero with increasing field because the Etingshausen coefficient for an extrinsic semiconductor becomes zero at high enough fields. He also shows that for a given extrinsic

semiconductor Peltier cooling will always be more effective than Etingshausen cooling.

For an intrinsic non-degenerate semiconductor with acoustic mode lattice scattering the expression for P becomes<sup>1</sup>

$$P = - \frac{3\pi}{16} \frac{k}{e} \frac{T}{K} \frac{n^2 \mu_e^3 + p^2 \mu_h^3 - np \mu_e \mu_h (\mu_e + \mu_h) (7 + 2E_g/kT)}{(\mu_e + \mu_h)^2}$$

where n and p are the densities of electrons and holes and  $\mu_e$  and  $\mu_h$  their mobilities.  $E_g$  is the energy gap of the material. There are now three terms in the expression. The first two represent the separate contributions of the two carriers, but unlike either the Hall or Seebeck effects in an intrinsic semiconductor the contributions are additive. This is because in the Etingshausen effect the magnetic field is effectively sorting the carriers according to their velocities and deflecting the slow carriers to one side (the cold side) of the sample and the fast carriers to the other (hot) side. With two carriers present this amounts to the transport of hole-electron pairs across the sample so that the third term in the expression for the Etingshausen coefficient is due to the transport of the ionisation energy. Thus the energy gap of the material appears in this term.

The expression for the Etingshausen effect in the intrinsic non-degenerate case simplifies for equal numbers of carriers, i.e.  $n = p$  and is a maximum for equal hole and electron mobilities,

when

$$P = \frac{3\pi}{16} \frac{kT\mu}{eK} (3 + E_g/kT)$$

This can be substituted into the expression for the figure of merit and  $Z$  then becomes

$$Z = \left(\frac{3\pi}{16}\right)^2 \frac{k^2 \mu^2 B^2 \sigma}{eK} (3 + E_g/kT)^2$$

Delves<sup>10</sup> examined the behaviour of  $Z$  in high magnetic fields and pointed out that because the Etingshausen coefficient of an intrinsic semiconductor does not go to zero at high fields there is an advantage in increasing the field. Both  $\sigma$  and  $K$  are also affected by the high field. To make allowance for the large magnetoresistance  $\sigma$  must be divided by the term  $(1 + \mu^2 B^2)$ . The total thermal conductivity  $K$  consists of two parts, an electronic component due to the transport of thermal energy by the carriers and a lattice component  $K_L$ . The electronic component is affected by the same magnetoresistance term as the electrical conductivity and at high enough fields the electronic component becomes zero. Thus for fields where  $\mu B \gg 1$ ,  $Z$  becomes asymptotic to the value

$$Z = \left(\frac{3\pi}{16}\right)^2 \frac{k^2 \sigma_0}{eK_L} (3 + E_g/kT)^2$$

where  $\sigma_0$  is the zero field conductivity. Expressed in terms of the carrier density and mobility this becomes

$$Z = \left(\frac{3\pi}{16}\right)^2 \frac{2k^2 n\mu}{K_L} (3 + E_g/kT)^2$$

This expression makes it possible to list the desirable properties of a material which is suitable for use in an

Ettingshausen cooling device. The material should be intrinsic with equal numbers of holes and electrons and preferably with equal hole and electron mobilities. It must have a high carrier mobility, both to increase  $Z$  and also so that the condition  $\mu B \gg 1$  can be satisfied at reasonably low magnetic fields. The lattice thermal conductivity should be low. At first sight it would appear that the energy gap should be high but this is not so because both  $n$  and  $\mu$  depend on the energy gap and a high gap would give a low carrier density. The low gap is also needed to give a material with low effective mass and hence high mobility. Delves<sup>10</sup> examined the dependence of  $Z$  on the energy gap in more detail, and so included the effect of degeneracy. He showed that the result would depend on the scattering mechanism. For acoustic mode lattice scattering  $Z$  rises as the energy gap becomes smaller and reaches a maximum with a small amount of band overlap. Harman<sup>11</sup> also examined the requirements for a suitable material and came to similar conclusions.

In general then it would appear that the class of materials of most interest are the semimetals which have a small band overlap, and very low energy gap semiconductors. Cooling is only likely to be effective at low temperatures because of the need for high mobilities. Most of the low gap semiconductors are un-suitable. For instance, HgTe and HgSe have very high electron mobilities but only a low hole mobility. This is

also true of the semimetal bismuth. Some improvement may be possible with alloys and the properties of HgTe-CdTe alloys have been investigated<sup>12</sup>. So far alloys of bismuth and antimony are the most promising<sup>13,14</sup> and one very small experimental permanent magnet cooling device has been constructed using bismuth<sup>15</sup>. In addition to the requirements listed above it is important to avoid ionised impurity scattering because of the less favourable temperature dependence of the mobility.

The only known material possessing the necessary small band overlap which also has nearly equal carrier mobilities is graphite. Graphite crystals have a layer lattice (see figure 5.2) with the atoms arranged in hexagonal arrays within the layers and only weak binding between the layers. Such a structure gives it highly anisotropic properties, but Delves<sup>10</sup> has shown that this is unlikely to give any advantage in a cooling device. Measurements on small single crystal flakes of natural graphite made by Soule<sup>16</sup> showed that in the basal plane the carrier densities are equal and the electron mobility is high, rising from  $10^4 \text{ cm}^2 \text{ V}^{-1} \text{ sec}^{-1}$  at  $300^\circ \text{K}$  to nearly  $10^6$  at  $4^\circ \text{K}$ . The hole mobility is only slightly less. The effective masses for holes and electrons are  $m_e^* \sim 0.04m_0$  and  $m_h^* \sim 0.06m_0$ <sup>17</sup>. It is thought that there is a small band overlap of the order of  $0.03 \text{ eV}$ <sup>18</sup>. Such properties appear very promising for Etingshausen cooling except that since the material has a low atomic weight it is likely to have a high lattice thermal

conductivity. However as the following paragraph will show this may not be a disadvantage.

In some semiconductors of very high purity and crystalline perfection the thermoelectric power is found to be enhanced at low temperatures because of the effects of phonon drag. This effect has been examined most thoroughly in Ge, Si and diamond<sup>19,20</sup> and is discussed by MacDonald<sup>21</sup>. The theory of the effect is complex since it involves interaction between the phonon and electron populations in the material. Qualitatively, as the temperature of the material is lowered sufficiently the additional component in the thermoelectric power is seen and this component continues to rise as the temperature is lowered further, reaching a peak and then falling off again because of the onset of boundary scattering effects similar to those encountered in thermal conductivity measurements. As for thermal conductivity the position of the peak depends upon the Debye temperature of the material and occurs at higher temperatures with increasing Debye temperature. The effect is likely to be greater in materials with high thermal conductivities but will fall off if the carrier density becomes too high. Parrott<sup>22</sup> showed that in similar circumstances a phonon drag component should also be seen in the Nernst coefficient, so that it is possible that the increase might outweigh the disadvantage of the high thermal conductivity and result in a high figure of merit for Etingshausen cooling. Wright<sup>23</sup> has made an estimate of the

magnitude of the effect which might be obtained in pyrolytic graphite. If phonon drag effects do occur they would result in a much higher figure of merit over part of the temperature range. Although the estimation did not result in spectacular amounts of cooling, it was sufficiently encouraging to warrant further investigation of graphite as a possible material for Etingshausen cooling.

#### 1.4 Description of the project

The previous two sections have discussed in a simple way the operation of an Etingshausen device to obtain useful cooling below room temperature, and have shown why graphite was chosen as a material which justified further investigation. A project to investigate the properties of a material for this purpose can be divided into the following four parts.

1. Preparation of the material in suitable form.  
Ideally it should be single crystal material with crystals of sufficient size to enable measurements to be made without too much difficulty.
2. Investigation of the structure of the prepared material.  
This will be particularly important if the prepared material is not single crystal since enough must be known about the structure and its defects to be able to assess their effect on the other measured properties.
3. Measurement of the thermal conductivity.

Because of its importance in the figure of merit for cooling the thermal conductivity needs to be known over the range of temperature in which cooling may be possible.

#### 4. Investigation of the thermomagnetic properties.

Since comparatively little work has been done on these effects some theoretical work will be required in addition to the experimental measurements.

Once the results from all four parts of the project are available it should be possible to assess whether graphite is a suitable material for Etingshausen cooling. In addition, since the investigations cannot be restrictively narrow, there should be a much better understanding of the basic properties of this particular material.

The project was divided into two. The present work is concerned with the first three parts. Work on the fourth part was undertaken by J.J. Mills and has already been written up<sup>24</sup>. Because of their importance to this work some of the results obtained by Mills will be summarised in the remaining sections of this chapter.

### 1.5 Summary of the results of the investigation by J.J. Mills of the thermomagnetic effects in pyrolytic graphite

#### 1.5.1 Experimental results

Measurements were made on a number of different bars of pyrolytic graphite of various degrees of perfection. They

yielded comparable results but since bar 22 has been most extensively investigated in this work (see chapter 2) only results from that bar will be given.

The variation of the resistivity with temperature for the samples is shown in figure 1.3. The resistivity relative to that at 300°K is plotted so that samples can be compared easily. The values of the resistivity at 300°K are

22 B	$4.4 \times 10^{-5}$ ohm cm
22 C	$4.5 \times 10^{-5}$
22 D	$5.3 \times 10^{-5}$
22 F	$9.4 \times 10^{-5}$
22 G	$26.2 \times 10^{-5}$
22 H	$43.3 \times 10^{-5}$

In agreement with other workers the less perfect graphites have a negative temperature coefficient. The better samples have a positive coefficient but the resistivity still does not change as steeply as single crystal material.

The average carrier mobility of the samples is shown in figure 1.4 as a function of temperature. Values of the average mobility were obtained from measurements of the magnetoresistance of the samples and have been corrected to the zero field values. It can be seen that the best samples are approaching the single crystal values. The slope is near the single crystal value at high temperatures but falls off at lower temperatures. If it is assumed that the saturation is due to the onset of

FIGURE 1.3

Temperature dependence of the relative resistivity of sections from bar 22

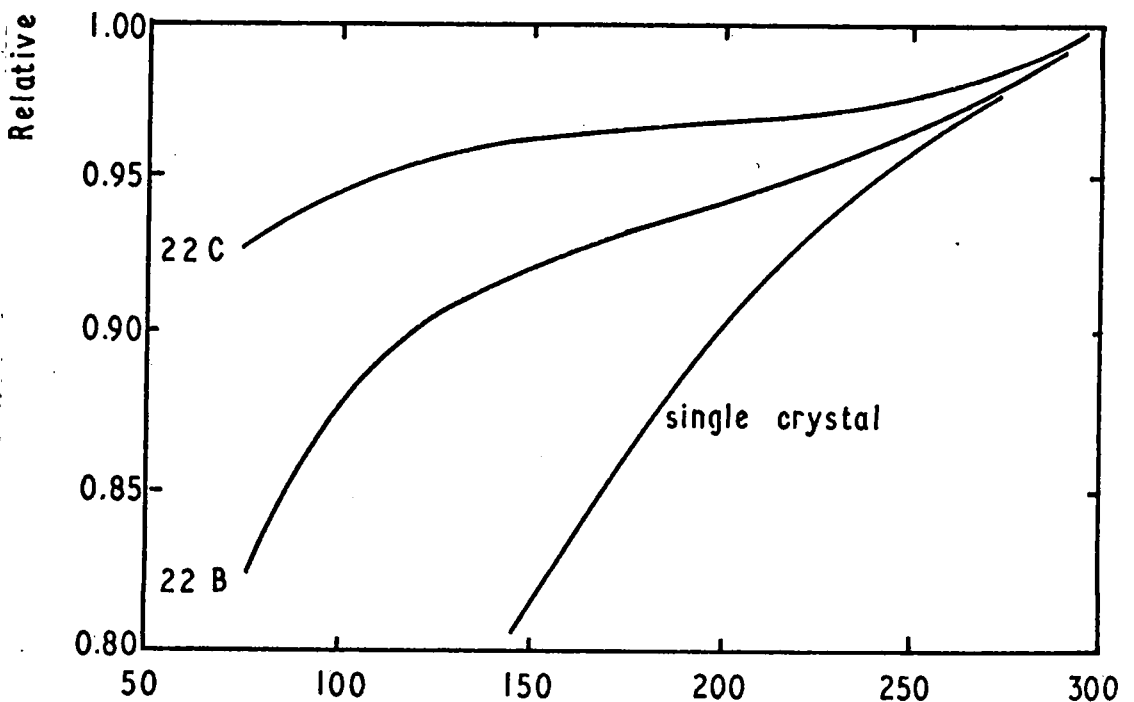
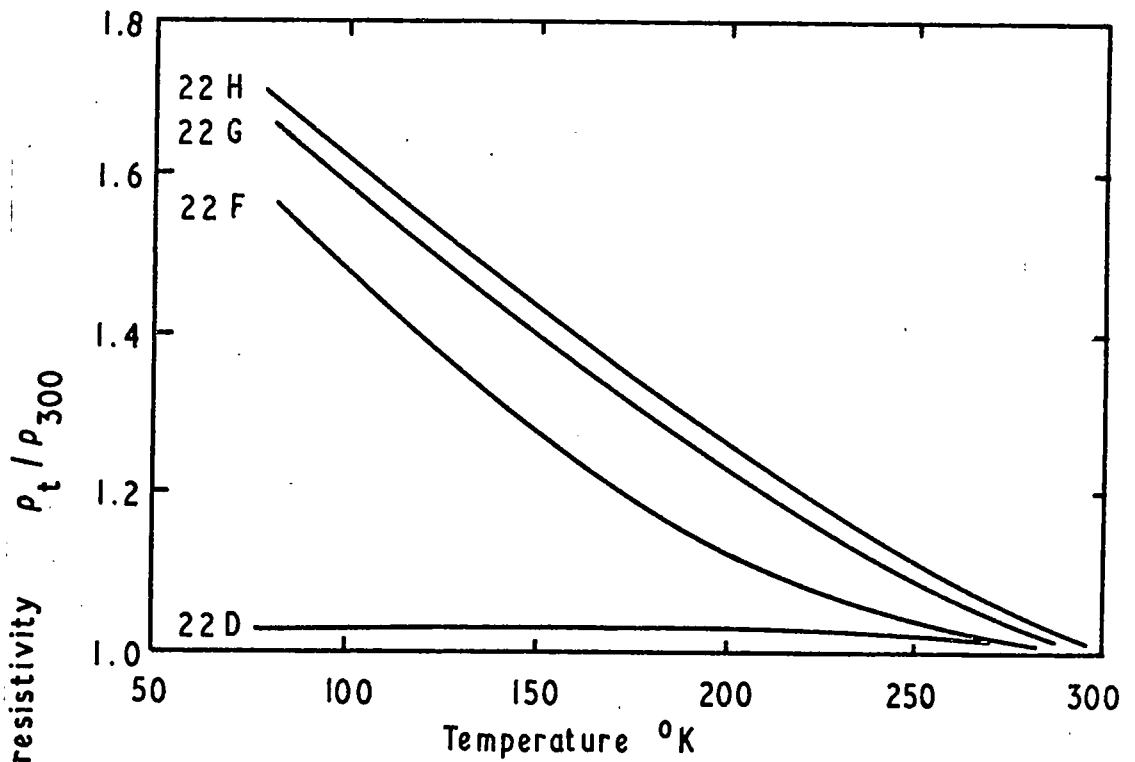
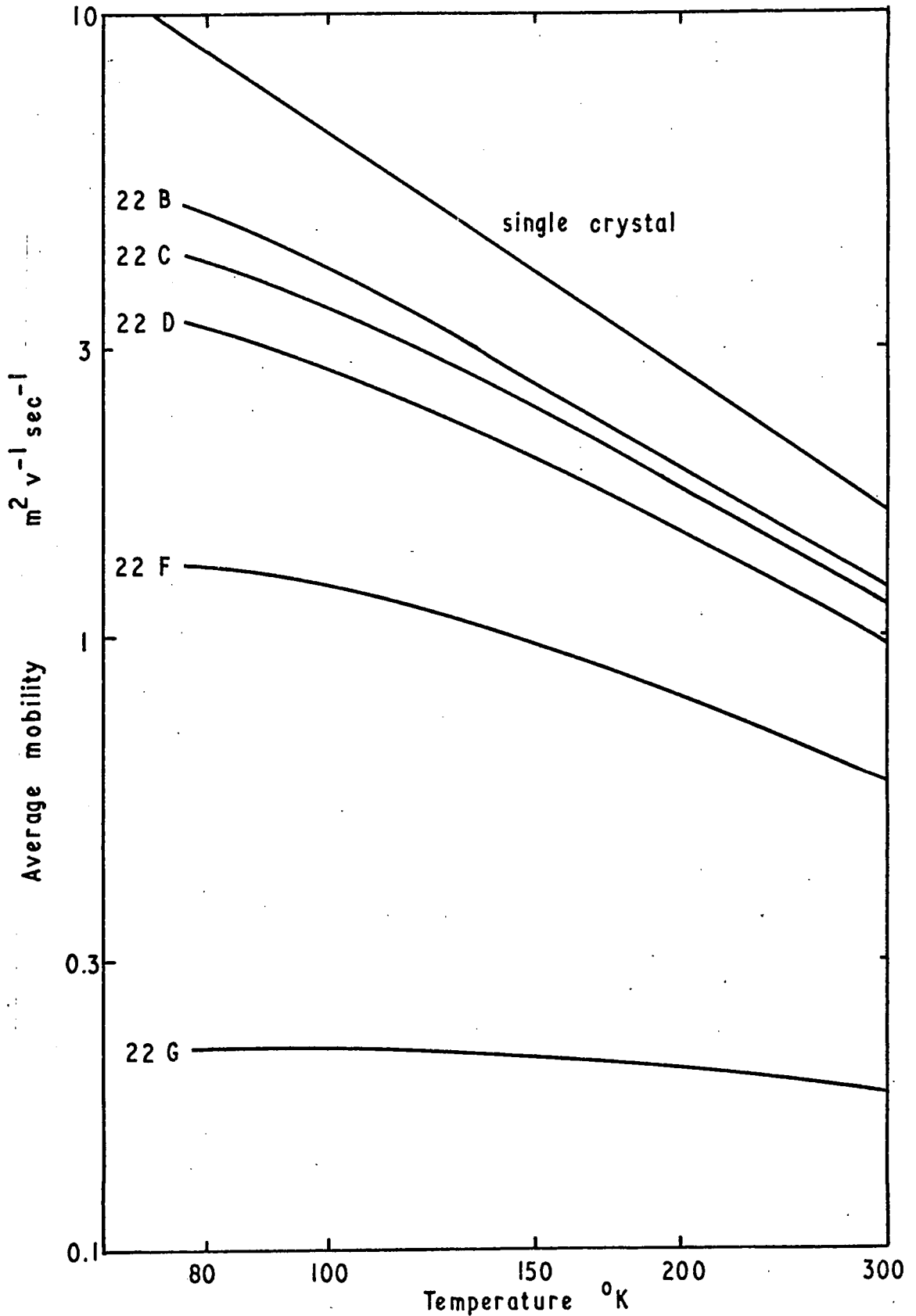


FIGURE 1.4

Temperature dependence of the zero field average mobility of sections from bar 22



crystallite boundary scattering then a crystallite size can be deduced from the saturation value. This gives the following values

22 B	3.8 $\mu\text{m}$
22 C	1.9
22 D	1.6
22 F	0.4
22 G	0.04
22 H	0.03

The carrier density of the samples showed little variation from sample to sample. The better samples had values near  $4 \times 10^{18} \text{ cm}^{-3}$  at  $300^\circ\text{K}$  falling to  $1 \times 10^{18} \text{ cm}^{-3}$  at  $80^\circ\text{K}$ . The mobility ratio also showed little variation from sample to sample and was a little over 1.1 at room temperature falling to a little less than this value at  $80^\circ\text{K}$ .

The Nernst coefficient was also measured as a function of temperature and the results are shown in figure 1.5. For the best samples values of this coefficient rose from  $3.2 \text{ cm}^2 \text{ deg K}^{-1} \text{ sec}^{-1}$  at  $300^\circ\text{K}$  to  $10.5 \text{ cm}^2 \text{ deg K}^{-1} \text{ sec}^{-1}$  at  $80^\circ\text{K}$ .

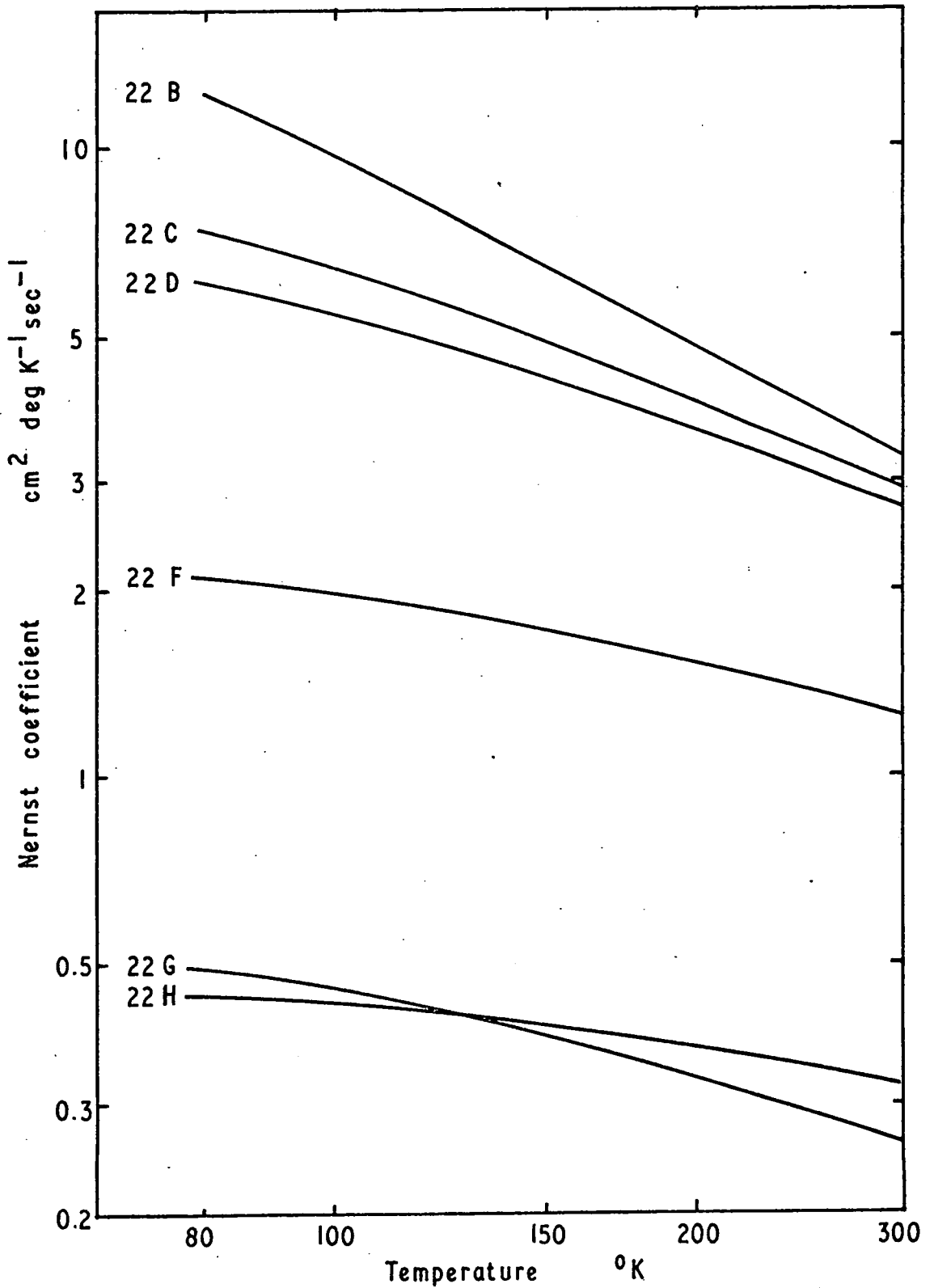
An attempt was made to measure the Etingshausen coefficient but with the apparatus available the effect could not be detected. This implies that the coefficient must be less than  $10^{-4} \text{ m}^3 \text{ deg K joule}^{-1}$ .

### 1.5.2 Theoretical results

A computer programme was written to determine the value

FIGURE 1.5

Temperature dependence of the Nernst coefficient of sections from bar 22

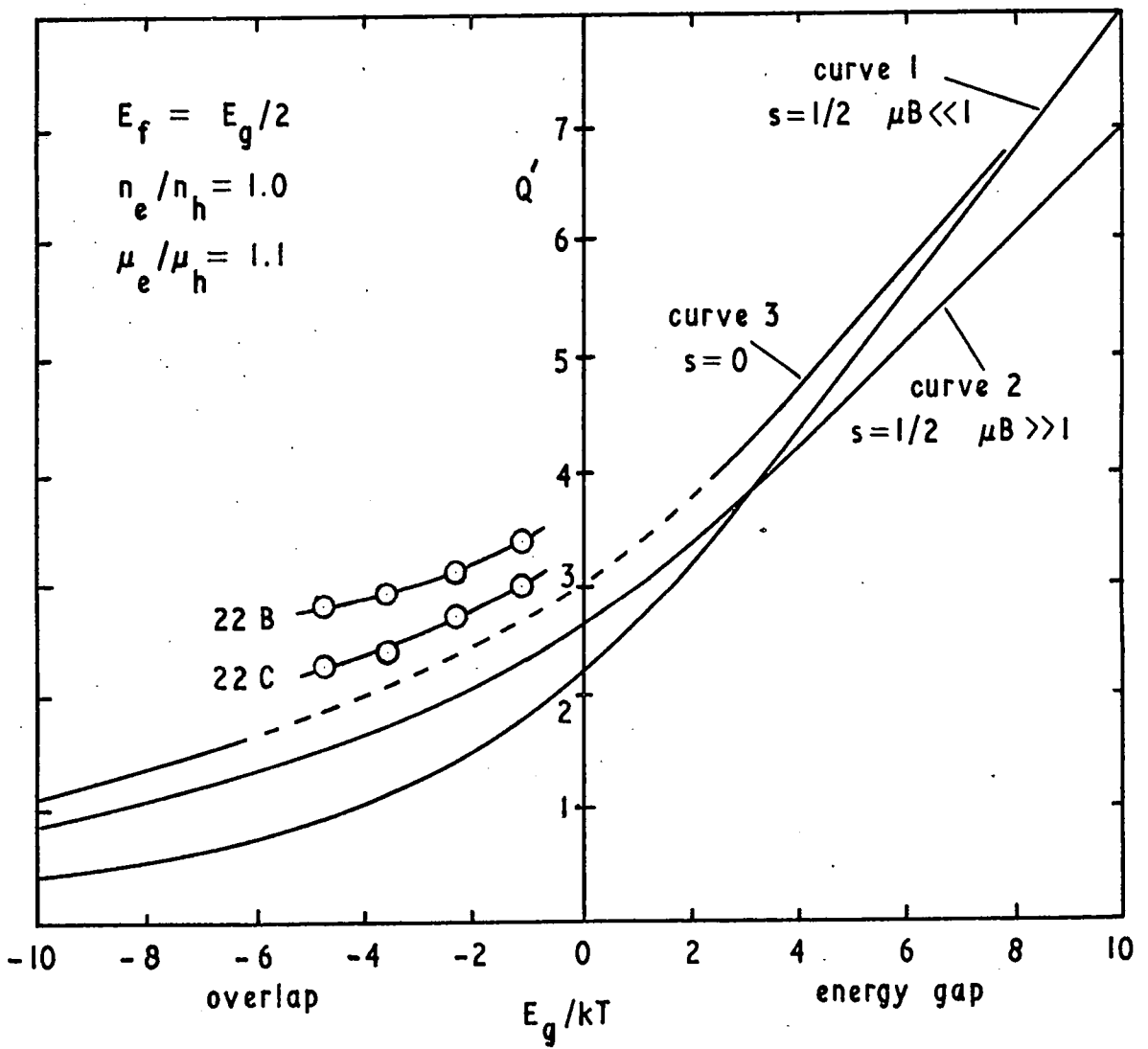


of the Nernst coefficient from theoretical considerations based on the known band structure of graphite. The assumptions made in the programme were that there were parabolic energy surfaces, that the Fermi level occurred at the centre of either the band gap or overlap, that there were equal numbers of electrons and holes, that the ratio of the carrier mobilities was 1.1 and that there was acoustic mode lattice scattering. The results were obtained in terms of  $Q'$  and the reduced band gap  $E_g/kT$  where  $Q' = eQ/k\mu_h$  with  $\mu_h$  the hole mobility. The programme covered the range from  $E_g/kT = -10$  to  $E_g/kT = +10$  and thus from band overlap through to band gap, and also from the fully degenerate through to the non-degenerate regions. If a constant band gap or overlap is assumed then the results effectively represent the variation of  $Q$  with temperature. Since the results are magnetic field dependent the two limits,  $\mu B \ll 1$  and  $\mu B \gg 1$ , were examined and are shown as curves 1 and 2 in figure 1.6. The computer programme was checked by using the fully degenerate and non-degenerate approximations to work out  $Q$  and showing that the values obtained were in agreement with the extremes of the curves produced by the computer.

To display the experimental results for  $Q$  on the same graph a value for  $E_g$  must be assumed. By trial of a number of values it was found that the experimental results would lie on a curve parallel to the theoretical curve only if an overlap of 0.03 eV was used. This value of overlap is in agreement

FIGURE 1.6

Comparison of the experimental values with  
 the theoretically obtained curves of  $Q' = \frac{e}{k} \cdot \frac{Q}{\mu_h}$   
 as a function of reduced energy gap



with that found by McClure<sup>18</sup>. The experimental values for samples 22 B and 22 C are shown in figure 1.6 assuming this overlap. The experimental results disagree with the theoretical expectations in two ways. The value of  $Q$  was higher than predicted and  $Q$  was found to be field independent. This caused some reappraisal of the assumptions made in the computer programme and other types of scattering were examined. It was found that in the case of neutral impurity scattering  $Q$  would be field independent and curve 3 in figure 1.6 was obtained for this type of scattering. This curve was not obtained by computer, but by working out values for the non-degenerate and fully degenerate extremes and interpolating between. The predicted values are now higher and lie closer to the experimental values, but the field independence leads to the important conclusion that in this type of graphite lattice scattering does not predominate even at the highest temperature measured. The type of neutral impurity scattering considered above can be obtained by scattering on uncharged defects, dislocations or grain boundaries. It would seem from the polycrystalline nature of the material that grain boundaries provide most of this scattering.

## CHAPTER 2

### MATERIAL PREPARATION

#### 2.1 Introduction

The previous chapter has outlined the reasons behind the investigation of graphite as a possible material for use in Etingshausen cooling devices. As in most device applications of this nature it is desirable to use single crystal material, so the object of the preparation must be to produce single crystals or failing that, as near single crystal material as possible.

Natural single crystals only occur in sizes up to a few millimetres but a few specimens have been separated and purified, and various electrical measurements made on them<sup>25,16</sup>. These measurements act as a valuable standard when assessing the properties of less perfect material, but natural crystals would clearly not be a suitable source of material for more extensive use.

The phase diagram of carbon has been determined<sup>26</sup> and since graphite sublimates at  $3600^{\circ}\text{C}$  it is not possible to use growth from the melt as a method of crystal production. It is therefore necessary to use a vapour phase method. Carbon has been produced by the breakdown of carbon compounds on to a hot substrate. This process is in common use commercially (for example in the production of carbon resistors) and quite

a lot is known about it. In general the pyrolysis temperatures are in the range 900 to 1500°C and a variety of gases and substrates are used. An extensive investigation of the preparation and properties of these pyrolytic carbons has been carried out by Grisedale et al<sup>27</sup>. The carbon produced depended greatly on the substrate. Loose sooty deposits were formed on surfaces contaminated with metal or metal oxides and dense compact deposits obtained on ceramics. The compact deposits were made up of packets of plane parallel sheets of carbon atoms arranged in hexagonal arrays. Within the packet each array was small in size and randomly rotated relative to its neighbours. The interplanar spacing was greater than that of graphite. In general the packets were randomly oriented with respect to each other but in some experimental conditions could be made to line up with the hexagonal layers parallel to the surface of the substrate. These carbons were all of relatively low density: up to 2.1 gm cm<sup>-3</sup> compared with the graphite theoretical density of 2.26 gm cm<sup>-3</sup>, and had an electrical resistivity around 1.5 x 10<sup>-3</sup> ohm cm and thermal conductivity around 0.08 watt cm<sup>-1</sup> deg C<sup>-1</sup>. Pirani and Fehse<sup>28</sup> and later Nishiyama<sup>29</sup> reported the properties of pyrolytic carbons deposited at much higher temperatures in the range 1500 to 2000°C and subsequently heat treated at temperatures up to 3000°C. The densities of the deposits were in the range 2.00 to 2.23 gm cm<sup>-3</sup>. The electrical resistivity depended

upon the heat treatment temperature, decreasing with increasing temperature, and had a value of around  $1.2 \times 10^{-4}$  ohm cm compared with around  $5 \times 10^{-5}$  ohm cm for natural graphite.

More recently an important systematic study of the properties of high temperature pyrolytic carbons has been made by Brown and Watt<sup>30</sup>. They investigated carbons prepared from methane, propane and benzene at pyrolysis temperatures in the range 1500 to 2200°C. The substrate used was a rod of commercial polycrystalline graphite clamped between water cooled electrodes and heated by the passage of a low voltage electric current. The rod and electrodes were contained in a vacuum vessel to allow the rod to be outgassed at a high temperature before deposition which took place at pressures in the range 25 to 150 torr. During deposition the surface temperature of the deposit was maintained constant. The properties of the deposit depended very little on the gas used or on the gas pressure. The deposition rate was slightly different with the various gases but depended more on temperature and pressure. Faster growth rates were obtained with increasing temperature and pressure. With these conditions all the carbons produced showed preferred orientation with the basal planes lined up parallel to the substrate but, except for those deposited above 2000°C, there were no x-ray reflections from a 3-dimensional lattice indicating that most of the deposits had not taken up the graphite crystal structure. The electrical resistivity

along the layer planes of the deposit was found to vary with the deposition temperature only, and fell to around  $1 \times 10^{-4}$  ohm cm for deposits formed at the highest temperatures. Across the deposit measurements were not very reliable but were up to 0.5 ohm cm. The most striking result was the dependence of the density of the deposit upon the pyrolysis temperature. Carbons deposited at  $1500^{\circ}\text{C}$  had a density of around  $1.5 \text{ gm cm}^{-3}$ , falling to about  $1.25 \text{ gm cm}^{-3}$  at  $1700^{\circ}\text{C}$  and rising again to  $2.0 \text{ gm cm}^{-3}$  at  $2000^{\circ}\text{C}$  and thereafter gradually approaching the theoretical density for graphite of  $2.26 \text{ gm cm}^{-3}$ . This dip in the density was later confirmed and examined over a wider temperature range by Brown, Clark and Eastabrook<sup>31</sup>. Further investigation of the density dip was carried out by Diefendorf<sup>32</sup> who showed that it was due to gas phase reactions and subsequent incorporation of sooty particles into the deposit. He showed that such reactions cannot occur if the gas pressure is lowered sufficiently. A series of carbons was produced from methane at  $1.7 \times 10^{-2}$  torr in which the density increased gradually from  $2.1 \text{ gm cm}^{-3}$  at a pyrolysis temperature of  $1100^{\circ}\text{C}$  up to  $2.25 \text{ gm cm}^{-3}$  at a temperature of  $2400^{\circ}\text{C}$ . The dip at  $1700^{\circ}\text{C}$  was completely absent.

Diefendorf also carried out experiments to examine whether the growth was epitaxial. To do this he used a bar of well oriented pyrolytic graphite as the substrate material and examined the coating obtained at different gas pressures.

At higher pressures,  $\sim 5$  torr, the coating grew evenly on all sides of the bar and was found to be oriented so that the c-axis of the coating was always normal to the substrate surface. At low gas pressures nucleation difficulties were encountered, but the deposits obtained grew much faster on the basal planes of the substrate and only a thin irregular deposit grew on the edges of the bar. This thin deposit was found to have the same orientation as the substrate giving some grounds for supposing that the growth could be epitaxial at very low gas pressures.

From the above description of previous work it would appear unlikely that the pyrolytic process could ever produce single crystals of any magnitude. Brown and Watt's estimate of the crystallite size of their high temperature deposits was only a few hundred Angstroms. However their work has shown that high temperature conditions could yield deposits with a true 3-dimensional graphitic structure and having the crystallites highly oriented. The a-axis electrical resistivity was also beginning to approach that of natural graphite indicating that provided neighbouring crystallites were sufficiently well aligned the a-direction properties of the polycrystalline material might become near enough to those of single crystals to allow a useful device to be made. It was decided therefore to try to develop the Brown and Watt method, concentrating on high temperature deposits, with a view to obtaining reproducibly

material that was truly graphitic, and which had as large a crystallite size as possible with the crystallites very accurately aligned.

## 2.2 Description of apparatus

### 2.2.1 General

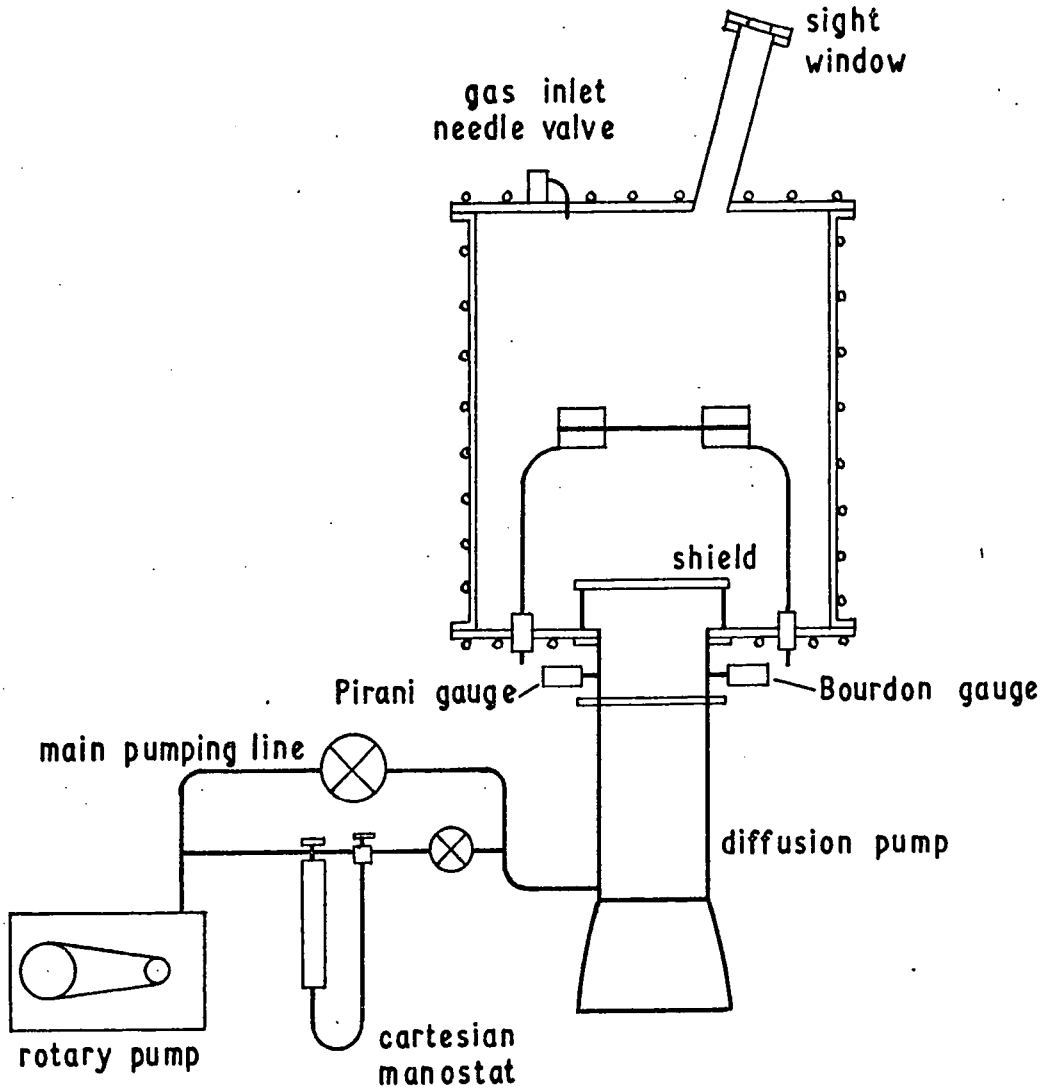
The apparatus was built within a very strictly limited budget. The use of sophisticated control gear was minimised and facilities that were thought to be only marginally necessary were not incorporated. During the course of the work the apparatus was elaborated in the light of experience, and parts of it were redesigned. Most of the economies proved justified but the most notable exception was in initially providing too small a power supply. Unless otherwise specified the apparatus will be described in its final form.

### 2.2.2 The furnace and vacuum equipment

A sketch of the furnace and vacuum equipment is shown in figure 2.1. The furnace consisted basically of a steel cylindrical vacuum vessel 12 in. diameter and 13 in. high. Copper water cooling tubes were soldered on to the base, lid and sides of the vessel. Heavy current electrical connections to the electrodes were made by bringing two pairs of 5/16 in. o.d. copper pipe through the base plate with Teflon insulated vacuum connections. These pipes also provided water cooling

FIGURE 2.1

Sketch of furnace and vacuum equipment



for the electrodes. A silica sight window was originally placed in the centre of the lid but this was found to soot up very quickly and was subsequently placed at the end of a relatively long angled tube out of the direct line of evaporation from the filament. The surface temperature of the growing deposit was measured through this sight window using a model L368 disappearing filament pyrometer manufactured by the Cambridge Instrument Co. Ltd. and capable of reading up to  $3600^{\circ}\text{C}$ . It was provided with a long focus objective and a magnifying eyepiece. Correction was made for the absorption of the silica window and for the c-direction emissivity of the bar<sup>33</sup>.

The 3 in. diameter pumping port in the centre of the base plate was fitted with a shield to protect the pump jets from possible debris and radiation from the filament. Two gauges were connected to the pumping port for pressure measurement, a barometrically compensated 4 in. dial gauge (Edwards High Vacuum Ltd., model CG 1B) for pressures from 760 torr down to 0.5 torr and a double filament Pirani gauge for pressures from 0.1 torr down to  $10^{-5}$  torr. The Pirani gauge was initially calibrated against a McLeod gauge. The furnace was evacuated by a 3in. diameter fractionating oil diffusion pump (N.G.N. Electrical Ltd., model AOP 125) with a speed of  $125 \text{ l sec}^{-1}$  and an ultimate pressure of  $5 \times 10^{-6}$  torr, backed by a rotary gas ballast pump with a speed of  $92 \text{ l min}^{-1}$  (N.G.N. Electrical

Ltd., model PSR 3). Once the system had been made reasonably leak free and the furnace outgassed by turning off the water cooling and allowing the furnace walls to rise in temperature, this pump combination was capable of producing a vacuum of  $10^{-5}$  torr in the cold furnace and of maintaining a vacuum of  $10^{-4}$  torr while a filament was being outgassed at  $2200^{\circ}\text{C}$ .

It was in the vacuum equipment that most of the economies of design were made. Had more money been available a baffle valve would have been fitted on top of the diffusion pump. This would have isolated the diffusion pump from the furnace and enabled growth runs to start immediately after outgassing without waiting for the diffusion pump to cool. It would also have avoided contamination of the pump oil by decomposition products from the furnace. Similarly a liquid air trap would have been a useful refinement since it would have aided quicker pump down times, lowered the ultimate vacuum attained and also condensed out vapour produced <sup>during</sup> growth and so relieved the load on the ballast mechanism in the rotary pump. However satisfactory graphite was produced without these items which would obviously be necessities for a production process.

### 2.2.3 Gas handling

The hydrocarbon gas used for pyrolysis was admitted to the furnace through a needle valve. A Rotameter flow gauge was used to monitor the gas flow which was usually held at

around  $20 \text{ ml min}^{-1}$ . Growth runs were made in the pressure range 50 to 150 torr and to maintain the pressure accurately a cartesian manostat (Edwards High Vacuum Ltd., Edwards-Greiner model 6) was fitted in the backing line. The control orifice provided with this manostat is 1 mm diameter and it was found that not only did it soot up but it did not have sufficient pumping speed to cope with the pressure surge when the filament was first heated up. An increase in diameter to 2 mm improved the performance on both counts with only a slight loss of stability. Control of the gas pressure with a much higher pumping speed could have been obtained by using the cartesian manostat to operate a contact controlling a magnetically operated valve in the main pumping line but this refinement did not prove strictly necessary and was therefore not incorporated. During deposition the rotary pump was operated with full gas ballast to prevent the build up of vapours in the system and the exhaust gases were vented to the outside.

It was decided in the first instance to use cylinder gas of ordinary commercial purity. Brown and Watt had already shown that the hydrocarbon used had more influence on the growth rate than on the graphite produced, but it seemed reasonable to use the simplest possible hydrocarbon to avoid any possible undesirable effects of intermediate breakdown products. However methane, the simplest hydrocarbon, was only available in cylinder form from the National Coal Board and the

analysis showed that it contained many impurities including oxygen. Propane was therefore used instead as the most likely impurities in the commercially available gas are other hydrocarbons which should have little effect. Shell-Mex and BP Gases Ltd. made available a supply of propane from their Thameside refinery, which produces propane of better purity than their other refineries, and very kindly supplied it in new cylinders without the addition of the usual 'stencing' agent.

#### 2.2.4 Electrode design

The requirements for the design of the electrodes gripping the graphite filament used as the substrate for the deposit are as follows :-

- a) There must be a sufficiently large area contact to carry the high currents used (up to 2000 A) and this contact must remain good at high temperatures
- b) Any junction between copper and carbon must be well cooled since these materials are not compatible at high temperatures.
- c) Allowance must be made for the linear expansion of the filament in heating up from room temperature to around 3000°C, and also for the low mechanical strength of the thin (0.2 cm) filament relative to the massive electrodes.
- d) It should be comparatively easy to replace the filament.

The final design which meets these requirements is sketched in

section in figure 2.2 and the photograph in figure 2.3 shows the electrodes in position in the furnace and enables the water cooling connections to be seen. The flat filament is clamped between massive graphite blocks which are in turn clamped between thick water cooled copper plates. The mating copper and graphite surfaces were ground flat before assembly to ensure good electrical contact. The assembly is held together with steel bolts fitted with spring washers. The water cooling connections to the copper plates which also served as electrical leads from the base plate were made of soft copper tubing. This soft tubing gives the electrode assembly great flexibility which is aided by the large diameter bends made in the pipe, and it enables the electrodes to be aligned accurately enough for the filament to be clamped between them without strain, though this must be done carefully because of the fragile nature of the filaments. The flexible electrodes also take up most of the expansion on heating up the filament, but there are difficulties here because the deposit has a lower a-direction expansion than the filament so that the deposit obtained is always longer at room temperature than the original filament, and there was always some strain present when the electrodes were unclamped after a deposition run.

It was soon found that in spite of the care taken in aligning the electrodes and ensuring the flatness of the graphite blocks, the high currents used inevitably led to some

FIGURE 2.2

Section through electrodes

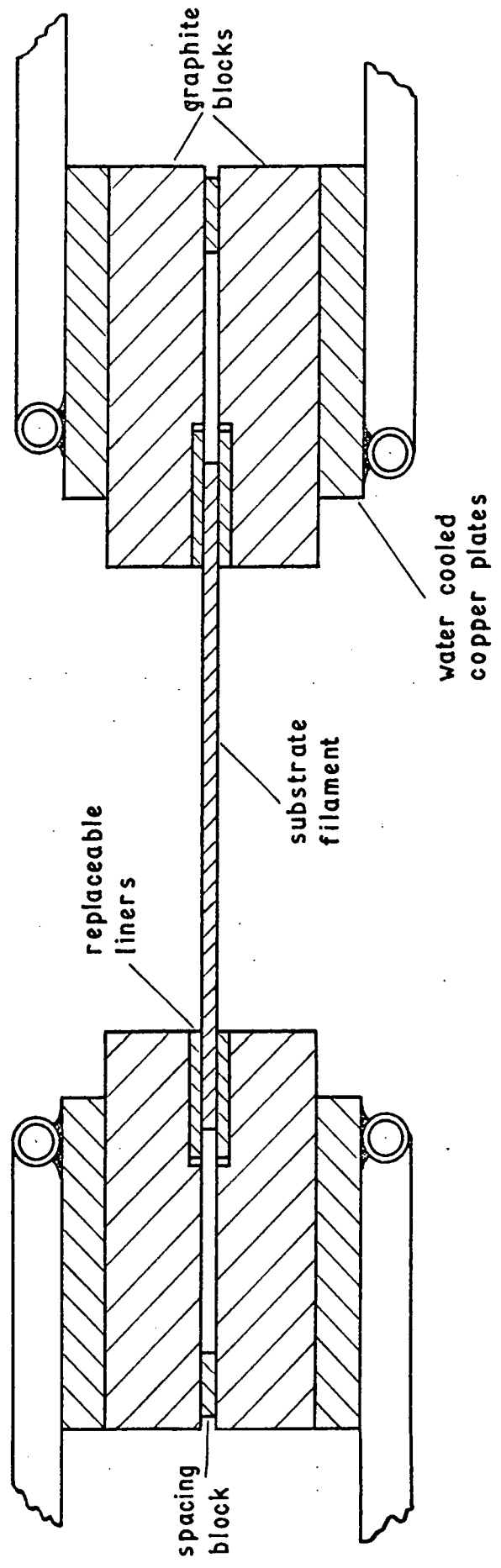


FIGURE 2.3

Deposition furnace showing  
the water cooled electrodes



degree of arcing at the contact between the filament and the blocks. The arcing was not sufficient to affect the current flow but the pitting it caused in the graphite blocks meant that they had to be ground flat again after each run. This extra work was avoided by the use of thin expendable graphite liners to the blocks and these could easily be replaced after each run. The contact area between the filament and liner was unchanged so that pitting continued to occur here but because the contact area between the liner and block was so much greater no arcing occurred at this contact and the blocks remained undamaged.

#### 2.2.5 Power supplies and controls

The original Brown and Watt method of growing pyrolytic graphite used resistance heating of the substrate as a means of obtaining the high deposition temperatures. However other workers, particularly at the Raytheon Company in the United States and to a lesser extent those at Imperial College, London had developed a method of growth using induction heating of the substrate. Because of space requirements in this method, coupling of the r.f. power to the work is inefficient and to allow for this a generator of approximately double the power output actually needed must be used. Purchase of an r.f. generator capable of giving 20 KW was completely beyond the financial allowance for this work so that it was decided to

use the very much cheaper resistance heating method. The influence of this decision on the graphite eventually produced will be described later in section 2.5.

The difficulty in making an economical design for the power supply for resistance heating the furnace is that the load resistance (the growing filament) is constantly changing and the supply must be capable of giving high voltage and low current at the beginning of a growth run and gradually changing to low voltage and high current at the end of a run. This means that the power rating of the supply (maximum voltage x maximum current) must be greatly in excess of the maximum power used to grow a filament and this supply is also used extremely inefficiently. The control equipment, if used in the usual simple straightforward way is equally inefficient.

The original power supply to the furnace was based on a welding transformer with an output of 22 V and 1000 A, supplied with a 415 V primary winding. The transformer output was controlled by a motor driven Variac. To avoid the expense of a Variac of the full power rating the one used was only capable of giving 30 A. It supplied the welding transformer directly at the beginning of a growth run, but once the voltage required across the filament had dropped sufficiently a 2.5 : 1 stepdown transformer was switched in between the Variac and the main transformer. This arrangement is somewhat simpler to switch than a series/parallel arrangement of the two Variac windings,

and proved satisfactory.

Considerable experience of the growth of pyrolytic graphite was obtained using this power supply but eventually it proved too small to grow the thick flat deposits required for further study, and was replaced by a supply based on a transformer giving 26 V and 2000 A. The 415 V primary of this transformer was controlled through a saturable reactor capable of handling the full power output and requiring a d.c. supply of up to 10 A for the control winding. The control characteristics of such an arrangement depend greatly on the load resistance. After the initial installation the control characteristics were determined for a number of different load resistances and plotted as a family of curves. The 'load curve' from a typical growth run was superimposed upon this to show the type of control that would be required, and it was immediately evident that very fine control of the d.c. current is required from 0 to 2 A but from 2 to 10 A the control could be quite coarse. The d.c. supply was therefore designed with a motor driven Variac supplying a bridge rectifier giving overall coarse control throughout the range, and an additional manually operated dropper for the fine control up to 2 A. This supply was adequate for all the bars of graphite actually grown since the largest obtained was taking 1600 A at 7.6 V at the end of growth and the run was limited by the water cooling of the electrodes.

### 2.3 Growth and assessment of the pyrolytic graphite

The material used for the substrate filaments was high purity nuclear grade graphite and because it has a particularly fine grain structure, Link EY9 grade manufactured by Morganite Carbon Ltd. was chosen. For the early experiments rectangular section filaments 3 x 2 mm and approximately 7 cm long were used. After insertion in the furnace all filaments were outgassed at a temperature at least 100°C higher than the growth temperature in a vacuum of  $10^{-4}$  torr.

The first runs attempted suffered from severe sooting problems and the sight window was obscured within a few minutes. Redesign of the sight window (as described in section 2.2.2) enabled this to remain clear but sooting at the beginning of a run remained a problem for some time. Early runs were at a comparatively low temperature, 1800°C, and propane pressure of 150 torr to give a relatively fast growth rate with a deposit of about 2 mm thickness in two hours. After growth the bars were assessed by three separate methods. The density was measured using kerosene as the immersion fluid as this is most likely to penetrate any pores in the material. X-ray powder photographs were examined for the appearance of 3-dimensional lattice lines indicating the onset of a true graphitic structure, and a section of the bar was polished and examined microscopically to look for flaws and the growth cone structure inspected under polarised light (see chapter 3). As would be expected these

low temperature deposits had low densities around  $1.4 \text{ gm cm}^{-3}$  and no 3-dimensional structure. The microscopic examination showed that the deposit was very badly laminated near the corners of the substrate filament and had widely divergent growth cones.

The next stage was to put up the deposition temperature to over  $2000^{\circ}\text{C}$  and bars were obtained at temperatures up to  $2200^{\circ}\text{C}$ . These deposits had much finer surface texture and densities of  $2.2 \text{ gm cm}^{-3}$ , close to the theoretical, so that density no longer became a sensitive method of assessment. The x-ray powder reflections had sharpened considerably (see chapter 5) and 3-dimensional lattice lines were showing, though apparently with a great deal of inconsistency from sample to sample. The growth cone structure was considerably finer but the corners remained badly laminated. To avoid the effects of corner laminations from this stage onwards the section of the starting filaments was increased to at least  $8 \times 2 \text{ mm}$  and it was found that at the centre part of the  $8 \text{ mm}$  flat the deposit was completely free from any laminations.

Although the deposits were now starting to become truly graphitic difficulties were still being experienced at the start of a growth run. The technique used was to establish the flow of propane at the desired pressure and then to heat the bar to the deposition temperature as quickly as possible. Because of the low thermal mass of the filament and the uninsulated furnace

the heating takes place very quickly and causes a very large surge in the gas pressure. The high pressure causes gas phase reactions and soot is formed during the short time the gas pressure remains high. At the same time the bar begins to grow and the initial deposits cause a greater relative change in the resistance of the bar than the later deposits, so that constant adjustment of the furnace controls is necessary to hold the surface temperature constant at the beginning of growth. It was felt that until the conditions at the beginning of a growth run were fully under control it would be unlikely that good quality reproducible material would be obtained, since soot particles included in the deposit at this critical stage could influence the growth of the rest of the deposit.

To help improve the starting conditions the propane pressure was reduced to 50 torr and it was found that the pressure surge was very much reduced and soot formation in the gas almost completely eliminated. At the same time the much slower growth rate meant that the bar resistance was changing more slowly and it was easier to hold the surface temperature accurately constant. Finally the starting conditions were brought completely under control by reducing the gas pressure just before switching on. After a little experience a reduction was found such that the initial pressure surge raised the pressure to near the desired value and the controlled pressure was reached very soon after switching on. A further

benefit of the lower gas pressure and slower growth rate was that the deposits obtained had an even finer surface texture and the growth cone structure was also correspondingly fine.

Control of the starting conditions with the consequent elimination of soot particles formed in the gas delayed the onset of the growth of a deposit on the filament. It was found that it was some minutes after the filament reached temperature before the deposit started to grow, but that after nucleation had occurred the growth rate was much as before, though occasionally for some unknown reason it was much slower. Such delay in nucleation was observed by Diefendorf<sup>32</sup> when trying to grow deposits on perfect or near perfect surfaces. After two weeks he failed to nucleate any growth on the basal plane of a purified single crystal of graphite at 800°C and 9 torr gas pressure and he observed a delay of two days using a pyrolytic graphite substrate at 1600°C and 1 atmosphere gas pressure. At 800°C the evaporation rate of carbon from the substrate would be negligible and at 1600°C only slow, but at the 2200°C working temperature considered here the evaporation rate is relatively high and it was supposed that nucleation could take place once carbon evaporation had made the surface of the filament sufficiently rough. To check the effect of surface roughness a filament was polished before insertion in the furnace and the nucleation delay became much longer. Since the growth cone structure from the deposit was also

slightly finer the filaments continued to be polished before use. Growth rate finally remained the one factor that could not be fully controlled. In most runs a reasonably constant rate that depended on the gas pressure was obtained, but occasionally and unpredictably a very much slower growth rate was obtained and it did not seem possible to find any reason for this.

Some experiments were performed to try to induce stress recrystallisation under constraint as described by Blackman and Ubbelohde<sup>34</sup>. In this method at the end of a deposition run the gas is pumped out of the furnace and the surface temperature is raised momentarily to around 2700°C. The major part of the deposit transforms suddenly from a rectangular sleeve to a cylindrical one, leaving some highly perfect graphite flakes near the substrate. This process was tried on several bars. One of them disintegrated explosively as also described by Blackman and Ubbelohde but although the transformation occurred in the rest a flake was found in only one of the cylinders. From the x-ray film the crystallite size was clearly high since a spotty ring was obtained, and spot counting gave an estimate of 1  $\mu\text{m}$ . However the crystallites were so poorly oriented that it was of little use and far too fragile for further measurements. Evidence of strain in the untransformed deposit is shown when it is separated from the substrate. In most cases the previously flat deposit curves to some degree.

During the course of taking x-ray powder photographs of the bars produced under properly controlled conditions, the cause of the inconsistency in the appearance of 3-dimensional lattice lines, mentioned earlier in this section, was resolved. In all deposits it was found that material taken from the side of the deposit nearest the substrate was much more graphitic than material taken from the surface of the bar, and once samples were always taken from the same part of the deposit the results became consistent. The inner layers from a well controlled high temperature deposit had all 3-dimensional lattice reflections present and a narrow line width indicating a reasonable crystallite size. The outer layers remained poorly graphitised. Powder photographs were thus no longer a sensitive means of assessing the quality of the graphite and better results were obtained by taking x-ray transmission photographs to determine the preferred orientation of the deposit. The quantitative and qualitative assessment of the graphite using this method is described in detail in chapter 3. It confirmed the difference in graphitisation between the outer and inner layers of a deposit.

Harvey, Clark and Eastabrook<sup>35</sup> first pointed out that, in this method of growth, temperature gradients could develop across the deposit because of the very low c-direction thermal conductivity of pyrolytic graphite. In the uninsulated furnace much of the power used to heat the growing bar is lost by

radiation from the surface. Since the heat is generated within the bar and must travel to the surface to be radiated it follows that the temperature of the inside of the bar must rise by an amount related to the thermal conductivity of the deposit. The lower the thermal conductivity in a direction perpendicular to the surface of the deposit the higher the internal temperature rise. Pyrolytic graphite is very anisotropic and although the deposit has a very high a-direction thermal conductivity (see chapter 4) the conductivity in the c-direction is extremely low, of the order of  $0.02 \text{ watt cm}^{-1} \text{ deg C}^{-1}$ . This means that the temperature difference across the deposit could be quite high and since it is the surface temperature that is maintained constant during growth, the temperature of the inner layers of the deposit will gradually rise as the bar grows. This would effectively anneal the inner layers at some temperature in excess of the deposition temperature and thus account for the increased graphitisation. The difference in graphitisation between the inner and outer layers indicates that the rise would have to be some hundreds of degrees for this to be the correct explanation, and the thermal conductivity measurement by Moore, Ubbelohde and Young<sup>36</sup> shows that such rises are possible.

It is possible to make a-direction measurements of the resistivity, thermal conductivity, magnetic and thermomagnetic properties on thin flat specimens of pyrolytic graphite. Such

specimens can easily be obtained by first cutting the deposit into a suitable shape and carefully cleaving it into thin sections with a razor blade. If the temperature profile across the deposit can be estimated sufficiently well then these sections enable the a-direction properties of the material to be found for a range of effective formation temperatures.

This was done for one particular bar and a number of property measurements made through the range with more interest centred on the better graphitised inner layers. The electrical and magnetic measurements were made by Mills<sup>24</sup>. The remaining sections of this chapter will describe the growth of the particular bar, estimate the temperature profile and demonstrate that the properties of the graphite produced at the estimated temperatures fit reasonably well with those found by other workers. In the following three chapters the measurement of preferred orientation, thermal conductivity and crystallite size as a function of formation temperature are described, and the overall properties are linked together in the final chapter.

#### 2.4 Details of the growth of bar 22

As was standard procedure, the furnace was cleaned of any soot formed during the previous deposition run and the electrode alignment checked. A substrate filament measuring 70 x 10 x 2 mm was inserted into the furnace and outgassed at a temperature of 2300°C and pressure of 10<sup>-4</sup> torr. It was noted that 220 A

at 14.3 V was required to keep the filament at 2200°C. After allowing the diffusion pump to cool down the cartesian manostat was set to control the propane pressure at 50 torr with a propane flow of 20 ml min<sup>-1</sup>. Just before switching on the pressure was reduced to 20 torr and the controlled pressure was reached within a few minutes of switching on. In this particular run there was little nucleation delay and growth started soon after the filament reached the deposition temperature of 2200°C. This was one of the runs when the growth rate was abnormally slow and after 2½ hours and the end of the time available the bar had not reached the desired size. It was therefore decided to continue the run the following day and in order to prevent any possible sooting on cooling down, the propane was pumped out of the furnace before switching off the current and the furnace was left under vacuum overnight. Because of the increased thermal mass of the bar and the expected longer time to reach deposition temperature, the following day's run was started with a low propane pressure so that there would be no possibility of low temperature deposition occurring. In spite of all these precautions the continued run took place at the normal deposition rate and after a further 1½ hours the bar had reached its desired size. At the end of the run the bar required 1300 A at 7.1 V to maintain it at a surface temperature of 2200°C.

Examination showed that the bar had a reasonably fine

surface texture. The deposit was 2.4 mm thick and until a section was polished and examined under the microscope the fine line marking the interruption in deposition could not be seen. Measurements of the deposit showed that the growth rates had been  $1.3 \times 10^{-5} \text{ cm sec}^{-1}$  for the first part of the deposition and  $2.6 \times 10^{-5} \text{ cm sec}^{-1}$  for the second. A more detailed description of the appearance of the polished section is given in section 3.2.1.

A piece of the deposit 15 x 3 mm was cut from the centre of the bar and parallel to its length and was cleaved into 8 sections to allow examination of the properties as a function of distance through the deposit.

## 2.5 Estimation of the temperature profile across the deposit

To estimate the temperature difference across the deposit at the end of growth some geometrical approximation is required. A better estimate is obtained by treating the deposit and substrate filament as two rectangular slabs whose thickness is small compared with the area of the slabs than is obtained by assuming cylindrical geometry.

Consider the heat flow in a direction perpendicular to the surface across a thin slice of the deposit situated a distance  $x$  from the substrate. The heat,  $q$ , passing outwards through this thin slice consists of the heat,  $Q_f$ , generated in the substrate filament together with the heat developed in that

part of the deposit between the substrate and the slice, i.e.

$$q = Q_f + V^2 \frac{xh}{\rho l}$$

where  $V$  is the voltage along the bar at the end of growth,  
 $\rho$  is the resistivity of the deposit along the length of the bar,  
 $l$  is the length of the bar and  $h$  is the extent of the slab in the perpendicular direction and approximates to the periphery of the bar.

If  $dT$  is the temperature difference developed across the thickness,  $dx$ , of the slice as a result of the heat flow

$$dT = - \frac{1}{Kh\ell} q dx$$

where  $K$  is the thermal conductivity of the deposit in a direction perpendicular to the substrate

so

$$dT = - \frac{1}{Kh\ell} \left( Q_f + V^2 \frac{xh}{\rho l} \right) dx$$

To find the total temperature difference,  $\Delta T$ , across the deposit, integrate across the whole of the deposit :-

$$\Delta T = - \frac{1}{Kh\ell} \left[ Q_f x + \frac{V^2 h}{2\rho l} x^2 \right]_0^d \quad (1)$$

where  $d$  is the thickness of the deposit.

$$\begin{aligned} \Delta T &= \frac{1}{Kh\ell} \left( Q_f d + \frac{V^2 h}{2\rho l} d^2 \right) \\ &= \frac{d}{Kh\ell} \left( Q_f + Q/2 \right) \end{aligned}$$

where  $Q$  is the total heat developed in the deposit.

If it could be assumed that all the power developed in the bar passed to the surface and was lost by radiation then the above expression could be used directly to obtain the temperature difference. Much of the heat is lost to the water cooled electrodes because of the high a-direction thermal conductivity of the pyrolytic deposit. However the heat lost by radiation can be calculated assuming

$$Q_r = \xi \sigma T^4 \quad \text{per unit area}$$

and using an integrated emissivity of  $\xi = 0.65$  for the c-direction of the pyrolytic skin<sup>33</sup>. This yielded a value of 3980 watts for bar 22 compared with the 9230 watts of electrical power used at the end of the run. Since the resistance of the substrate filament is known from the power required at the beginning of the growth run, the proportion of the total power that is developed in the filament at the end of the run can be calculated, and was found to be 770 watts, only about 8 percent. This low proportion is to be expected because of the much higher a-direction electrical conductivity of the pyrolytic graphite deposit. Once this proportion is known the temperature difference across the deposit can be calculated assuming a c-direction thermal conductivity of  $0.02 \text{ watt cm}^{-1} \text{ deg C}^{-1}$ <sup>36</sup> and was found to be 870 deg C. With a surface temperature of  $2200^\circ\text{C}$  the inner layers of the pyrolytic deposit had risen to  $3070^\circ\text{C}$  and would be expected to have properties corresponding

to this effective annealing temperature.

To find the temperature profile across the deposit it is necessary to return to equation (1). The temperature,  $T$ , at the point  $x$  is given by

$$T = - \frac{1}{Kh\ell} \left( Q_f x + \frac{V^2 h}{2\rho\ell} x^2 \right) + \text{constant of integration}$$

which can be written in terms of  $Q$ , the power developed in the deposit as

$$T = - \frac{1}{Kh\ell} \left( Q_f x + \frac{Q}{2d} x^2 \right) + \text{constant}$$

The temperature profile thus has a small linear component proportional to the power developed in the substrate and a square term proportional to the power developed in the pyrolytic skin. Since the relative proportions of power in the substrate and skin are known the profile can be worked out and temperatures assigned to each of the 8 samples cleaved from the deposit.

## 2.6 Comparison of the estimated temperatures with annealing studies

The property of pyrolytic graphite which is measured most commonly and reliably is the a-direction resistivity because of the comparative simplicity of the measurement, and it is often used as a method of assessing the improvement in quality of the material. In the course of his work on the thermomagnetic properties of pyrolytic graphite Mills<sup>24</sup> measured the resistivity

of all the samples from bar 22 as a function of temperature. He also measured the magnetoresistance and from this deduced the average carrier mobility. Both these measurements have also been made by Klein<sup>37</sup> on a series of graphites annealed separately after deposition. Figure 2.4 shows Klein's results for the room temperature resistivity and figure 2.5 the mobility, plotted against the annealing temperature, and also shows the results of the same measurements on the sections of bar 22 plotted against the estimated temperature at the end of the growth run. The extremely good agreement between the two sets of curves justifies the temperature profile estimation made in the previous section and allows other properties to be measured as a function of the effective formation temperature with a reasonable degree of confidence. Meers<sup>38</sup> has also made similar annealing studies and his results for the resistivity show the same general temperature dependence.

Once the temperature profile through a deposit grown by resistance heating can be estimated with reasonable success, the apparent disadvantage can be turned to good use since it allows samples to be obtained which have been annealed at temperatures over 3000°C without having to use a separate furnace to reach such high temperatures. Fortunately many of the a-direction properties can be measured on thin sections so this type of deposit can be used. However should these measurements indicate that a useful device could be developed

FIGURE 2.4

Comparison of the room temperature resistivity of sections from bar 22 with annealing studies

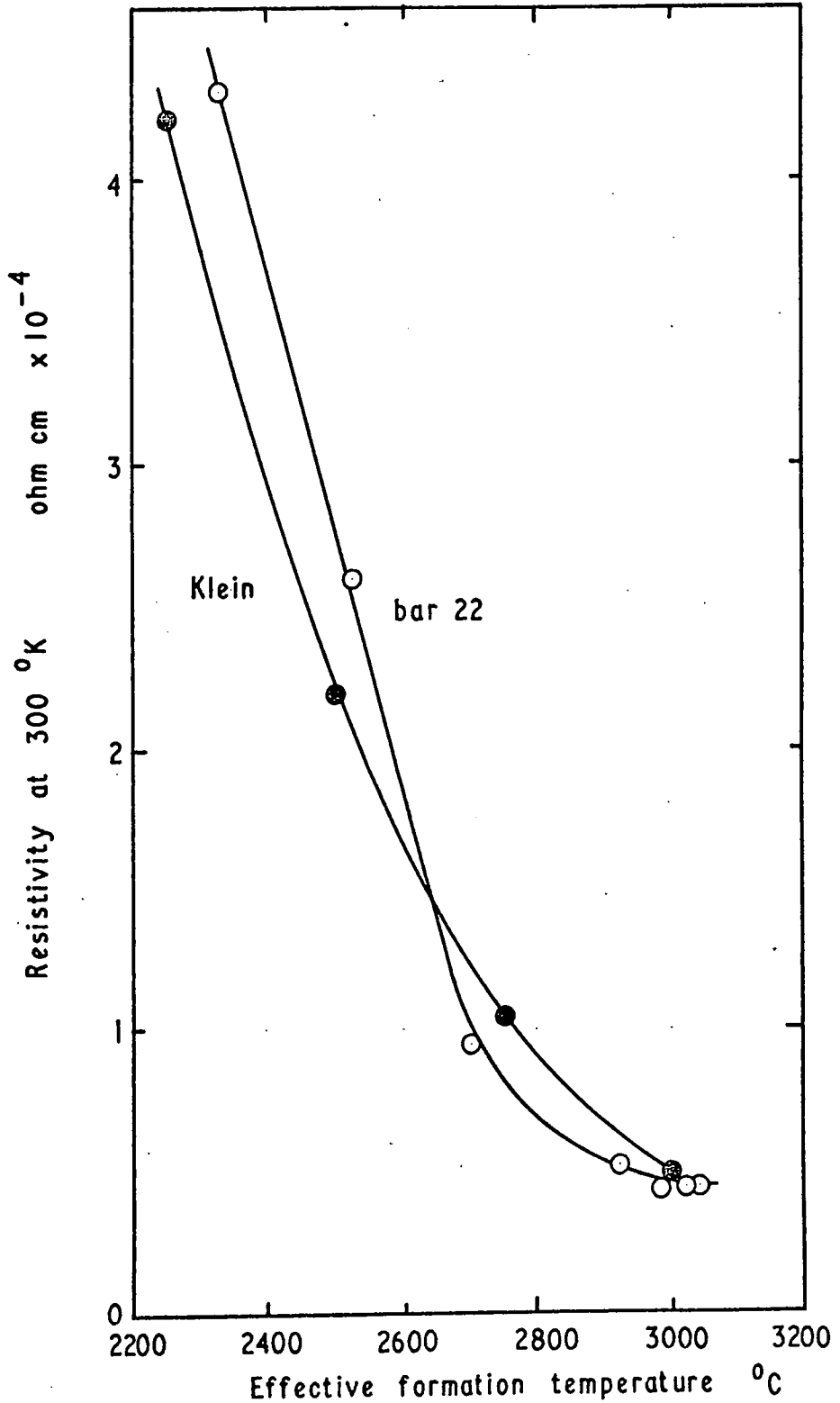
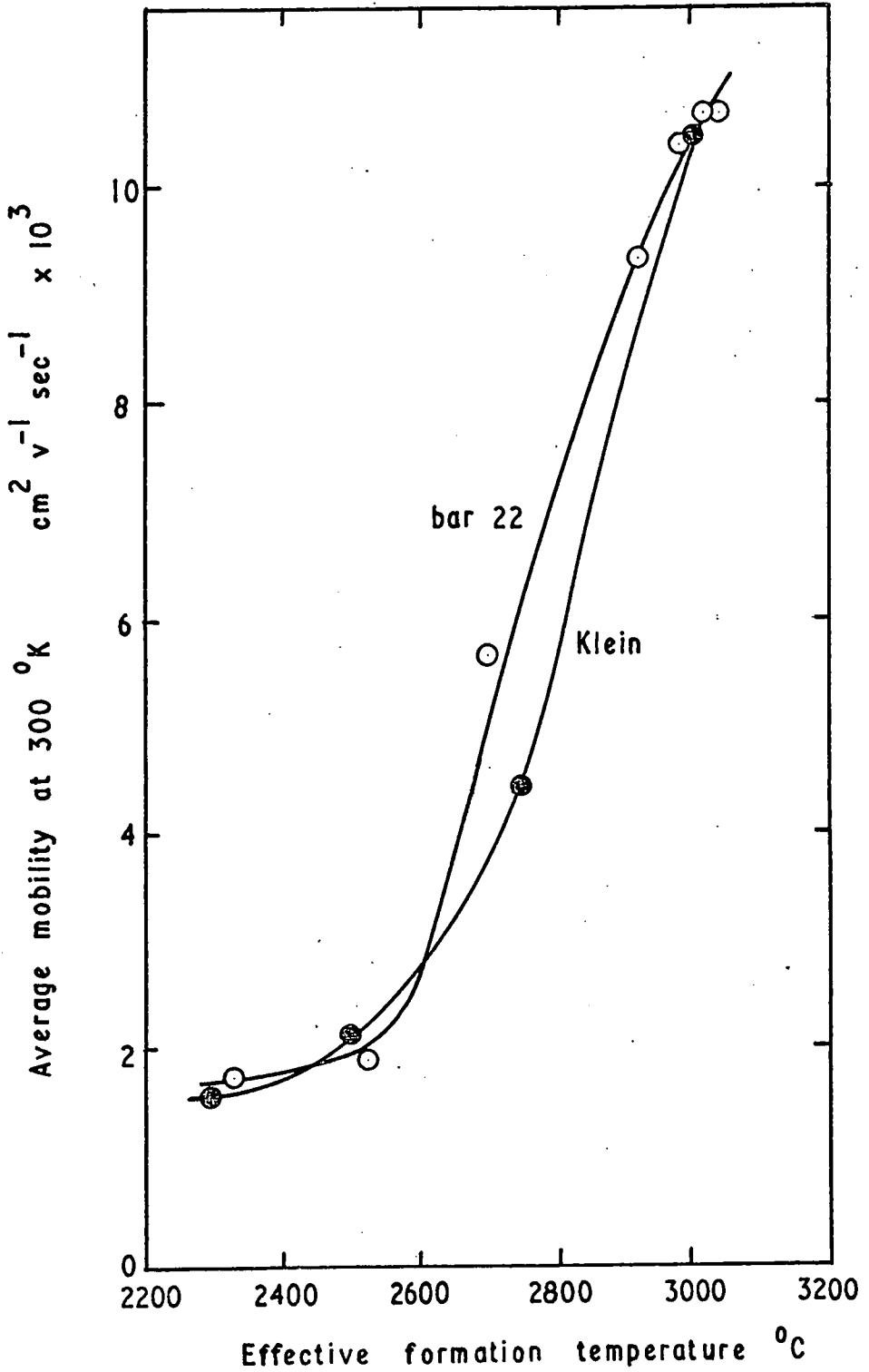


FIGURE 2.5

Comparison of the room temperature average mobility of sections from bar 22 with annealing studies



it is highly unlikely that thin samples could be used for this. It would then be necessary to anneal massive deposits evenly in a separately heated furnace at a temperature in excess of any reached during deposition in order to achieve uniformity through the material. Since there is evidence that applied stress during annealing can improve some properties, particularly the preferred orientation, the hot pressing method described by Moore, Ubbelohde and Young<sup>39</sup> would seem to be the most suitable method of annealing. In their furnace, samples can be heated up to 3200°C while under a load of 1500 Kgm.

Temperature gradients through the deposit would only be expected in the resistance heated method of deposition. It would not be expected if the substrate were maintained at temperature by heating in a tube furnace and Harvey, Clark and Eastabrook<sup>35</sup> who first suggested the reason for the difference in properties through the deposit, prepared one sample in a tube furnace and found, as expected, that the deposit had uniform properties. It is also to be expected that uniform material would also be obtained from inductively heated deposits but so far there has been no direct evidence of this. However workers from the Raytheon Company in the United States (for example Guentert<sup>40</sup>) often report in their papers that resistance grown material has better properties for the same nominal deposition temperature than inductively grown material. This presumably is because the resistance heated samples were cut

from a part of the deposit effectively formed at a higher temperature. If good comparison is to be made between different workers' results it is important to realise that in the resistance heating method the surface temperature is not a reliable means of specifying growth conditions.

## CHAPTER 3

### PREFERRED ORIENTATION

#### 3.1 Introduction

Pyrolytic graphite, as explained earlier, is a polycrystalline material in which the crystallites are aligned with their basal planes parallel to the deposition plane. No directional relation other than this exists between neighbouring crystallites which are otherwise randomly oriented relative to each other. It might reasonably be expected then, that if the crystallite basal planes are accurately parallel the a-direction properties of the bulk material might approach that of single crystal material whereas the c-direction properties would be far removed from it. In the detailed study of bar 22 in which the a-direction properties were measured as a function of distance from the substrate, and thus as a function of formation temperature, it was thought that the preferred orientation, i.e. the accuracy of alignment of the crystallites, would probably affect the a-direction properties obtained for the bulk material, so the preferred orientation was one of the first parameters measured.

#### 3.2 Qualitative description of the preferred orientation

##### 3.2.1 Optical examination

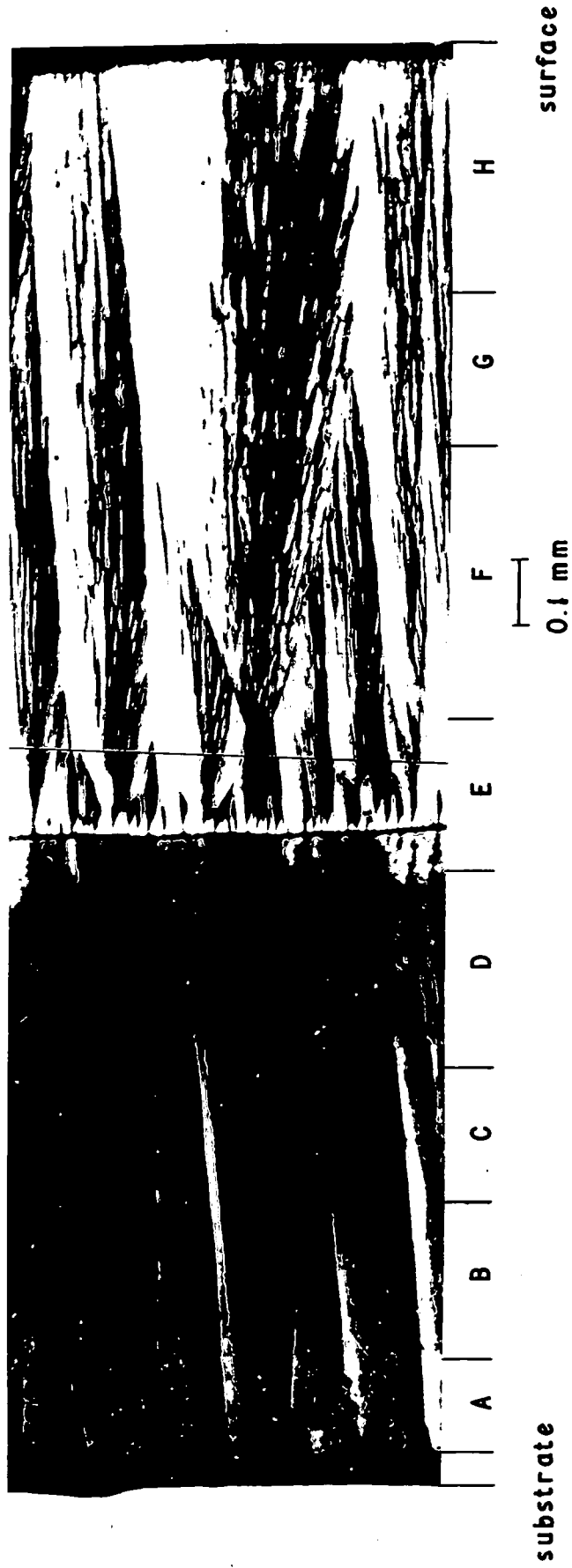
A section through the bar was polished with successively

finer grades of Carborundum, followed by 2 and 1  $\mu\text{m}$  alumina and finished with Hyprez  $\frac{1}{4}$   $\mu\text{m}$  diamond paste used with Hyprez polishing medium on a special pad. The polishing was done by hand but to keep the surface as flat as possible the bar was held in a large diameter jig. The polished surface was then examined under a metallurgical microscope. The surface appeared even with no voids or flaws in the part of the deposit near the centre of the filament, apart from the join between the sections deposited at the different growth rates (see section 2.4). Towards the corners of the filament the deposit had cleaved irregularly. With polarised light the growth cone microstructure can be seen and a photograph of a section through the bar with crossed Polaroids is shown in figure 3.1. The figure also shows how the bar was cleaved into sections for examination of the properties as a function of distance from the substrate.

Clearly the different growth rates have resulted in a very different microstructure. The fast growth rate of the outside layers has given well defined cones which are strongly divergent and the inside layers grown at a much slower rate have much less structure and what cones there are diverge only slowly. It would be reasonable to suppose that the coarser cone structure of the outside layers would give much poorer preferred orientation than the more even structure of the inside layers and this was borne out by subsequent measurement. It is

FIGURE 3.1

Polished section through bar 22 showing the cleaved samples



the coarse cone microstructure that gives the surface of bars of pyrolytic graphite their characteristic bubbly appearance.

### 3.2.2 X-ray examination

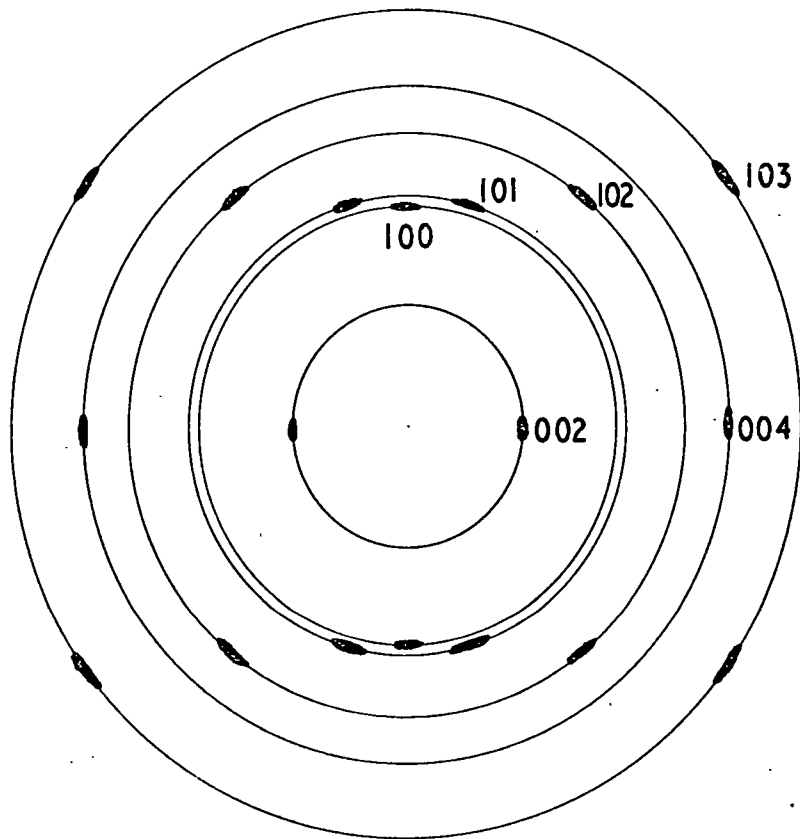
Small rods were cleaved from each section and x-ray transmission photographs were taken on a Philips Universal Flat Plate camera using nickel filtered copper radiation with the x-ray beam both perpendicular and parallel to the plane of deposition. Had the specimen consisted of a randomly arranged aggregate of crystallites, photographs from both directions would merely give a series of powder rings. The preferred orientation produces directional differences. With the x-ray beam perpendicular to the plane of deposition the (002) reflection was absent from all photographs. This in itself indicates some degree of orientation. Since the (002) reflection occurs at a Bragg angle of  $26^\circ$  ( $2\theta$ ) the conclusion is that none of the crystallites are misoriented as much as  $77^\circ$  away from the plane of deposition. Because of the random rotation of the crystallites the (100) and (101) reflections appear as complete powder rings in this direction and there are progressive changes through the bar. The surface layers gave the asymmetrical (10) powder ring typical of a 2-dimensional turbostratic structure. With increasing distance from the surface the profile of the (100) ring became symmetrical, then the (101) ring began to show with the increasing graphitisation

of the layers formed at higher temperatures. Moving inwards still further the rings become much sharper and the (101) ring increases in intensity until it is much more intense than the (100) ring. These changes are the same as would be obtained in the (100) and (101) reflections from powder photographs taken from samples of increasing graphitisation. (For a fuller description of the crystallography of graphitisation see chapter 5)

With the x-ray beam parallel to the plane of deposition more information is obtained about the preferred orientation. With no preferred orientation complete powder rings would be obtained. In the extreme case of perfect orientation with all the crystallites perfectly parallel to the plane of deposition the pattern of spots obtained would not be that of single crystal material, but because of the random rotation of the crystallites would be similar to a rotation photograph of a single crystal with the spots occurring in a series of layer lines. The diagram in figure 3.2 shows the pattern that would be obtained superimposed upon the powder rings. For intermediate degrees of orientation the powder rings split up into arcs centred upon the layer line spot positions and with increasing orientation the length of the arcs decreases. In the series of photographs through the bar the outer layers gave very long diffuse arcs. With increasing depth from the surface the arcs became shorter and less diffuse, the two neighbouring (101) arcs could be

FIGURE 3.2

X-ray transmission pattern of graphite with  
the x-ray beam parallel to the layer planes



distinguished and seen separately from the (100) arc. The (002) arcs in particular become sharper and more intense as they contract. The inner layers, sections B, C and D from the part of the bar deposited at the slower growth rate and having less structure, all gave photographs in which the arcs had contracted into blurred spots and little difference could be seen between them.

Although these transmission photographs serve to provide a qualitative description of increasing orientation, they do not provide a quantitative measure since it is not possible to measure the lengths of the arcs on the films. Alternative methods are required to obtain the preferred orientation quantitatively and these are discussed in the next section.

### 3.3 Measurement of the preferred orientation

Preferred orientation in pyrolytic graphite is usually defined<sup>40</sup> in terms of an orientation function  $n(\delta)$  which is the density of basal plane normals per unit solid angle relative to the symmetry axis of the distribution, i.e. relative to the basal plane normal. This density function can be obtained by measuring the integrated intensity of the (002) reflection as a function of the angle  $\delta$ . In practice if the distribution obtained is normalised to a maximum intensity of unity little error is introduced by measuring peak rather than integrated intensities. The measurement can be made

directly by using a rod sample on a counter diffractometer fitted with a texture attachment. This attachment disconnects the normal 2:1 drive for the specimen and allows the specimen to be set accurately to any given angle relative to the x-ray beam. It is an expensive accessory and not generally available with most diffractometers.

The most straightforward alternative is a film method using a cylindrical cassette that fits into a standard powder camera. The method was first described by Richards<sup>41</sup> and a drawing of the cassette used in this work is shown in figure 3.3. The cassette is designed to fit on to the beam trap of a Philips 11.46 cm diameter powder camera and has a hole in the side to allow the specimen to be mounted on the rotating table. The specimen can be aligned optically in the usual way after loading the cassette since the cassette is designed to be light tight. An indexed film taken with this cassette using a fairly well oriented graphite specimen is shown in figure 3.4 and it can be seen that all reflections now appear as straight lines. In the particular case of the (002) reflection the geometry is such that the arcs which were obtained from the x-ray transmission photographs with the x-ray beam parallel to the basal plane now appear as straight lines and so can be measured using a microdensitometer. The geometry is also the same as that used in the diffractometer method so that results can be compared, and as in that method provided the resultant profile is normalised

FIGURE 3.3

Cassette to fit a Philips 11.46 cm  
diameter x-ray powder camera

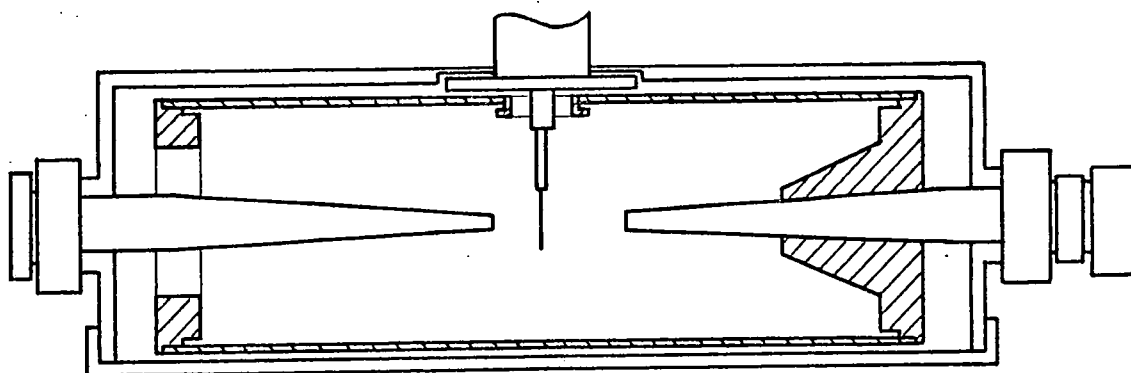
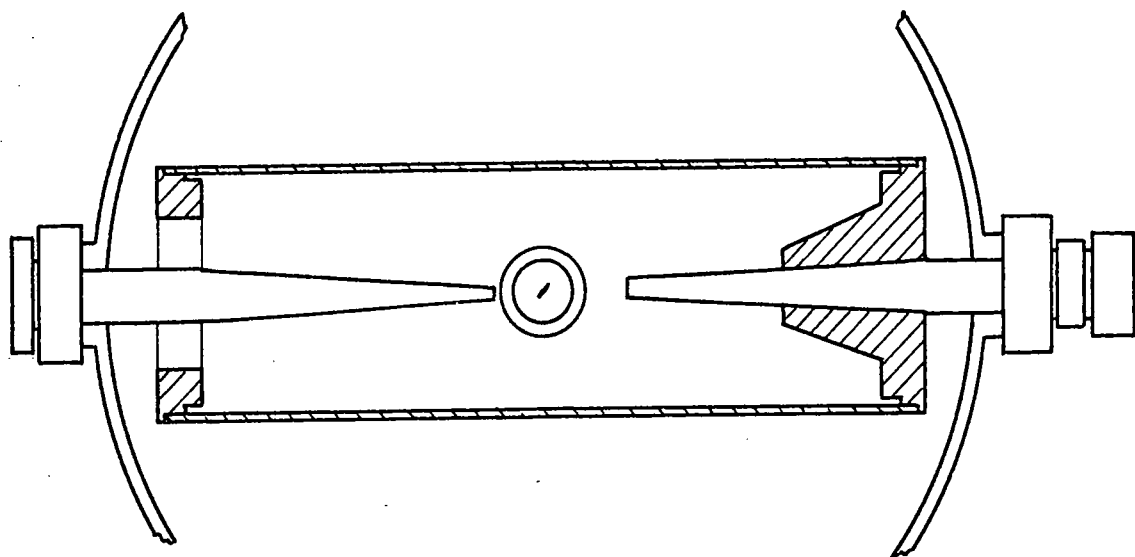
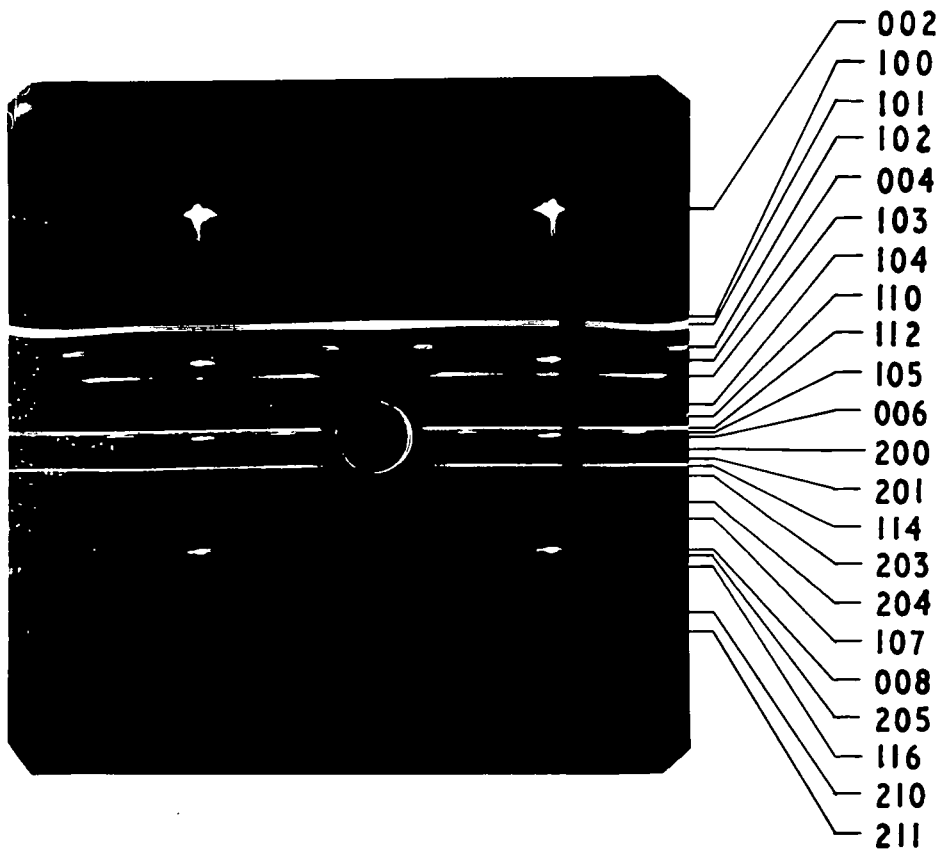


FIGURE 3.4

A graphite orientation photograph



a straight scan of the microdensitometer along the length of the line can be used.

The film shown in figure 3.4 was exposed for  $3\frac{1}{2}$  hours using nickel filtered copper radiation and this long exposure was necessary to bring up all the lines for indexing. However the (002) lines are grossly overexposed. When a film with a suitable density for measurement of the (002) lines on the microdensitometer is made it is found that the exposure needed is only between 1 and 10 minutes for rod samples with section approximately  $0.5 \times 0.1$  mm. The poorly oriented specimens require the longer exposure since the intensity is spread out over a longer length. The instrumental broadening of the experimental arrangement was found by obtaining an exposure using a piece of single crystal magnesium oxide of similar size and shape to the graphite specimens and measuring up a suitable low angle spot.

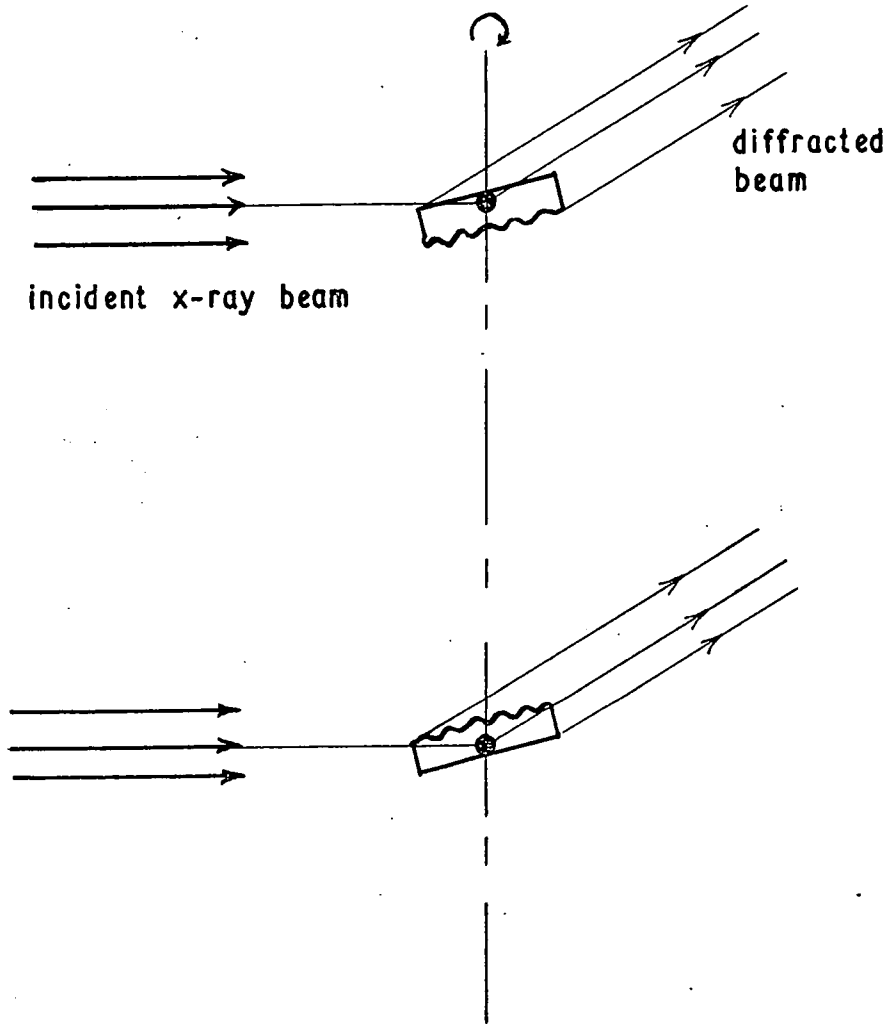
Two minor experimental difficulties were encountered and resolved. The first concerned film handling. The range of film densities that can be satisfactorily accepted by the microdensitometer is fairly limited so that it is necessary to expose the film to be in this range. (A full description of the use of the microdensitometer is included in chapter 5.) It is particularly important to keep the film background as low as possible. The film available, Ilford blue sensitive film for spectroscopy, is relatively fast and coarse grained so the

background level cannot be very low. However in practice it was found to be unacceptably high. The cause was traced to fogging from the dark green safe light used in the dark room. Normally this fogging is of little importance. An acceptable background level was obtained when the films were handled in complete darkness.

The second difficulty showed up when the first films were measured and the profiles were found to be double peaked. This is rather unlikely though Parry<sup>42</sup> has reported an exceptional case of a double peaked profile. The cause was eventually traced to errors in specimen alignment and the diagram in figure 3.5 shows how this comes about. For every complete rotation of the specimen there are two positions in which an (002) reflection can be obtained. It is easy to see that if the centre of rotation does not coincide with the centre of the specimen a double peaked profile is obtained. That the double peaks were due to the experimental conditions rather than the material was confirmed when the known single crystal specimen of magnesium oxide, which was used to obtain the instrumental broadening, also gave double peaks. The synchronous motor used for specimen rotation in the Philips powder cameras is a slow speed one driving the specimen at one revolution per minute. Since the exposures required were all ten minutes or less it was a simple matter to close the x-ray shutter for half a minute in each revolution thus completely eliminating the second peak.

FIGURE 3.5

Error in specimen alignment leading to a double peaked profile of the diffracted beam



The complete experimental procedure was thus as follows. A suitable graphite specimen was prepared by cleaving and cutting with a razor blade, and was then mounted in the camera. The film was loaded into the cassette which was placed in the camera and the specimen was then aligned optically as well as possible. The exposure was made as described above and the film developed. The (002) line on the film was measured on the microdensitometer using the motor drive to scan the film and taking readings at timed intervals since the instrument did not have a distance scale. The motor speed was obtained separately, and the film calibrated by measuring the distance between the peaks of the two (002) lines. To allow for the relation between film transmission and x-ray intensity the readings were plotted on logarithmic graph paper and the best smooth curve drawn through them to eliminate fluctuations due to film grain. These curves were then used as a measure of the preferred orientation.

### 3.4 Experimental results

Orientation films were taken with specimens from sections B, C, D, F, G and H of the bar. Section E was excluded since it contained the join and no other measurements could be made on it. In addition a flake from the surface and a specimen from section A were included as representing the extremes of the bar. The films were measured up and the profiles obtained

were normalised to a peak intensity of unity. Sections F, G, H and the surface layer produced profiles so broad that it was not necessary to correct for instrumental broadening. Profiles for sections B, C and D were corrected for instrumental broadening using the profile obtained for the single crystal MgO specimen. This correction was made by subtracting the squares of the widths of the two profiles. The resultant profiles for all the sections are shown in figure 3.6 and profiles for sections B, C and D are also shown on an enlarged scale in figure 3.7. It can immediately be seen that apart from section A the profiles divide into two groups. Sections F, G and H have much broader profiles consistent with the coarse cone structure of figure 3.1 and sections B, C and D lie close to each other and are very much narrower.

Three different ways of designating the widths of the profiles are in use. The most usual is the width of the profile at half peak intensity, the half width. An alternative suggested by Stover<sup>43</sup> is to fit the curves to the function  $\cos^m \delta$  when the exponent  $m$  is used as a measure of the profile width. The third and less commonly used method is to fit the profiles to a Gaussian curve and use the variance as a measure of width. Guentert and Klein<sup>44</sup> suggest that the  $\cos^m \delta$  function is the most meaningful since they propose that the anisotropy ratios in the electrical conductivity of pyrolytic graphite i.e. the ratio of the a- and c-direction measured conductivities,

FIGURE 3.6

Relative crystallite misorientation  
of sections from bar 22

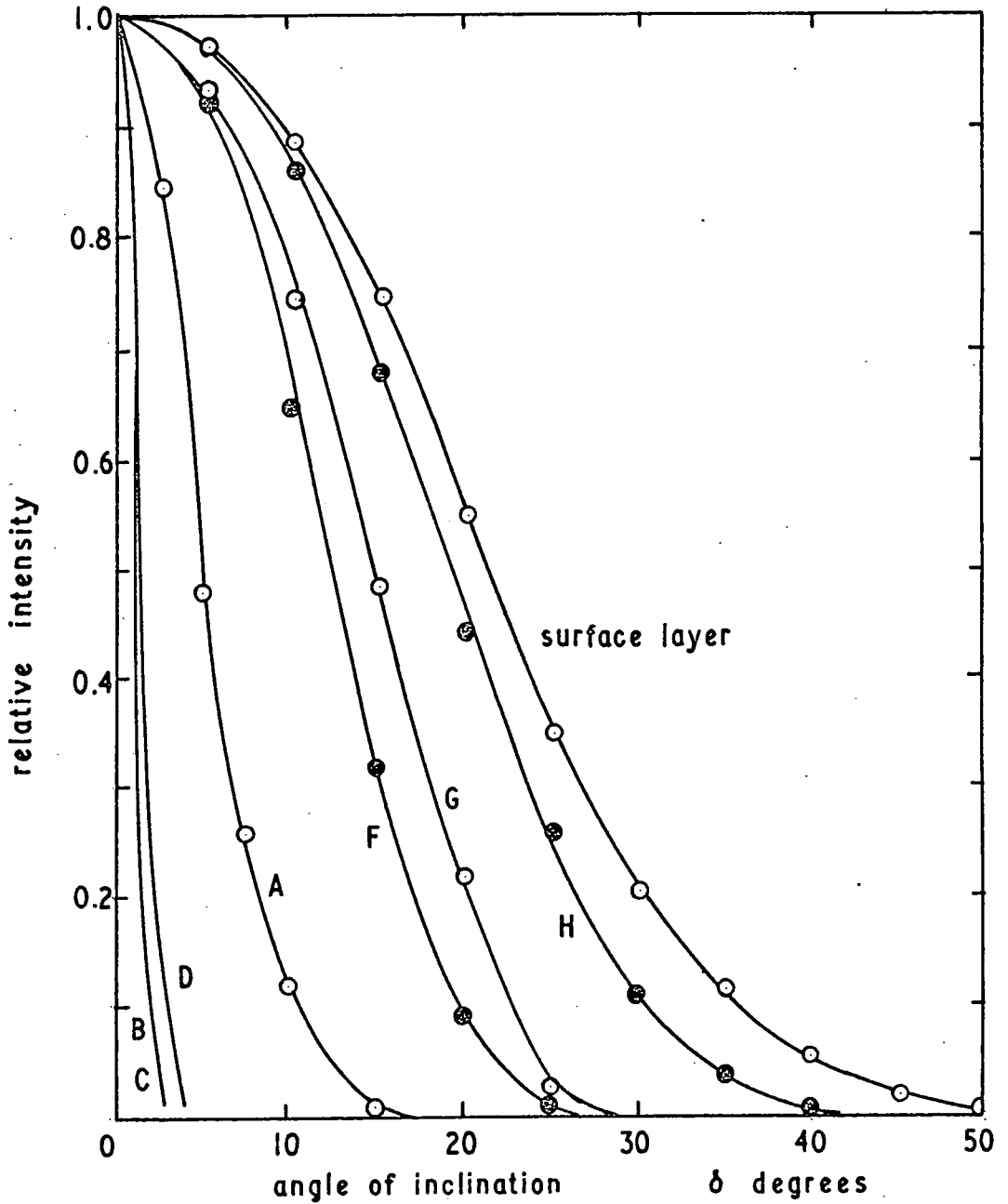
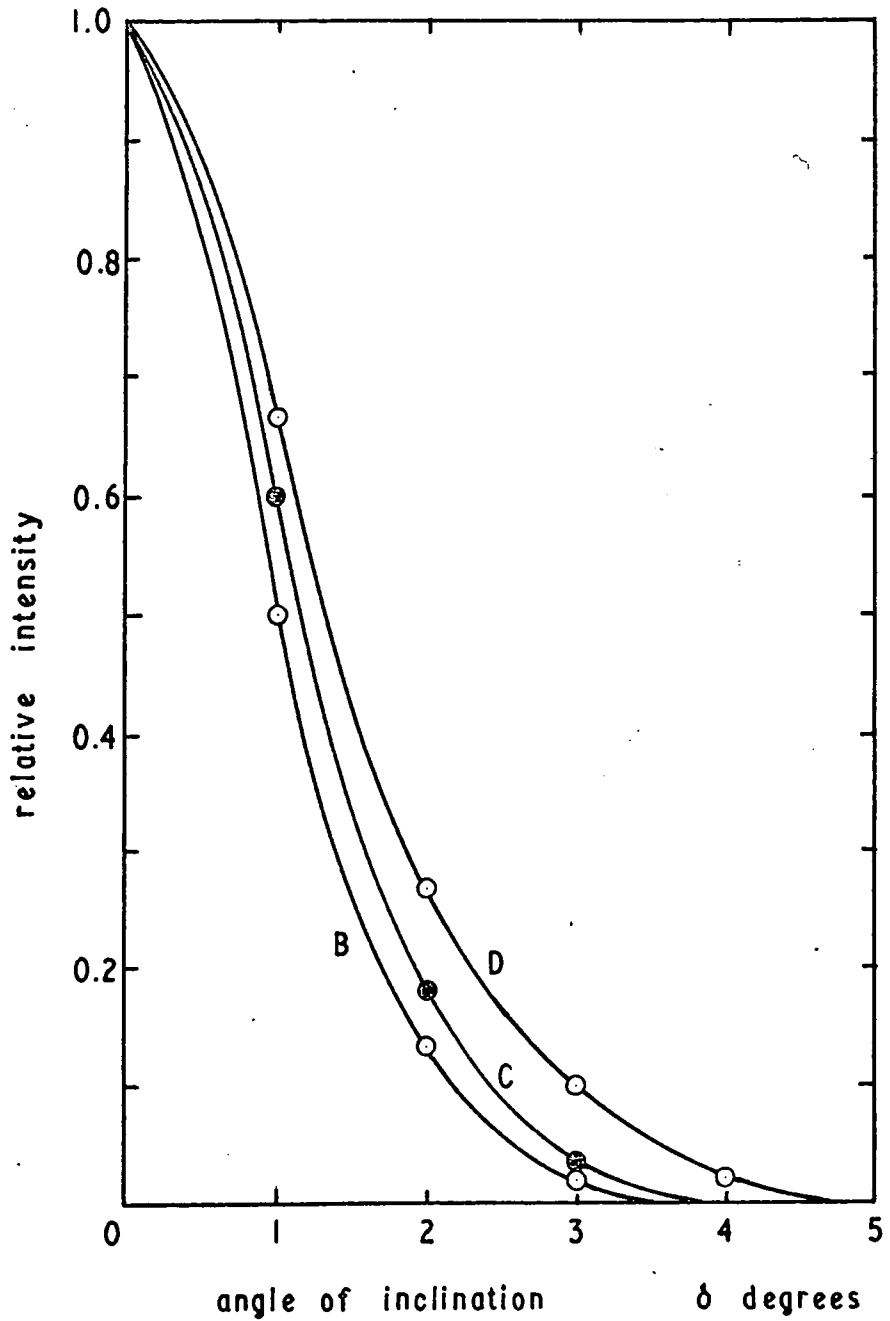


FIGURE 3.7

Relative crystallite misorientation  
of sections B C and D from bar 22



can be related to the intrinsic anisotropy ratio of a single crystal through the expression

$$\sigma_{\parallel}/\sigma_{\perp} = \frac{(m+2)\sigma_a/\sigma_c + 1}{2\sigma_a/\sigma_c + (m+1)}$$

where  $\sigma_{\parallel}/\sigma_{\perp}$  is the measured anisotropy ratio of the electrical conductivity of the pyrolytic graphite, and  $\sigma_a/\sigma_c$  is the intrinsic ratio of single crystal material. Not unnaturally they conclude that reliable c-direction measurements can only be made on extremely well oriented material.

The curves obtained were fitted to  $\cos^m \delta$  functions. The fit was made by plotting the log of the intensity against  $\log \cos \delta$  and measuring the slope of the best straight line fit. The curves gave a reasonable fit to the function though on some there was a systematic deviation from the line towards the tail of the profile. The results of the fitting process are shown in the table

Section	Formation temperature °C	Half width angular degrees	m
A	3040	9.5	140
B	3020	2.0	3000
C	2980	2.2	2600
D	2910	2.4	2200
F	2700	25.3	37
G	2550	29.4	25
H	2330	38.2	18
Surface	2200	42.3	11

An attempt was also made to fit the profiles to Gaussian curves but in this case there was so much systematic deviation from a straight line that such a fit was clearly meaningless. Bragg and Packer<sup>45</sup> however obtained an extremely good fit to Gaussian curves in their measurements on pyrolytic graphite. Fischbach<sup>46</sup> showed that the three different parameters used for specifying the profile width could be related and suggested that

$$\beta \approx 1.18\sigma \approx 1.18 m^{-\frac{1}{2}}$$

where  $\beta$  is the half width,  $\sigma$  is the variance of the profile and  $m$  is the exponent of the  $\cos^m \delta$  fit.

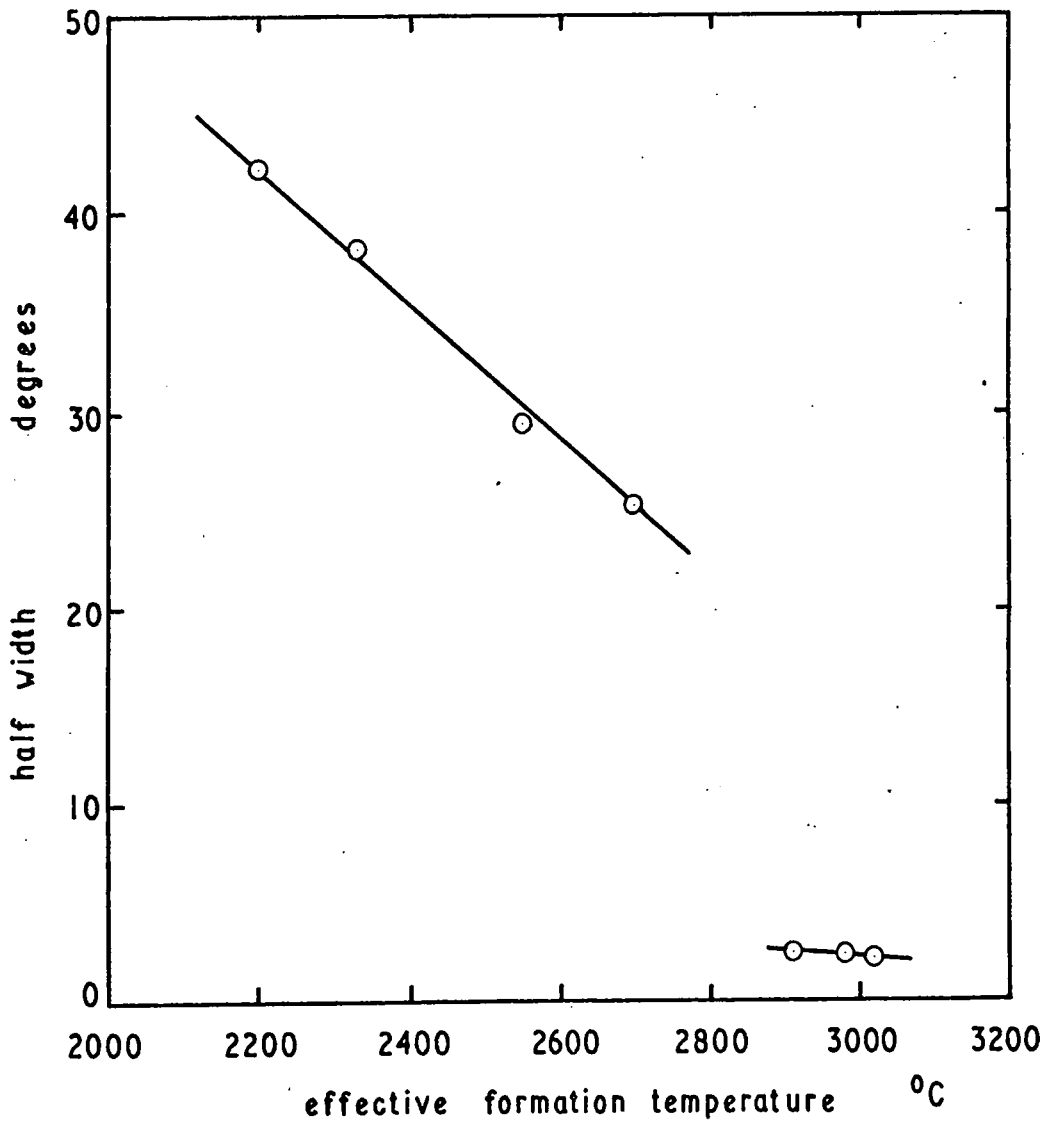
### 3.5 Discussion

Apart from section A, there is a systematic improvement in the preferred orientation with increasing formation temperature. No other measurements were made on section A since it was clearly damaged in breaking away from the substrate and it is this damage that probably accounts for the poor orientation.

In figure 3.8 the half widths for all the sections except A are plotted against the estimated formation temperature and the graph shows the difference in texture produced in the two parts of the bar. The even texture of the inner layers gives much improved alignment of the crystallites. Both sets of results appear to be linearly related to the formation temperature but with different slopes. Such a relation has not been reported in any previous work on pyrolytic graphite. The

FIGURE 3.8

Crystallite misorientation of sections from bar 22 as a function of formation temperature



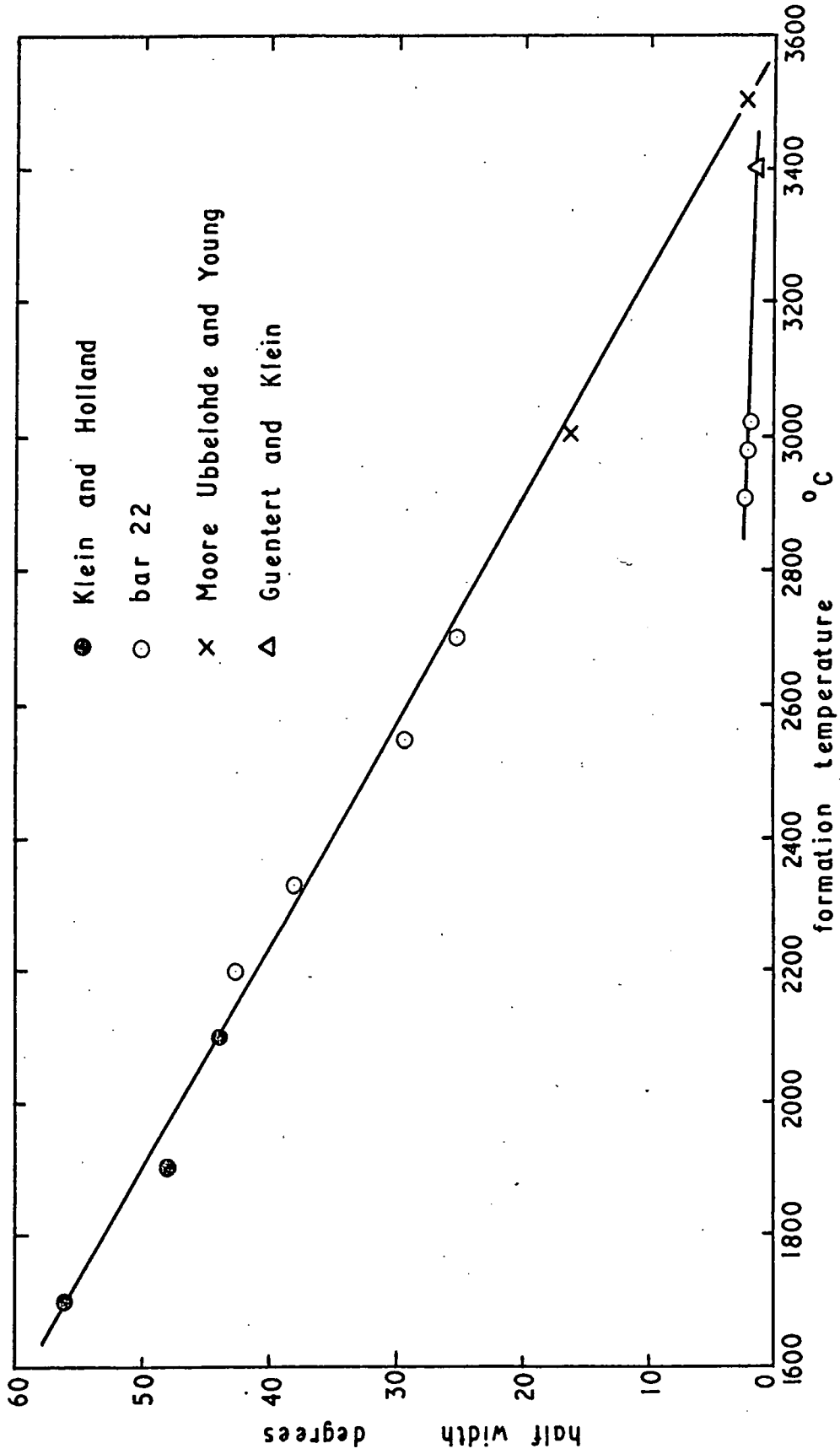
material with the coarser structure shows a greater relative improvement in alignment with increasing temperature.

In figure 3.9 the results are plotted again together with other workers' results over a much wider temperature range. At the low temperature end the graphites reported by Klein and Holland<sup>47</sup> were prepared in a resistance heated furnace and so should be free from temperature gradients. The deposition temperature is thus a true indication of formation temperature. At the high temperature end the results reported by Moore, Ubbelohde and Young<sup>39</sup> are on graphites prepared in a similar manner to bar 22, but subsequently annealed in a separate furnace at the temperatures shown. These temperatures are in excess of any produced as a result of gradients in the relatively thin initial deposits and so represent a true formation temperature for the material. All these results and the results from the coarse textured part of bar 22 lie on the same straight line which is remarkable considering the variations that there must have been in the methods of preparation. It indicates that the highest temperature reached during deposition or subsequent unconstrained heat treatment has more effect on crystallite alignment than any other process variable.

The angular misalignment of the even textured inner layers of bar 22 is much lower than the general line. Pyrolytic graphite with angular misalignment as low as  $0.6^\circ$  has been prepared by hot pressing a conventionally deposited material at

FIGURE 3.9

Crystallite misorientation as a function of formation temperature



temperatures around  $2900^{\circ}\text{C}$  and with a load of  $500 \text{ Kgm cm}^{-2}$  <sup>39</sup>. The hot pressed material may subsequently be annealed at higher temperatures. The degree of crystallite alignment of the inner layers of bar 22 is more of the order of the hot pressed material than the unconstrained material. Unfortunately it is not possible to get a more direct comparison since the temperatures used in the preparation of the hot pressed material are not sufficiently specified. Guentert and Klein<sup>44</sup> report results on 'highly stress annealed' material and this is shown plotted in figure 3.9. Their result is reasonably consistent with the inner layers of bar 22.

It would appear that provided growth conditions can be sufficiently controlled to grow even textured deposits at a slow growth rate, good crystallite alignment can be obtained without recourse to any of the stress methods of annealing, though it is possible that the interruption of the growth of the bar with the consequent cooling and reheating introduced some form of stress annealing which would account for the improved alignment.

## CHAPTER 4

### MEASUREMENT OF THE THERMAL CONDUCTIVITY

#### 4.1 Introduction

In view of the importance of the lattice thermal conductivity in the figure of merit for Etingshausen cooling, measurements of the a-direction thermal conductivity of the samples were required as a function of temperature, working below room temperature, in order to obtain information that would allow a reasonable extrapolation down to near the liquid helium range where an Etingshausen device might be expected to give useful cooling.

It was decided to make a direct measurement of the thermal conductivity, i.e. to measure the temperature gradient set up by a known quantity of heat passing along the bar, rather than use any of the many comparison methods since apart from the difficulty of obtaining a standard with known and similar conductivity over the temperature range, there would be geometrical difficulties because of the thin flat shape of the graphite samples. Thermal diffusivity methods were also rejected because in order to convert the measurement to thermal conductivity values for both the density of the sample and its specific heat as a function of temperature must be known. Pyrolytic graphite is a good conductor of heat in the a-direction so the apparatus must be designed for this and since it was thought that there might be

some advantage at a later stage in making measurements in a magnetic field to eliminate the electronic component of the thermal conductivity, the cryostat was designed to enable it to fit between the pole pieces of a magnet. In the event because the measured thermal conductivity was so high the electronic component was always negligible in the temperature range considered and measurements in a magnetic field were unnecessary.

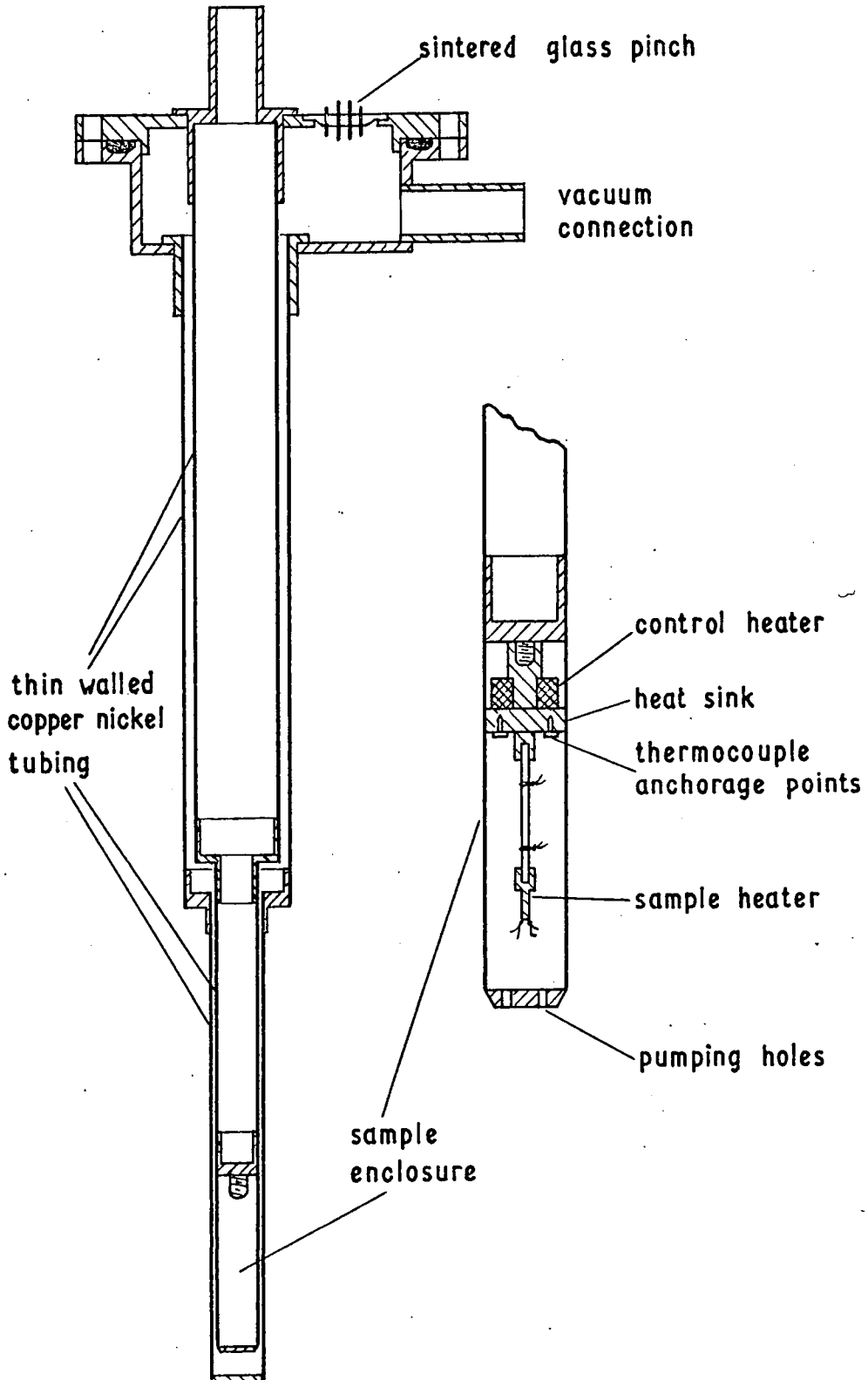
## 4.2 Description of the apparatus

### 4.2.1 The cryostat

The cryostat was designed to make measurements in the range from room temperature down to the lowest temperatures possible using liquid nitrogen, and was also designed to fit between the pole pieces of the magnet already being used for thermomagnetic measurements. The second requirement dictated the overall shape of the cryostat since the pole piece gap is only  $1\frac{1}{2}$  in. and the apparatus would have to be fitted into a tail Dewar. It followed therefore that the only possible shape for the cryostat was also tail shaped. Using the direct method of measurement it is important that all forms of heat loss from the sample and its heater be minimised; the sample must be in an evacuated enclosure and it is desirable that temperature differences in the enclosure are kept small so that radiation losses are negligible. A sketch of the cryostat is shown in figure 4.1 and it consists basically of one tail shaped vessel within the

FIGURE 4.1

Sketch of cryostat for thermal conductivity measurements



other with the sample enclosure suspended from the bottom of the inner vessel. The annular space between the two vessels, including the sample enclosure, can be evacuated through a  $\frac{1}{2}$  in. diameter vacuum connection in the cryostat head. The O-ring flange at the top gives a vacuum tight connection between the two vessels and allows the whole inner one to be lifted out to give access to the sample. All electrical connections are brought out by means of a 12 lead sintered glass pinch which is soldered into the top plate. The leads in this pinch are small tubes which allow wires to be brought through without interruption and they are then soldered into place to give a vacuum tight seal. A suitable refrigerant can be placed inside the inner vessel to cool the sample and the outer vessel was also immersed in the same refrigerant. To keep the O-ring flange and the glass pinch at room temperature the tail sections of the vessels were made from specially drawn thin walled copper-nickel tube chosen for its poor thermal conductivity. The wall thickness was made as thin as possible for the one atmosphere pressure difference both to minimise conduction losses and also to save space. 0.010 in. wall thickness was used in the  $1\frac{1}{4}$  in. diameter top section and 0.006 in. wall thickness in the  $\frac{5}{8}$  in. diameter bottom section. To give sufficient rigidity and also directional accuracy the ends of the copper-nickel tubes were soldered into the cryostat using long bushes and different melting point solders. To further ensure the correct location

of the inner vessel it passed through a 3-pronged locating bush at the junction between the two diameters in the tail, and a silver steel peg fitting into a reamed hole was provided in the O-ring flange to prevent rotation. The bottom of the inner vessel was closed with a relatively massive copper plug provided with a threaded boss that allowed different sample holders to be screwed into place. The copper block which acted both as sample holder and heat sink for the conductivity measurements was provided with a narrow shank between the sample and the threaded connection to the boss. A 15 ohm heater was wound on this shank and cast in Araldite to make good thermal contact and this heater enabled the sample to be maintained at any desired temperature above the refrigerant temperature. A can in good contact with that part of the block below the heater completed the sample enclosure and acted as a radiation shield. Holes were drilled in the bottom of the can to ensure a good vacuum inside.

To cover the complete temperature range without using large powers in the control heater a number of different refrigerants were used. Crushed ice in water covered the range from room temperature down to  $273^{\circ}\text{K}$ , crushed solid carbon dioxide in methanol the range from  $273^{\circ}\text{K}$  down to  $200^{\circ}\text{K}$  and liquid nitrogen from  $200^{\circ}\text{K}$  to  $77^{\circ}\text{K}$ . Further reduction in temperature to about  $65^{\circ}\text{K}$  was obtained by pumping on the nitrogen through a vacuum connection provided in the top plate.

#### 4.2.2 The vacuum system

The cryostat was evacuated using a 2 in. glass mercury diffusion pump supplied by the General Electric Co. Ltd., and backed by a model 1SC30 Edwards High Vacuum Ltd. rotary pump. A liquid nitrogen trap was provided and pressure measured using a calibrated McLeod gauge. Once all the soldered joints in the cryostat had been made leak free this system easily maintained a vacuum of  $10^{-6}$  torr. A large vacuum reservoir was provided in the backing line so that the diffusion pump could be operated for relatively long periods without using the rotary pump which could then be used for pumping on the liquid nitrogen when the lowest temperature measurements were being made.

#### 4.2.3 Temperature measurement

The temperature gradient along the sample was measured using copper-constantan thermocouples. These were made from 40 gauge enamelled wire to minimise heat losses. To make any heat losses quite definite the thermocouples were thermally anchored to the heat sink before passing up to the cryostat head. The length of wire between the contact on the sample and the anchorage point was also made as long as possible to keep down heat losses. Because of the high thermal conductivity of the samples and also to further minimise heat losses, temperature differences along the sample were limited to around 1 deg K. At  $77^{\circ}\text{K}$  this means a difference in output from the thermocouples

of only  $16 \mu\text{V}$  and it is thus vitally important that no stray voltages appear. As it is easy to generate voltages of the order of a few microvolts, extreme care was necessary in the preparation and handling of the thermocouples since strain alone can give strays when the temperature along the wire is changed. After experimenting with spark welded junctions it was found that more reliable junctions were obtained by twisting the wires together and soldering. Between the heat sink and the glass pinch in the top plate the wires were insulated both thermally and electrically with Refrasil sleeving. The wires passed through the pinch, held in place by soldering, and were continuous to either the cold junction or the terminal block. The cold junctions were immersed in a Dewar containing water at room temperature. The temperature in the Dewar held constant over periods of the order of a day and it was found more satisfactory to measure this temperature (to  $0.1^\circ\text{C}$  with a mercury in glass thermometer) than to overcome the usual difficulties encountered with keeping a stirred icebath at constant temperature. The two cold junctions were joined together thermally but not electrically before immersion in the Dewar. This ensured that any variations in the water temperature would not affect the temperature difference measured along the sample, but would only affect the average temperature assumed. Each pair of thermocouples was checked for reliability over the whole of the temperature range after mounting in the cryostat. In spite of

the precautions taken to prevent strain in the wires it was still necessary to keep temperature conditions constant both along the length of the thermocouples and over the outside of the glass pinch. Once this pinch and the final terminal block had been enclosed in thermally insulating boxes to prevent slight temperature differences due to air draughts no more trouble was experienced. Tables published by the National Bureau of Standards<sup>48</sup> were used to convert the output from the thermocouples to temperature.

Measurement of the voltage appearing between the copper leads of the thermocouples after the temperature gradient had been established allowed the thermoelectric power to be measured at the same time as the thermal conductivity. Since both the thermoelectric power and the temperature gradient are low the voltages measured were only a few microvolts so the precautions to eliminate stray voltages, already described, were even more necessary for this measurement.

#### 4.2.4 Sample mounting, contacts and the heater

The graphite sample was cemented directly into a slot in the heat sink using a silver dispersion (Silverdag, Acheson Colloids Ltd.). This made a good electrical and thermal contact to the sample that remained reliable during repeated changes from room to liquid nitrogen temperatures. Before cementing into place the sample was also carefully coated with the dispersion

along the end faces and sides of the bar for a short distance to ensure adequate thermal contact to all the layer planes. Some experiments were made using copper plated contacts but these would not take repeated thermal cycling.

Contacts for attaching the thermocouples for measuring the temperature gradient along the sample were made by first passing a 40 gauge wire tightly round the sample. Thermal contact was completed by adding a thin fillet of silver dispersion between the wire and the sample and the thermocouples were soldered to the wire. The distance between the contacts was measured using a travelling microscope which was also used for measuring the cross sectional area of the sample.

The 5 ohm sample heater was made by winding 40 gauge constantan wire on to a thin mica former 3.5 mm square. Both this heater and the control heater were wound noninductively to prevent any possible magnetic effects. The heater was sandwiched between two sheets of 0.005 in. copper foil and cast in Araldite. The foil was extended from the heater to form a slot for cementing to the sample with silver dispersion and the finished heater and slot measured 7 x 4 x 1 mm. Potential and current connections to the heater were made with 40 gauge copper wire and the leads thermally anchored to the heat sink. The length of wire between the heat sink and the heater was made as long as possible.

#### 4.2.5 Supplies and measuring equipment

An a.c. supply was used with the control heater. Currents of up to 0.7 A from a 9 V transformer were sufficient to cover the temperature range. The output of the transformer was controlled with a Variac and it was found that the temperature of the sample was held sufficiently constant if the Variac was fed from a constant voltage transformer to eliminate fluctuations in the mains voltage.

A 2 V accumulator was used to supply the sample heater since an accumulator in good condition and given careful treatment during charging and use provides an extremely stable current for long periods of time if only small currents are required. The voltage from a freshly charged accumulator falls rapidly when it is first used but then reaches a steady value which it holds until nearing discharge. The accumulators were always discharged until the steady voltage was reached before using for the sample heater. The heater power was obtained by measuring the voltage appearing across a sub-standard 1 ohm resistor in series with the heater to give the current, and by using the potential leads to find the voltage directly across the heater. Both measurements were made using a model 3387B Tinsley potentiometer and were taken to the nearest millivolt. Typical values were 0.8 V and 0.25 A giving a heater power of 0.2 watts.

The output from the thermocouples was measured using a Pye precision decade potentiometer, catalogue number 7600.

This is a precision low resistance instrument in which the use of special thermofree switches and high quality manganin resistance wire enables the instrument to be almost entirely free from stray thermoelectric voltages. The smallest switched dial division is  $0.1 \mu\text{V}$  and by a special procedure using the calibrated current standardisation dials it is possible to interpolate between. This sensitivity can only be achieved if the potentiometer is used with a suitable galvanometer. Greatest sensitivity is obtained when the potentiometer is used in a low resistance circuit but because of the need to use 40 gauge wires for the thermocouples their resistance could not be reduced below about 35 ohms. Thus a very sensitive galvanometer was required and a Pye galvanometer preamplifier feeding a Pye Scalamp galvanometer number 7903/S was used. This combination has a sensitivity of 11,000 mm per microamp and was more than sufficient to detect change in the lowest dial reading. It was not necessary to use the most sensitive position on the galvanometer shunt. The galvanometer preamplifier was sensitive to vibration and had to be suitably mounted; it also drifted badly when first switched on because of thermal effects caused by the lamp warming the case and could not be used for the first hour. As with all sensitive detectors of this nature there was a great deal of capacitative pick up, but this was greatly reduced by earthing suitable points in the circuit and by using screened leads. The potentiometer was

provided with a reversing switch so that any stray voltages in the external circuit, particularly the galvanometer circuit, can be averaged out. A certain standing voltage is to be expected with a galvanometer amplifier so reversal is necessary for the most accurate readings. Switching to select either thermocouple or the copper leads for thermoelectric power measurement was done with a Pye thermofree switch of the same design as those used in the potentiometer. This switch together with the terminal block was enclosed in a thermally insulated box. The precautions taken to prevent stray thermoelectric voltages in the thermocouple circuits have already been described, but in spite of this care it was found that there was a small standing voltage of less than a microvolt on the leads used for measuring the thermoelectric power of the sample. This was corrected for by making a measurement of its magnitude after the apparatus and sample had stabilised at the measuring temperature but before the sample heater was switched on.

At the lowest measurement temperatures the thermocouple voltages were measured to the nearest  $0.1 \mu\text{V}$  to achieve sufficient accuracy with the small change in thermocouple outputs at these temperatures. At higher temperatures the thermocouple voltages were only taken to the nearest microvolt. The thermoelectric voltage along the sample was measured to the nearest  $0.1 \mu\text{V}$  since it was not found possible to hold conditions stable for long enough to use the fairly complicated interpolation

procedure. Because of the small temperature gradients used the thermoelectric voltage was as low as  $4 \mu\text{V}$  over part of the temperature range, but because it was higher at the lowest temperatures measured where the accuracy of temperature measurement is falling off, the overall accuracy probably remained about the same.

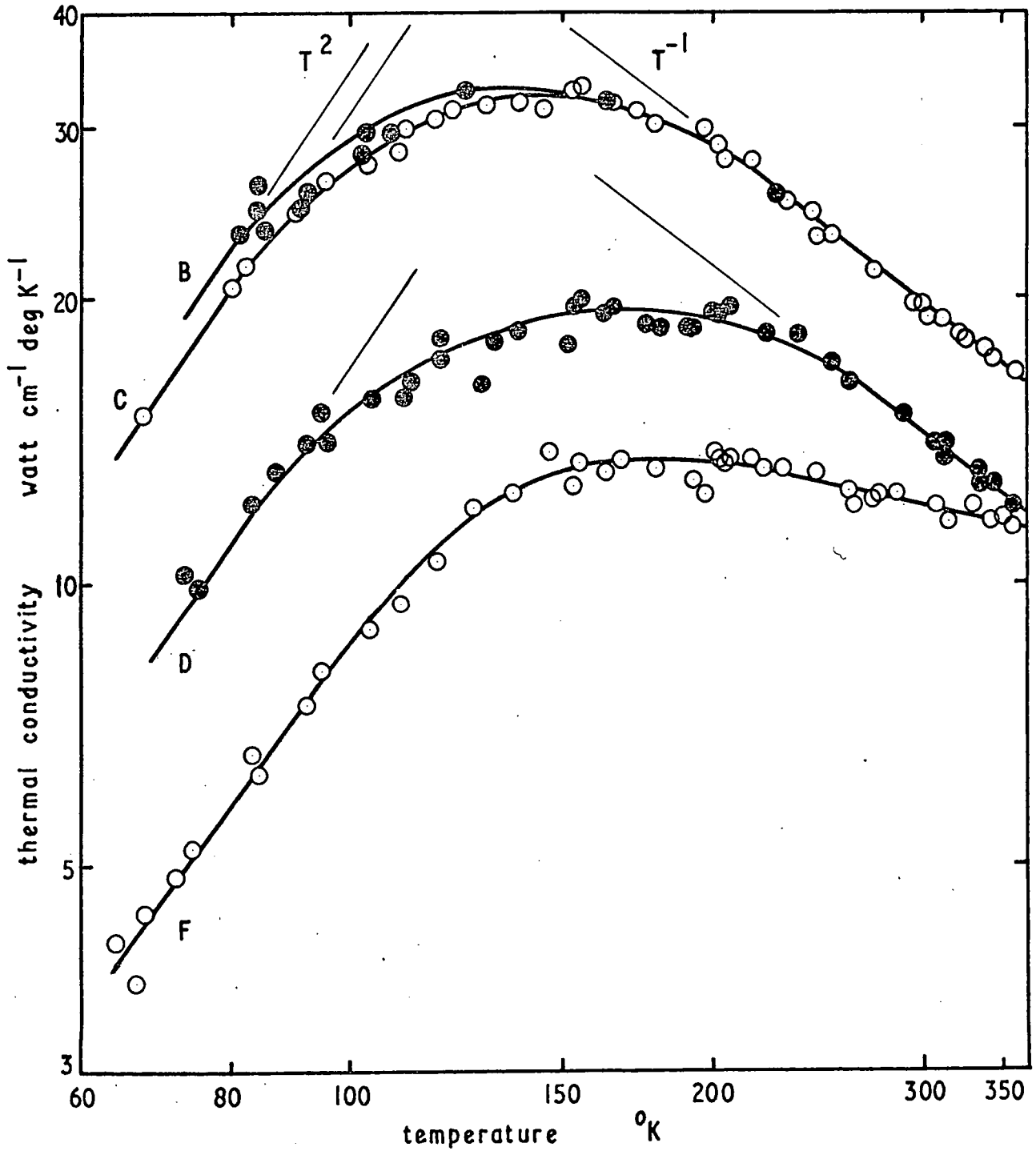
### 4.3 Experimental results

#### 4.3.1 Thermal conductivity

The results of the thermal conductivity measurements that were made on four of the sections from bar 22 are shown in figure 4.2. It can be seen that samples B, C and D have the same temperature dependence, varying as  $T^2$  on the low temperature side of the peak and as  $T^{-1}$  on the high temperature side. The magnitude of the thermal conductivity increases as the formation temperature is increased. Sample B reaches a peak of  $34 \text{ watt cm}^{-1} \text{ deg K}^{-1}$  at a temperature of  $140^\circ\text{K}$ . Samples B and C are very little different and lie together on the high temperature side of the peak. Sample F is rather different. It also has a temperature dependence near  $T^2$  on the low temperature side of the peak but the behaviour on the high temperature side does not show a  $T^{-1}$  dependence. For all the samples the peak position moves to lower temperatures with increasing thermal conductivities. The results can be compared with those of Hooker, Ubbelohde and Young<sup>49</sup>. They measured a

FIGURE 4.2

Temperature dependence of the thermal conductivity of sections from bar 22



series of samples hot pressed at  $2850^{\circ}\text{C}$  and one sample additionally annealed at  $3500^{\circ}\text{C}$  and obtained similar curves. The hot pressed samples had maximum values between 22 and 28 watt  $\text{cm}^{-1} \text{ deg K}^{-1}$  between 140 and  $160^{\circ}\text{K}$  which lie between the curves for samples C and D and are comparable with them. The annealed sample peaked at  $120^{\circ}\text{K}$  with a value of 40 watt  $\text{cm}^{-1} \text{ deg K}^{-1}$ . The peaks extended over a larger temperature range than in the present work and as the range of measurement was not so large it is not easy to be sure of the temperature dependence on either side of the peak but it would appear likely that the curves are approaching the  $T^2$  and  $T^{-1}$  asymptotes so that the two sets of results are in good agreement.

There are no results available from single crystal graphite to act as a standard of comparison. The nearest are measurements on flakes of natural graphite made by Smith<sup>50</sup>. These were specially selected flakes and microscopic examination of the surfaces showed deformation lines which indicated that the crystallite size was around  $10^{-2}$  cm. The thermal conductivity curves obtained peaked at near  $80^{\circ}\text{K}$  and reached a maximum value of 32 watt  $\text{cm}^{-1} \text{ deg K}^{-1}$ . At low temperatures the curve had a  $T^2$  dependence but on the high temperature side the approach to the peak was somewhat steeper than  $T^{-1}$ . The curves from three different flakes tended to lie together on the high temperature side of the peak.

Taylor<sup>51</sup> has measured the thermal diffusivity of two

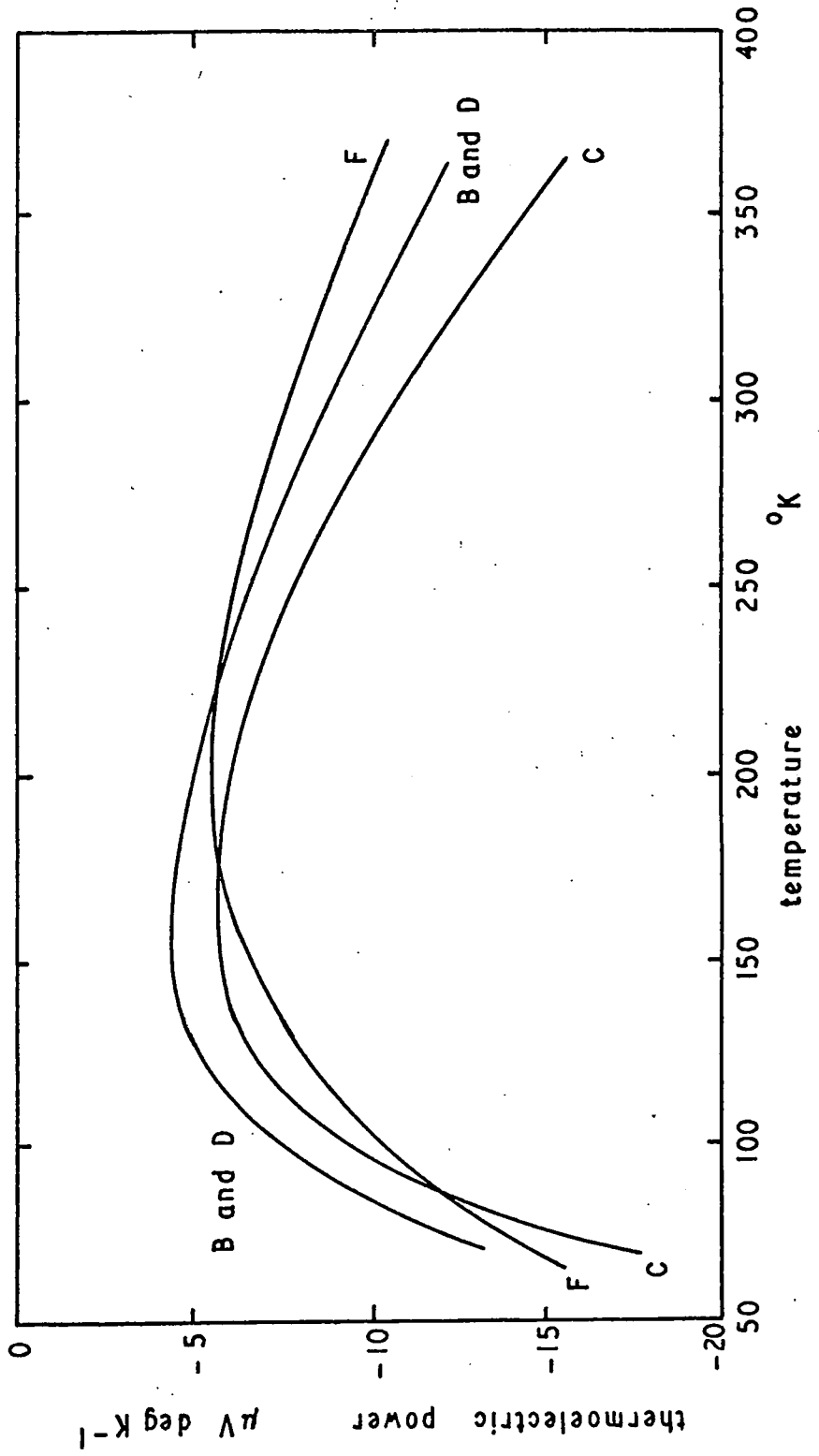
samples of pyrolytic graphite and taken the measurements up to  $900^{\circ}\text{K}$ . Little detail of the material preparation is given. One was as-deposited material annealed at  $2900^{\circ}\text{C}$  and the other was said to be structurally more perfect and annealed at  $3300^{\circ}\text{C}$ . The thermal conductivity of the better quality material reached a value of  $38.5 \text{ watt cm}^{-1} \text{ deg K}^{-1}$  at  $140^{\circ}\text{K}$  which is in good agreement with sample B although the estimated formation temperature for this sample is not as high as  $3300^{\circ}\text{C}$ .

#### 4.3.2 Thermoelectric power

The results of the thermoelectric power measurements taken at the same time as the thermal conductivity are shown in figure 4.3. The graph shows the thermoelectric power relative to copper. In order to avoid confusion the individual points have not been shown but the amount of scatter was very similar to that obtained in the thermal conductivity measurements. Curves from all the samples lie very close together with samples B, C and D having essentially the same temperature dependence. As in the thermal conductivity measurements the shape of the curve for sample F is somewhat different. The results can be compared with those of Tyler and Wilson<sup>52</sup> for polycrystalline artificial graphites and Blackman, Saunders and Ubbelohde<sup>53</sup> for pyrolytic graphite. Tyler and Wilson measured a series of graphites of different crystallite sizes over the temperature range  $30$  to  $300^{\circ}\text{K}$ . They found that lampblack graphite with

FIGURE 4.3

Temperature dependence of the thermoelectric power of sections from bar 22



poor crystal structure and an estimated crystallite size of under 500 Å had a positive thermoelectric power. The better graphites had negative values that gradually increased (negatively) as the temperature decreased, reaching a peak at about 45°K and falling sharply towards zero at lower temperatures. The height of the peak increased with larger crystallite size reaching 13 μV deg K<sup>-1</sup> for a graphite with crystallites estimated at 6700 Å. Blackman, Saunders and Ubbelohde measured a series of pyrolytic carbons deposited at between 1600 and 2000°C and one stress recrystallised sample. The carbons prepared below 2000°C had positive thermoelectric power in agreement with Tyler and Wilson. The recrystallised sample and the 2000°C sample had a similar shape to the Tyler and Wilson curves but with the negative peak occurring at 100°K. The shape of their curve for the recrystallised material was similar to the present work between 300 and 100°K but again a peak occurred at 100°K. In the present work there was no sign of a peak being reached down to the lowest temperatures measured.

In the course of obtaining the thermomagnetic coefficients for the same samples Mills<sup>24</sup> made an independent measurement of the thermoelectric power and obtained results in very good agreement with those obtained during the course of thermal conductivity measurements and he also found no peak at 100°K. Mills also included the thermoelectric power for sample 22 G. The curve was parallel to that of sample F but smaller in

magnitude. This agrees with the measurements of both Tyler and Wilson, and Blackman, Saunders and Ubbelohde which showed that the thermoelectric power of the more defective graphites becomes positive.

Two attempts have been made to predict the thermoelectric power theoretically. In the more recent Klein<sup>54</sup> used a very simple two band model of graphite. Since the thermoelectric power represents the difference between the effects due to positive and negative carriers he found that the predicted curves for essentially single crystal material are very sensitive to the values of the ratios of both the carrier densities and the carrier mobilities and gave a series of curves for different carrier mobility ratios. None of these curves gives a temperature dependence in agreement with the experimental results, but he suggested that his theory could account for the results if it is assumed that the mobility ratio is changing throughout the temperature range.

The earlier theoretical prediction is that of Mrozowski and Chaberski<sup>55</sup> and is based upon the relatively simple band model with touching bands proposed by Wallace<sup>56</sup>. No details are given of any of the calculations but curves are shown for a number of different heat treatment temperatures from 2300 to 3000°C. They also considered that with the improvement in the structure of material given the higher treatment temperatures there might be a contribution due to phonon drag and showed

curves both with and without that contribution. Their curves give positive thermoelectric powers for the lower treatment temperatures. The curve for  $3000^{\circ}\text{C}$  is always negative and with the contribution due to phonon drag has a large negative peak at around  $50^{\circ}\text{K}$  in agreement with the peak found by Tyler and Wilson. The general overall shape of this curve is similar both in magnitude and temperature dependence to the results obtained on samples B, C and D of bar 22 in the temperature range from  $68^{\circ}\text{K}$  upwards. It would appear that the peak obtained by Blackman, Saunders and Ubbelohde cannot be attributed to phonon drag since it is obtained at too high a temperature. Possibly the increase obtained at the lowest temperatures measured in the present work is the beginning of a peak which would occur at some lower temperature and which could be attributed to phonon drag. Thermodynamic arguments predict that the thermoelectric power must fall to zero at  $0^{\circ}\text{K}$ . This will be discussed further in chapter 6 in connection with other measurements.

#### 4.4 Estimation of the crystallite size

To obtain an estimate of the crystallite size from the thermal conductivity measurements some understanding of the theory of the lattice thermal conductivity of a crystalline solid is necessary. In general for a perfect isotropic crystal the lattice thermal conductivity  $K_L$  is given by

$$K_L = \frac{1}{3} C_v \bar{v} l$$

where  $C_v$  is the total specific heat per unit volume of the lattice,  $\bar{v}$  is an average velocity of the phonons and  $l$  is the mean free path of the phonons, (Drabble and Goldsmid, reference 57). The most important process in limiting the thermal conductivity is three phonon Umklapp interactions and for temperatures well below the Debye temperature the expression for the phonon mean free path for these interactions is

$$L_u = A \exp \frac{\theta}{bT}$$

where  $A$  and  $b$  are constants and  $\theta$  is the Debye temperature. For higher temperatures the mean free path for Umklapp scattering is proportional to  $\theta/T$ . The thermal conductivity will thus go on rising as the temperature is lowered until the phonon mean free path is of the order of the size of the crystal. The mean free path then becomes temperature independent as the temperature is lowered further and in this boundary limited region the thermal conductivity will have the same temperature dependence as the specific heat. For an isotropic perfect crystal the specific heat varies as  $T^3$  and the thermal conductivity falls off as  $T^3$  in this region. Thus curves for a series of samples in which the only difference is the physical size of the crystal should lie together on the high temperature side of the peak. As the size of the crystal is increased each curve will rise to a higher maximum value which will occur at successively

lower temperatures. Berman<sup>58</sup> showed that the same argument also holds for polycrystalline solids when the peak in the thermal conductivity curve would occur when the phonon mean free path becomes of the order of the crystallite size. So in principle the crystallite size can be estimated either from the peak position or from the boundary limited asymptote to the low temperature side of the curve. The second method can be used if an accurate knowledge of the specific heat is available, but because of the anisotropy of graphite the behaviour of the specific heat is extremely complicated. This will be discussed further in the next section but it accounts for the  $T^2$  dependence on the low temperature side of the peak. Several authors, for example Slack<sup>59</sup> and Hooker, Ubbelohde and Young<sup>49</sup>, have attempted to calculate the specific heat due to the modes contributing to the a-direction thermal conductivity and hence obtain the crystallite size but since it has been shown by Bowman and Krumhansl<sup>60</sup> that the specific heat is very structure dependent this is a rather dubious process, though interesting theoretically.

Smith and Rasor<sup>61</sup> have developed a method of estimating the crystallite size of graphite from the peak position aided by the theoretical work of Hove and Smith<sup>62</sup>. They argue simply that if the only sources of resistive phonon scattering are boundary scattering and Umklapp processes and that these contribute equally to the thermal resistivity at the peak, then for two different samples the crystallite sizes and the peak

temperatures can be related by

$$L_1/L_2 = \exp \frac{\theta}{2} \left[ \left( \frac{1}{T_1} - \frac{1}{T_2} \right) \right]$$

This removes the difficulty of giving a value to the constant A in the expression for Umklapp mean free paths and theory predicts that the constant b should have a value near 2 for these processes. On the basis of the work by Hove and Smith it is suggested that a value of 1000°K be used for the Debye temperature. Using as a standard a synthetic graphite where the peak occurred at 300°K and which had an independently measured crystallite size of  $6 \times 10^{-5}$  cm they obtained a value of  $0.6 \times 10^{-2}$  cm for the flake natural graphite referred to in section 4.3.1 which peaked at 80°K and for which deformation lines on the surface indicated a crystallite size of about  $10^{-2}$  cm.

Using the recommended Debye temperature and the same standard, crystallite sizes were calculated from the peak positions of the four samples measured and these are shown in the table overleaf. Also shown in the table for comparison are the estimated sizes obtained by Mills<sup>24</sup> from his low temperature measurements of the carrier mobility in the same samples. This estimation followed the method of Klein<sup>37</sup> in which the low temperature saturation of the mobility is attributed to the onset of boundary scattering and the crystallite size is estimated from the saturation value. The results from the two independent methods are in reasonable agreement except

for sample F. In this sample the rather different temperature dependence of the thermal conductivity probably makes the Smith and Rasor method less valid.

Section	Estimated formation temperature, °C	Crystallite size (μm)	
		from K	from μ
B	3020	3.3	3.8
C	2980	2.9	1.9
D	2910	2.1	1.6
F	2700	1.3	0.4

As will be seen in chapter 5 these estimates also compare well with the direct measurement of crystallite size using x-ray methods. However in spite of this agreement it is worth looking a little closer at the assumptions made in the Smith and Rasor method. It is only in Umklapp scattering that the approach to the peak is exponential. If the scattering is predominantly from imperfections in the crystal then a  $1/T$  temperature dependence will be obtained in agreement with most people's measurements. In practice an exponential dependence is seldom seen in any substance; artificial sapphire is one of the few crystals to show the expected relationships throughout the temperature range. Even in structurally near perfect crystals a  $1/T$  dependence is often obtained because imperfections due to isotopes are sufficient at reasonably low temperatures to prevent Umklapp scattering dominating. For example in the work of Geballe and Hull<sup>63</sup> on enriched germanium the isotopically

more pure specimen approached the peak more steeply than  $T^{-1}$  but did not reach exponential dependence. Ziman<sup>64</sup> has estimated the comparative phonon mean free paths for isotope and Umklapp scattering for various substances over a range of temperatures and calculates that for carbon the effect of isotope scattering should still be seen down to about 140°K. His conclusions for carbon are based on work by Berman<sup>58</sup> on rather defective graphites so may not hold for pyrolytic graphite. Like sapphire graphite has a high Debye temperature for a-direction conduction and if sufficiently perfect should show an exponential dependence if the crystallite size is large enough for the peak to occur at a low temperature. The natural graphite flakes measured by Smith<sup>50</sup> approached the peak somewhat steeper than  $T^{-1}$  but most measurements on good quality pyrolytic graphite still show a  $T^{-1}$  dependence. The exception is the measurement by Taylor<sup>51</sup> on a pyrolytic graphite sample annealed at 3300°C. This sample was said to be structurally more perfect than as-deposited material annealed at 2900°C and was supplied by R.J. Diefendorf of the General Electric company, U.S.A. It showed an extremely sharp peak of 38.5 watt cm<sup>-1</sup> deg K<sup>-1</sup> at 140°K with an exponential dependence from 900°K down to 350°K. If this measurement is a reliable one it indicates that the speculations of Ziman on the importance of isotope scattering in carbon are not correct and that an exponential dependence can be obtained in pyrolytic graphite of sufficient structural perfection. It is also some

justification of the otherwise empirical method of Smith and Rasor.

#### 4.5 Discussion

Following the simple arguments put forward in the previous section it can be deduced from the results shown in figure 4.2 that samples B and C must be very similar structurally. The curves lie together on the high temperature side of the peak, presumably because of a common source of thermal resistance, and the curve for sample B rises to a higher peak at a lower temperature because of its increased crystallite size. Sample D must have an additional source of thermal resistance as the high temperature values for the thermal conductivity are so much lower. This could either be due to additional structural defects within the crystallites or to increased misorientation of the crystallites. Since the measurements of chapter 3 show little difference between the degree of misorientation of samples C and D but a large difference between D and F it seems unlikely that misorientation is sufficient to account for the increase in resistance which must therefore be attributed to increased structural imperfection.

The thermal conductivity of samples B and C which have the largest crystallite sizes and greatest structural perfection is very high. It is probably too high to obtain useful cooling from an Eттingshausen device, but before this can be assessed

in the liquid helium range it is necessary to extrapolate the results down to those temperatures. Since this is the boundary limited region the phonon mean free path is temperature independent and the thermal conductivity should follow the temperature variation of the specific heat. There have been a number of measurements of the specific heat of graphite<sup>65,66,67</sup> and there is general agreement that down to about 20°K the specific heat varies as  $T^2$ . This dependence is due to the anisotropic lattice vibrations. Early work on the thermal conductivity of synthetic graphites<sup>58</sup> gave a steeper temperature dependence, near  $T^{2.6}$ , and excited a great deal of interest since this was the first known substance in which the temperature variation of the specific heat and the thermal conductivity in the boundary limited region were different. However it was shown by Hove and Smith<sup>62</sup> that the steeper dependence of the thermal conductivity could be attributed to the pitch binder used in making the graphite. This provided isotropic regions in the aggregate which were sufficient to account for the observed difference, and thus data on the temperature dependence of the specific heat can be used to aid the extrapolation of the thermal conductivity down to liquid helium temperatures.

There have been a number of theoretical studies of the specific heat of graphite. The electronic component of the specific heat seems to be reasonably well understood from the band structure, but because of its anisotropy analysis of the

elastic vibrations of the lattice is a difficult problem. A good summary is given by Bowman and Krumhansl<sup>60</sup>. The problem was simplified by the work of Komatsu<sup>68</sup> who showed that to a good approximation the lattice vibrations could be divided into independent 'in-plane' and 'out-of-plane' modes. This is because the weak binding between the layers means that the shear interaction between the planes, described by the elastic constant  $c_{44}$ , is always small. The major part of the heat capacity is in the out-of-plane modes which correspond to bending of the lattice planes. This model can be used to show that above about 20°K the specific heat should vary as  $T^2$  in agreement with the experimental results. Below this temperature it is predicted that there should be a change to a  $T^3$  dependence. DeSorbo and Nichols<sup>67</sup> measured the specific heat of a number of different graphites down to 1°K. The good quality flake natural graphite showed the expected transition to  $T^3$  behaviour below about 10°K, but lampblack graphite with its high proportion of structural defects, particularly stacking faults, had a higher specific heat and did not show the transition. These results were analysed by Bowman and Krumhansl who suggested that the random stacking of the lampblack graphite decreased the interplanar shear modulus  $c_{44}$  and allowed bending vibrations of the layer planes to be excited at much lower temperatures, accounting for both the increased specific heat and the lack of transition to  $T^3$  behaviour. The same experimental results

were analysed independently by Komatsu<sup>69</sup> who came to the same conclusion that the transition would become lower as  $c_{44}$  decreases and also that  $c_{44}$  would be very sensitive to the structure and would decrease with defects, particularly with stacking faults.

On the basis of the work on the specific heat it would be expected that the lattice component of the thermal conductivity of good quality graphite would continue to decrease as  $T^2$  down to some temperature below  $20^\circ\text{K}$  and then become  $T^3$  dependent, with the transition temperature becoming higher as the quality of the graphite increased. The one measurement made by Holland, Klein and Straub<sup>70</sup> of the thermal conductivity of a sample of pyrolytic graphite heat treated at  $3250^\circ\text{C}$  showed this sort of behaviour. It peaked at about  $120^\circ\text{K}$  with a value near  $40 \text{ watt cm}^{-1} \text{ deg K}^{-1}$  and fell as  $T^2$  down to near  $20^\circ\text{K}$ , steepened to near  $T^3$  until the electronic component became significant below  $10^\circ\text{K}$ . With the application of a magnetic field to remove the electronic component the steeper fall continued down to  $2^\circ\text{K}$ . (In figure 1 of the paper by Holland, Klein and Straub a curve has been drawn through all the experimental points and they suggest an overall slope of  $T^{2.7}$  on the low temperature side. A better fit to the experimental points is obtained by a  $T^2$  line down to  $20^\circ\text{K}$  and a  $T^3$  line below that. The transition can be seen very clearly.)

The transition to a steeper temperature dependence is

obviously of importance in a potential cooling device and it is likely that a lower lattice component of the thermal conductivity would be obtained at helium temperatures from a good quality graphite showing the transition than from a poor quality graphite having a much lower peak thermal conductivity. In addition the poor quality graphite is likely to have inferior thermomagnetic properties. To illustrate this, if sample F, the poorest quality graphite measured, is extrapolated downwards as  $T^2$  the value obtained is greater below  $7^{\circ}\text{K}$  than that for the good quality sample measured by Holland, Klein and Straub. There would therefore seem little point as far as a possible device is concerned in trying to reduce the thermal conductivity by the deliberate introduction of defects into the material.

## CHAPTER 5

### MEASUREMENT OF THE CRYSTALLITE SIZE

#### 5.1 Introduction

The thermal conductivity measurements described in chapter 4 were used, following the method of Smith and Rasor<sup>50</sup>, to give a crystallite size for sections of bar 22 which was in reasonable agreement with the values deduced from the mobility measurements made by Mills<sup>24</sup>. However these are both indirect methods and it was thought desirable to attempt to obtain the crystallite sizes directly by x-ray methods. As will be seen below, the technique is not an easy one and although the c-direction layer thickness can be obtained relatively straightforwardly, obtaining the a-direction layer size is complicated by the graphite crystal structure and the incidence of stacking faults.

#### 5.2 Crystallite size determination from x-ray line broadening

The Bragg equation,  $2d \sin \theta = n\lambda$ , which relates the angle  $\theta$  at which an x-ray reflection occurs with the crystal lattice spacing and the wavelength of the incident radiation, can be simply deduced using ordinary principles of optical diffraction. The equation only specifies the position of the reflection and assumes an infinite crystal. Scherrer<sup>71</sup> first showed that the width  $\beta$  of an x-ray line obtained from a powder

aggrégate is related to a mean crystallite dimension,  $D$ , through the equation

$$D = \frac{K\lambda}{\beta \cos \theta}$$

where  $K$  is a constant near unity whose value depends on the exact definitions of  $D$  and  $\beta$  and also to a lesser extent on the crystallite shape. As with the Bragg equation a simplified derivation of the Scherrer equation can be made using optical diffraction methods. In this derivation rays diffracted at a small angle on either side of the Bragg angle are examined, and the phase change for each successive crystal plane obtained. The resultant amplitude of the reflection from  $n$  crystal planes is

$$n a \frac{\sin \alpha}{\alpha}$$

where  $a$  is the amplitude of the ray from each crystal plane and  $\alpha$  is half the phase difference between the first and last plane in the crystal. The intensity is proportional to the square of the amplitude, i.e.

$$I \propto \frac{\sin^2 \alpha}{\alpha^2}$$

Two definitions of  $D$ , the crystallite dimension, are in common use. The first is the cube root of the crystallite volume and is only suitable if the crystallites are of a more or less regular shape, and all lines from the powder pattern are of a similar width. Graphite crystallites are platelike

with a large a-direction dimension and small c-direction one, and give a powder pattern with narrow (hk0) lines and broad (00 $\ell$ ) lines. In this case the definition of D which is suitable is the extent of the crystallite in the direction perpendicular to the reflecting planes.

In considering the definition of  $\beta$ , the line breadth, it must be emphasised firstly that this is the pure diffraction breadth separated from all other sources of broadening, such as strain in the crystal or the instrumental broadening. It will be seen that the choice of definition depends on the method of separation used.

The first definition and the easiest to obtain is the half width, which is the width of the line at half peak intensity. However it has little mathematical significance as it provides no information about the shape of the profile. Scherrer originally suggested that the instrumental broadening could be obtained by photographing a powder with large crystallite size using identical geometrical conditions to the unknown, and then directly subtracting the half width from the half width of the unknown to obtain the diffraction broadening.

The second, and mathematically more meaningful definition is the integral breadth of the line

$$\beta = \frac{\int I d(2\theta)}{I_{\max}}$$

which is the integrated area divided by the peak intensity.

This takes into account the shape of the line. A number of methods have been proposed for separating out the diffraction broadening. Warren<sup>72</sup> showed that when both the instrumental profile and the diffraction profile could be described by Gaussian curves,  $e^{-kx^2}$ , then the squares of the integral breadths should be subtracted. Jones<sup>73</sup> showed that a powder containing a distribution of crystallite sizes was more likely to have a diffraction profile following a Cauchy distribution,  $\frac{a}{\pi(a^2 + x^2)}$ ; and assuming that the instrumental profile was still a Gaussian he performed a Fourier analysis to find the 'fold' of the two curves and produced a set of curves for correcting for instrumental broadening. These are relatively easy to apply. However there is no real reason to suppose that the instrumental profile is always a Gaussian.

Following on this, Stokes<sup>74</sup> gave a procedure for the separation of instrumental from diffraction profiles using full scale Fourier analysis of the curves. This makes no assumptions about the shape of the curves, so is a more correct process than any so far described. However it is rather tedious and lengthy though the ready availability of computers makes it more possible.

The separation methods described so far assume that fully annealed powders are used, i.e. that there is no strain. If there is strain present a component proportional to  $\tan \theta$  and independent of the wavelength  $\lambda$  is added to the broadening<sup>77</sup>,

and this must be separated if the broadening due to crystallite size is required. If the powder yields a large number of lines then Kochendorfer<sup>75</sup> showed, using half widths, that plots of  $\beta/\tan \theta$  versus  $\theta$  and  $\beta \cos \theta$  versus  $\theta$  could be used to separate out the strain from the crystallite size broadening. Warren and Averbach<sup>76</sup> showed how the Fourier analysis method of Stokes should be extended to separate the strain. This method also requires several orders of x-ray lines and is based on the finding that the strain component is likely to have a profile represented by a Gaussian distribution. In addition the Fourier analysis method turns out to be very sensitive to the exact background level assumed in the determination of the line profiles, and choosing the optimum background level also requires more than one (hkl) line. The complete method has been well described by Warren<sup>78</sup>.

More recently Tournarie<sup>79</sup> and Wilson<sup>80</sup> have suggested the use of variance as the measure of the width of an x-ray line profile. It is possible to separate out the instrumental, crystallite size and strain contributions to the line broadening without recourse to the elaborate mathematical methods of Fourier analysis.

Variance is defined as the mean square deviation of  $2\theta$  from its mean value

$$W_{2\theta} = \langle (2\theta - \langle 2\theta \rangle)^2 \rangle$$

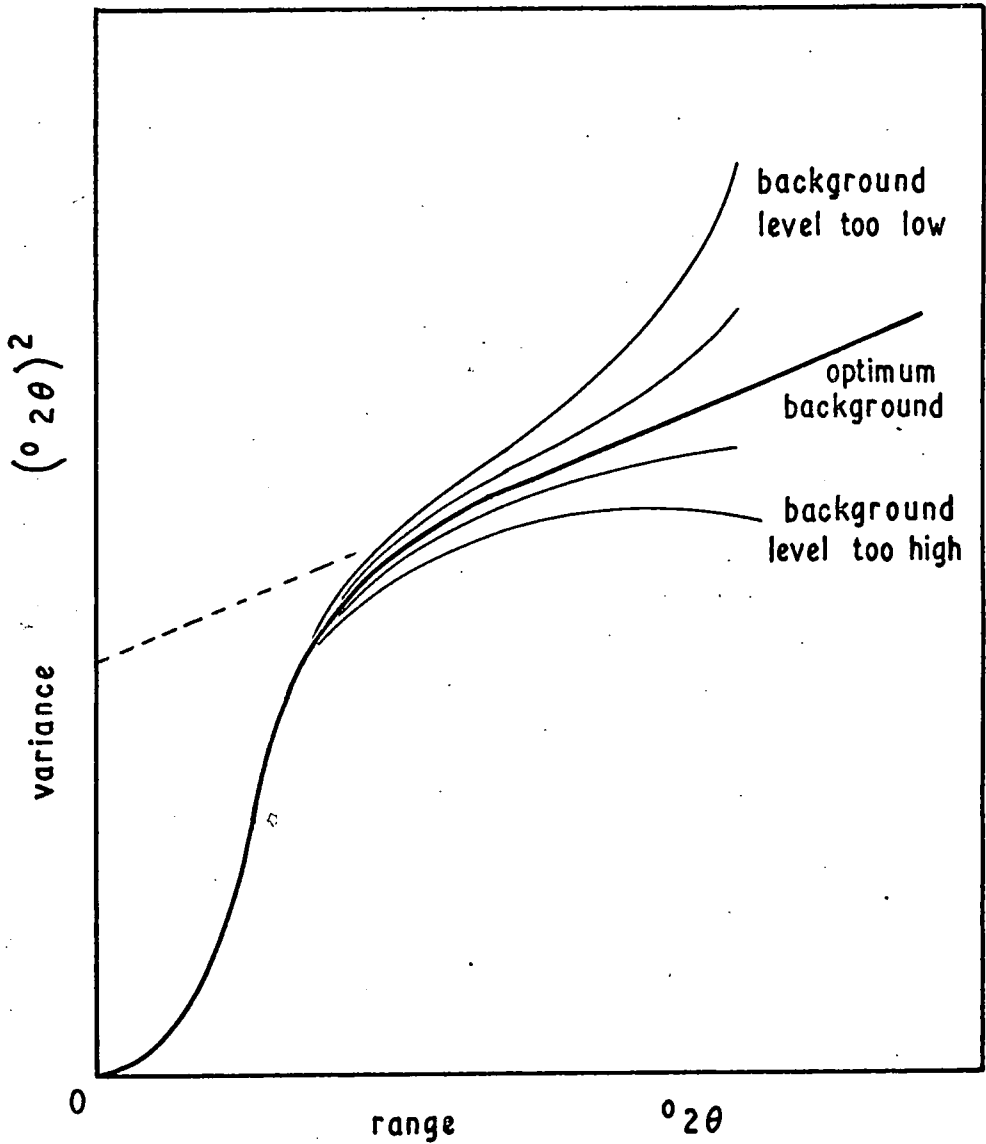
$$\begin{aligned}
&= \frac{\int_{2\theta_1}^{2\theta_2} (2\theta - \langle 2\theta \rangle)^2 I(2\theta) d(2\theta)}{\int_{2\theta_1}^{2\theta_2} I(2\theta) d(2\theta)} \\
&= \frac{1}{I_{\text{total}}} \int_{2\theta_1}^{2\theta_2} (2\theta)^2 I(2\theta) d(2\theta) - \langle 2\theta \rangle^2
\end{aligned}$$

The basis of the method is the examination of the variance of a line profile as the range of integration is changed. Variance is only meaningful for a truncated distribution since if the limits are taken to infinity the variance becomes infinite. Wilson<sup>81</sup> showed that for any profile which approaches the background according to an inverse square law, the variance in the region of the tails of the profiles is a linear function of the range of integration. The outline of the simple derivation of the Scherrer equation given at the beginning of this section gave an expression for the intensity of the line which satisfies this condition, and the Cauchy distribution deduced by Jones<sup>73</sup> for a range of crystallite sizes also approaches the background according to an inverse square law. A plot of the variance of a profile as a function of the range of integration would therefore appear as shown by the optimum curve in figure 5.1 with the curve becoming linear as the tail region is approached. The variance of a Gaussian curve, however, becomes independent of the range of integration in the tail region provided a sufficiently large range is taken.

The variance of the 'fold' of any two profiles can be shown, (Wilson<sup>81</sup>), to be simply the sum of the variances of the

FIGURE 5.1

Variance of an x-ray line profile as a function of range showing the effect of error in the background level



two individual profiles, and it is this property of variance that allows the various components to be separated out. The procedure for doing this is as follows. The line profile from the unknown powder is obtained, and a second profile also obtained from a standard powder using identical geometrical conditions. The standard powder should be an aggregate of very large (a few  $\mu\text{m}$ ) unstrained crystallites. A plot is made of the variance of the standard as a function of range and the slope and intercept of the linear region of the tails found. This represents the instrumental broadening. A similar plot is made from the unknown powder line profile. If there is no strain in the sample then the linear tail region will have the same intercept as the linear tail region of the standard, and the difference in slopes gives the crystallite size broadening. If the sample is strained then the Gaussian strain term will add a range independent component to the variance of the line and the intercept of the linear tail region will differ from the intercept of the standard. The difference gives the variance of the strain. Wilson showed that the strain variance  $W_{2\theta}$  can be related to the root mean square strain  $e$  by

$$e = \frac{1}{2} (W_{2\theta})^{\frac{1}{2}} \cot \theta$$

To obtain the crystallite size from the slope Wilson showed that when using variance the Scherrer equation must be modified to the form

$$\frac{W_{\theta}}{(\theta_2 - \theta_1)} = \frac{K\lambda}{4\pi^2 D \cos \theta} + \text{second order term}$$

where  $W_{\theta}/(\theta_2 - \theta_1)$  is the slope of the linear region of the variance-range curves. The second order term, called the taper parameter, is related to the exact crystallite shape and consequently also to the particular crystal plane giving the line, and in general may be neglected so that the crystallite size may be obtained simply from this equation. The value of  $K$  also varies slightly with crystallite shape and crystal plane, but in practice when using variance as a measure of line breadth, with  $D$  as the average dimension of the crystallite perpendicular to the crystal plane giving the reflection, an average value of 1.16 is suitable.

As in the Fourier analysis method the variance of a profile is extremely sensitive to the exact background level chosen and if the method is to be of use a technique for optimising the background level must be found. Langford and Wilson<sup>83</sup> showed that an error in the background level adds a cubic term to the variance-range curve. If a family of variance curves for different background levels is plotted as shown in figure 5.1 it is found that the lines curve away increasingly on either side of the optimum linear one. It is thus a simple matter to optimise the background level.

In summary, the advantages of the variance method over the Warren and Averbach Fourier method of analysing line profiles

is the comparative simplicity of the computation. Although slightly tedious the determination of variances can be carried out straightforwardly with a desk calculator and the use of a computer is not necessary. More important with graphite where the number of x-ray lines available for analysis is limited, the background level can be optimised and the strain component separated out without the use of a second x-ray line. Recently Aqua<sup>84</sup> has made a study of the various methods of analysis of line profiles and has shown that the variance method yields results in agreement with the Fourier analysis method of Warren and Averbach.

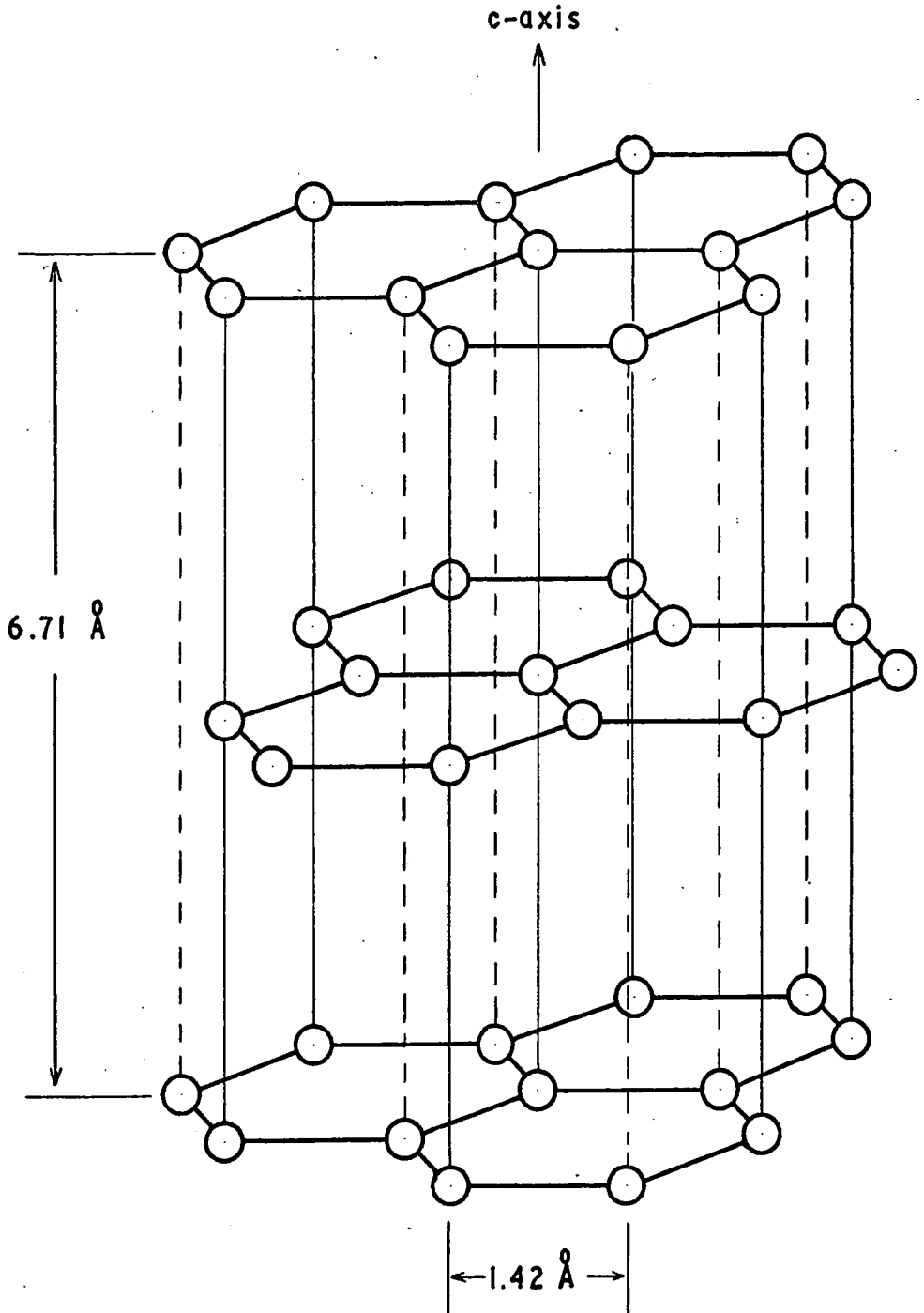
### 5.3 Line broadening in graphite

The previous section outlined quite generally methods of determining crystallite size from x-ray line broadening. It is necessary now to consider the method in relation to the specific crystal structure of graphite.

The graphite crystal lattice is shown in figure 5.2. It is a layer structure with carbon atoms in the layers arranged in a hexagonal array with lattice spacing  $1.46 \text{ \AA}$ . The layers are  $3.354 \text{ \AA}$  apart and are stacked so that alternate layers are displaced as shown in the diagram, giving a stacking sequence ABABAB'... A third layer position, C, is also possible and the stacking sequence ABCABC.... gives the rhombohedral modification of the graphite structure<sup>85</sup>. Most graphite

FIGURE 5.2

The crystal structure of graphite



contains a small proportion of this modification in the form of an occasional C layer. Such an error in the stacking sequence is termed a 'mistake' or stacking fault.

Before considering the detailed effects of stacking faults the alterations in the powder pattern obtained as the material changes from carbon to graphite will be described. Even the atoms in a carbon black show some kind of order as they are still arranged in hexagonal arrays in single layers. Although these layers stack themselves up physically there is no relation between them and each layer is randomly translated and rotated relative to the next. Such two dimensional crystals are termed 'random layer lattices', and in graphite the term 'turbostratic' is used to indicate that there is no order between successive layers. They give a powder pattern with very diffuse  $(00\ell)$  lines at positions indicating the closest that two layers can approach without any form of crystal binding. They also give broadened  $(hk0)$  lines indicating the size of the layers. There are no  $(hk\ell)$  lines as there is no 3-dimensional order. The profile of the  $(hk0)$  lines is now very asymmetrical with a very long high angle tail. Warren<sup>86</sup> calculated an approximate form for the profile of any random layer lattice line and showed that the half width  $\beta$  is related to the layer size  $D_{hk}$  by

$$\beta = \frac{1.84 \lambda}{D_{hk} \cos \theta}$$

The Scherrer constant of 1.84 is nearly double that for 3-dimensional crystals. Note that it is necessary to use the half width since integral breadth and variance become meaningless with the long tailed profile. Warren also showed that the (hk0) lines are displaced from their expected positions (specified by the a-spacing of the hexagons) by an amount

$$\Delta(\sin \theta) = \frac{0.16\lambda}{D_{hk}}$$

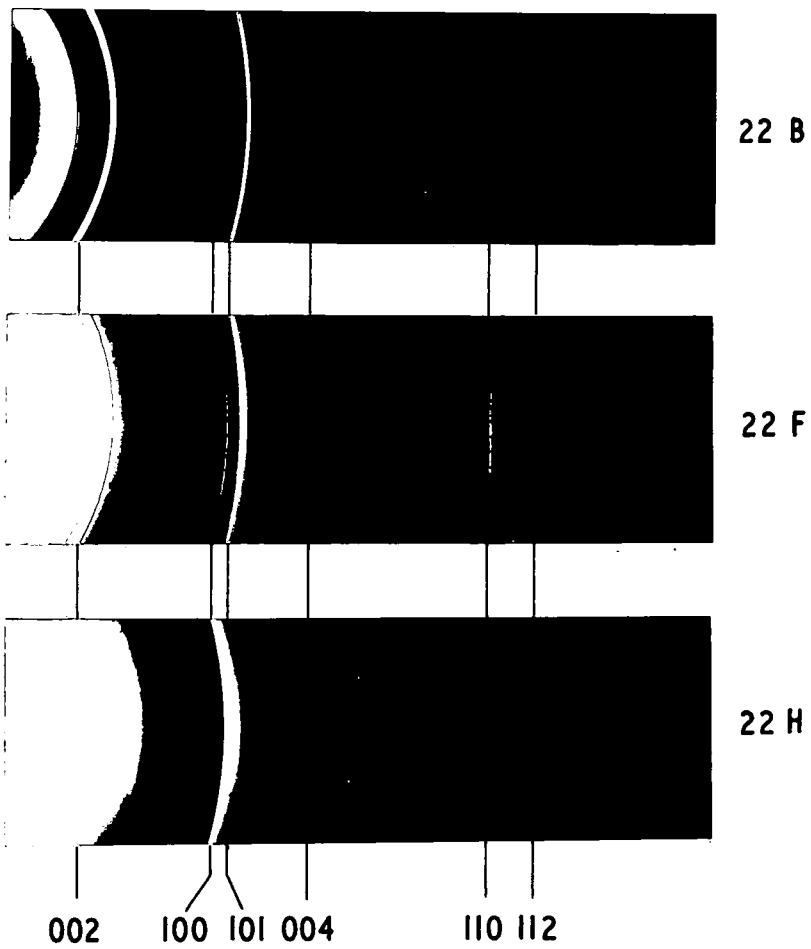
thus explaining the apparent contraction of the lattice in small crystals which had already been observed. Wilson<sup>87</sup> made a more exact calculation of the profile which will be considered later.

As graphitisation begins some of the layers become bound in the correct graphite positions and as a consequence move closer together. The average c-spacing thus goes down and the (00 $\ell$ ) lines become sharper and move towards higher angles. At the same time the (hk0) lines become less asymmetrical and (hk $\ell$ ) lines begin to appear diffusely. With increasing graphitisation more (hk $\ell$ ) lines appear and they sharpen, the (hk0) lines become symmetrical and the (00 $\ell$ ) lines also sharpen and move towards the position appropriate to a c-spacing of 3.354 Å. The change is illustrated in figure 5.3 which shows prints from x-ray films for three stages of graphitisation.

A stacking factor, p, can be defined as the chance that an additional layer added to the crystal will contain a stacking

**FIGURE 5.3**

X-ray powder photographs showing the effects of increasing graphitisation



fault. Franklin<sup>88</sup> investigated the graphitisation process and showed that turbostratic material has a c-spacing of 3.44 Å, the closest approach of two unbound layers. By assuming that only two other spacings are possible, 3.354 Å for a correct graphite layer and an intermediate value when a stacking fault occurred, she related the mean c-spacing to the stacking factor. This was slightly refined by Bacon<sup>89</sup> to give the Bacon-Franklin expression for the stacking factor

$$d = 3.44 - 0.086(1 - p) - 0.064p(1 - p)$$

This expression becomes insensitive for values of p below 0.2, that is to say once less than 1 in 5 layers are incorrectly stacked the c-spacing differs little from the graphite value of 3.354 Å. If it is desired to determine the stacking factor in well graphitised material an alternative method must be used.

Graphite crystallites are platelike with a large a-direction dimension and small c-direction thickness. One would therefore expect a powder film of a well graphitised sample to give sharp (hk0) lines corresponding to the large layer size, and broader (00ℓ) lines corresponding to the small thickness. (hkℓ) lines should have an intermediate width depending on the exact direction of the crystal plane. However in practice the (hkℓ) lines are usually broader than the (00ℓ) lines, (see figure 5.3). This is because stacking faults contribute to the width of the (hkℓ) lines, Wilson<sup>77</sup> p.87, and the integral breadth of the line is

$$\beta = \frac{\lambda^2 \ell}{c^2 \sin 2\theta} \cdot p$$

Since the intensity follows a Cauchy distribution the integral breadth and variance are simply related<sup>90</sup> and for variance the equation becomes

$$\frac{W_{\theta}}{(\theta_2 - \theta_1)} = \frac{2\lambda^2 \ell}{\pi^2 c^2 \sin 2\theta} \cdot p$$

Until recently it was not thought that stacking faults contributed to the width of the (hk0) lines since with  $\ell = 0$  the above expression becomes zero. However layer sizes determined from the width of the (hk0) line have often been around an order of magnitude smaller than those obtained by direct methods such as electron microscopy<sup>91</sup>. This has led to theories of a mosaic texture<sup>92</sup> which assume that the mean free path for the scattering of x-rays can be very much less than that for electrons or phonons. Eeles and Wilson<sup>93</sup> pointed out that there is in fact a contribution from the stacking faults to the width of the (hk0) line but that this is not obtained in the usual derivation of the line profiles, since the derivation uses an approximation that is not valid in the special case of small graphite crystals. The derivation, Wilson<sup>77</sup> p.38, is made in terms of reciprocal space in which each infinite crystal plane appears as a point. A small crystal gives a smeared out x-ray intensity surrounding the point and a platelike crystallite, as in graphite, will appear

as a rod in reciprocal space which in the limit of the random layer lattice has infinite extent. The line joining a point in reciprocal space to the origin has length  $s_0 = 2 \sin \theta / \lambda$  and the intensity diffracted with a Bragg angle between  $\theta$  and  $\theta + d\theta$  is proportional in reciprocal space to the intensity lying between concentric spheres of radii  $s$  and  $s + ds$ . The line profile can be obtained if the integral over the space between the two spheres can be determined. In practice this is too difficult mathematically except in a few special cases, and a solution is usually obtained by replacing the spheres by their tangent planes. For regular shaped small crystals this is a reasonable approximation, but it was realised, Warren<sup>86</sup>, Wilson<sup>87</sup>, that in the extreme case of random layer lattices with an infinite rod in reciprocal space the approximation is not valid. A better approximation in this case is obtained by replacing the spheres by tangent paraboloids and the random layer lattice line profiles were calculated in this way. Eeles and Wilson suggested that the more exact tangent paraboloid approximation should also be used for reasonably graphitised samples in which the rods still have a fair extension in reciprocal space. This leads to the stacking fault contribution to the width of the (hk0) lines which is expressed in terms of the variance as

$$W_s = W_u + \frac{W_w^2}{4S_0^2}$$

where  $W_s$  is the measured variance of the (hk0) line and  $W_u$  is the variance obtained from the tangent plane approximation. The last term represents the contribution of the stacking faults and Wilson<sup>123</sup> has shown that this term is expressed in terms of the stacking factor,  $p$ , and the range of integration by

$$W_w^2 = \frac{1}{3\pi^2 I_\sigma} \left( \frac{2\sigma^3}{S_o} \right)^{\frac{1}{2}} - \frac{2\sigma}{\pi^4 S_o I_\sigma^2} + \frac{a^2}{\pi^4 I_\sigma} \left( \frac{\sigma}{2S_o^3} \right)^{\frac{1}{2}}$$

where  $I_\sigma = \frac{2}{\pi a} \arcsin \left\{ \frac{\pi}{a} \left( 2S_o \sigma \right)^{\frac{1}{2}} \right\}$ ,  $S_o = 2 \sin \theta / \lambda$ ,  
 $a = p/2c = p/6.71$ ,  $\pm \sigma =$  range of integration

The procedure for obtaining the a-direction layer size from an (hk0) line is thus as follows. The line profile is analysed to obtain a variance-range plot as described in the previous section. The stacking factor  $p$  is obtained from a variance-range plot of an (hkl) line. The correcting factor is then computed for the appropriate range and subtracted point by point from the original variance-range plot and the resulting line used to determine the crystallite size.

## 5.4 Practical considerations

### 5.4.1 Choice of Debye-Scherrer camera or diffractometer

Two methods are in use for obtaining line profiles; a Debye-Scherrer powder camera in which the powder lines are obtained on a film which must then be measured up with a

microdensitometer to obtain line profiles, and a counter diffractometer with the counter feeding a chart recorder so that the line profiles are obtained directly. At first sight the diffractometer is the more desirable instrument as not only is the profile obtained directly but because of the focussing properties it is possible to get an instrumental line width of less than  $0.25^{\circ}$ ; The sensitivity of the crystallite size determination increases as the ratio of the powder line width to the instrumental line width increases. However in practice the diffractometer is subject to a number of aberrations which both shift line position and distort the profiles and for accurate work corrections have to be made<sup>94</sup>. The error that is of most importance in this work is that due to specimen transparency. Perfect focussing is only obtained if the x-ray beam is reflected from a curved sample which it is not able to penetrate. The use of a flat sample gives little error but graphite has such a low absorption coefficient that the beam is able to penetrate a considerable distance and the profile is distorted as a result. A further disadvantage is that relatively large quantities of material are required for preparing the powder samples and since a small bar of graphite was being cleaved into thin sections to examine the variation through the bar it was difficult to obtain sufficient material.

Using a Debye-Scherrer camera special precautions must be taken to obtain a low instrumental line width but even so it

is difficult to obtain a reproducible width very much less than  $0.5^{\circ}$ . Corrections for specimen transparency are opposite to that of the diffractometer giving distorted and displaced profiles for high absorption specimens, so the low absorption of graphite is an advantage. Only very small quantities of material are required to prepare the powder samples and these two advantages are sufficient to justify the choice of a Debye-Scherrer camera in spite of the larger instrumental width and the need for measuring up the film.

The camera used was a 11.46 cm diameter Philips camera used with a Philips PW 1008 generator and nickel filtered copper radiation. The camera was mounted on a high intensity arm, that is to say viewing the line focus end on, and to ensure identical geometrical conditions the same arm and camera were used throughout the series. Before the film from the final sample, 22 D, could be obtained the copper insert tube failed and had to be replaced. This necessitated realigning the camera arm and because of this, and the possible change in the exact shape of the focus, a new standard film was taken to correct this particular sample for instrumental broadening.

The most common use for Debye-Scherrer cameras is for powder identification or determination of lattice spacings where only line positions are required. Exact line profiles do not matter except in so far as the lines must be narrow enough to enable measurement of position to be sufficiently

accurate, and it is usual to use a slit collimator on the camera. The resultant lines are 'umbrella' shaped with a distorted profile but remain in the same position. The longer length of the sample seen by the x-ray beam with a slit collimator means that exposure times are reduced by a factor of three. To avoid distorted profiles a round collimator 1 mm diameter was used in this work.

To obtain lines suitable for measuring on the microdensitometer special film, Ilford Industrial CX, was used. This is an extremely fine grain film giving a very low background, but is about three times slower than Industrial G which is mostly used. The films were developed for 4 minutes in Ilford Phenisol x-ray developer and fixed in Ilford Hypam fixer with hardener added. To ensure uniform conditions fresh solutions were used each time.

The combination of fine grain, slow film and the round collimator means about a tenfold increase in exposure time over the usual conditions. Because of its low absorption graphite already requires a rather longer exposure than more absorbing substances, and it was found that an exposure of up to 300 hours was necessary to obtain a suitable density on the film. The better graphitised samples with much narrower line widths needed a shorter exposure time to give the same peak density.

#### 5.4.2 Choice of standard

As explained in section 5.2 instrumental broadening is allowed for by taking a film of a powder sample consisting of large strain free crystallites. A crystallite size of a few  $\mu\text{m}$  is sufficiently high. Ideally the standard is a fully annealed sample of the same substance as the unknown so that there will not be any error due to differences in absorption. It is not possible to obtain such a graphite standard. However diamond, as it is also carbon, has the same absorption as graphite and it is readily available graded to size in the form of metallurgical polishing pastes. A 6  $\mu\text{m}$  polishing paste was used and the diamond was separated out by dissolving the paste medium in carbon tetrachloride and allowing the diamond particles to settle. A little of the clay mineral used to assist polishing was left with the diamond but this only appeared as a very faint pattern on the film well away from the (220) line which was used as the standard. It was assumed that the diamond was relatively strain free.

#### 5.4.3 Sample preparation

To keep the instrumental line width low the prepared sample must have the smallest possible diameter, but in order to keep the geometrical conditions the same the prepared samples must all have the same diameter and be packed reproducibly. This means that the usual method of coating a glass filament

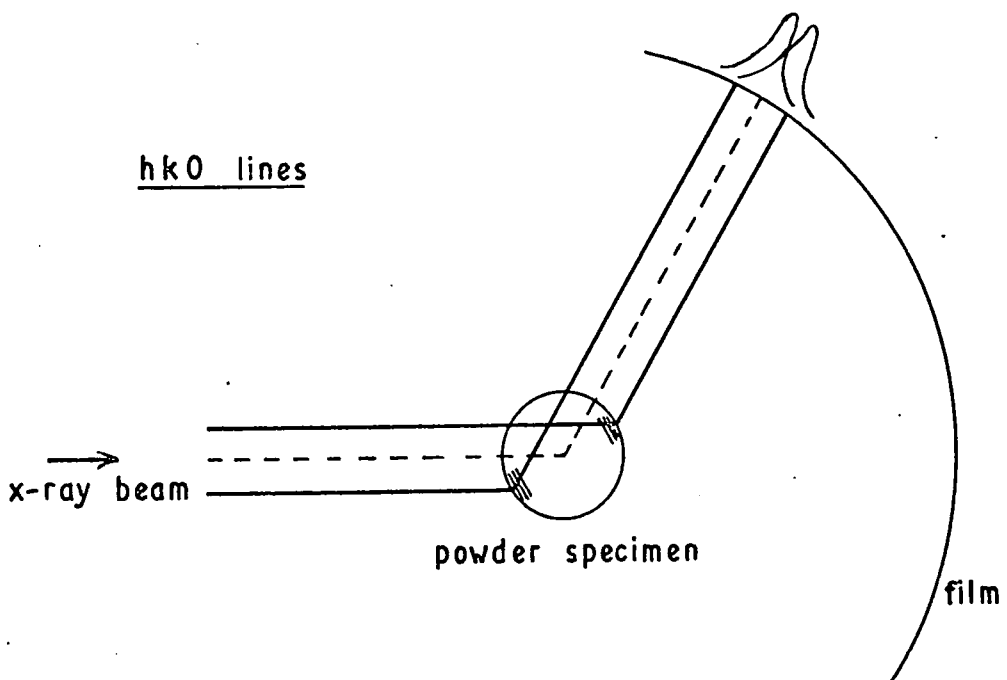
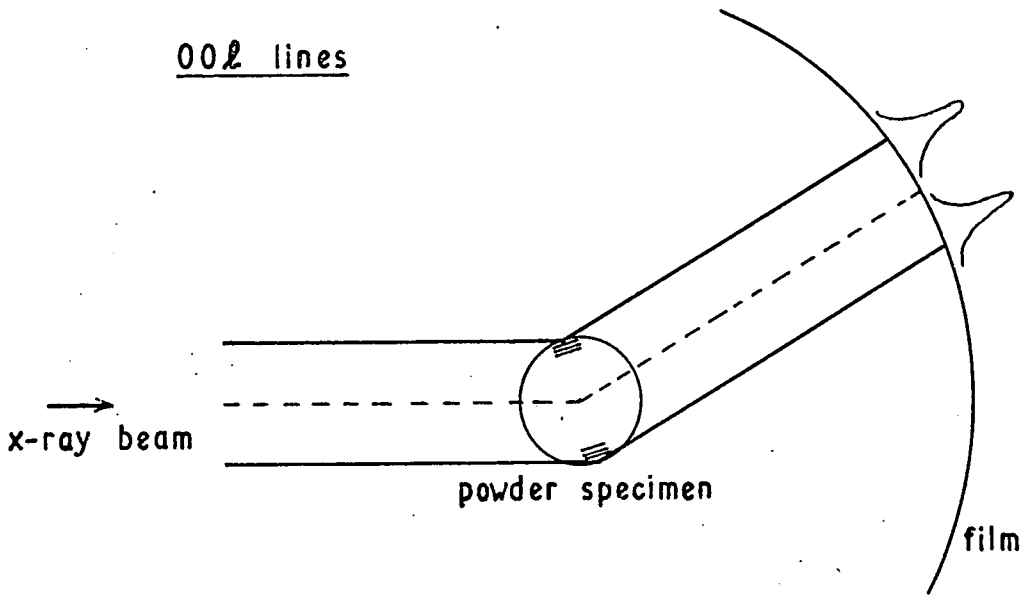
with powder using collodion is unsuitable. Specimens of known diameter can either be prepared by mixing the powder with collodion and extruding the mixture, or by packing the powder into a capillary tube. The latter method was adopted. Thin walled capillary tubes made of low absorbing Lindemann glass were used. The capillaries were supplied nominally as 0.3 mm diameter, but each length was found to taper considerably. They were further selected by passing an etched wire inside until it jammed and the capillary was broken off at this point. All the prepared sample diameters were measured with a travelling microscope and found to lie between 0.26 and 0.27 mm diameter. The thin walled capillaries are very fragile and a fair degree of manual dexterity was required to load the material without shattering the capillary.

The original Scherrer equation for line width and all the subsequent refinements assume that the specimen is a randomly arranged powder aggregate. It is extremely difficult to pack graphite powder with its platelike crystallites without getting preferred orientation, as the particles tend to line up parallel to any surface. Nelson and Riley<sup>95</sup> first reported the effects of preferred orientation in graphite powder samples, and showed that doubling of the lines occurs. This is because in cases of a high degree of orientation the specimen can be considered as a tube in which all the layer planes are perpendicular to the radii and filled with a small quantity of randomly oriented

material. The precise effect depends on the crystal reflection but the simple geometrical construction in figure 5.4 for the  $(00\ell)$  and  $(hk0)$  reflections shows that it is effectively only the material in the tube at the opposite ends of the appropriate diameter that produces the reflections which therefore result in two peaks. The construction also shows that for  $(00\ell)$  lines the peak separation is of the order of the normal line width but for  $(hk0)$  lines the peak spacing is less than the normal line width so that with preferred orientation an abnormally narrow  $(hk0)$  line would be obtained. First attempts at obtaining graphite powder specimens produced this effect with the  $(110)$  line narrower than the diamond standard. Since the  $(00\ell)$  peak separation is  $\cos \theta$  dependent the two peaks can easily be seen in the low angle  $(002)$  line. Fitzer, Fritz and Overhoff<sup>96</sup> made an extensive study of this problem and found that if the graphite powder was mixed in the correct proportions with a fairly thick grease a reproducible randomly oriented specimen could be prepared. As they were using a diffractometer they also wanted to put up the specimen absorption and so used a silicone grease. It was found that the method also worked well for loading capillaries for a Debye-Scherrer camera. In this case the increase in absorption was not wanted so Apiezon L vacuum grease was used instead. The graphite powder was first passed through a number 120 sieve to remove any large particles and then mixed with grease in the proportion

FIGURE 5.4

The effect of preferred orientation in a graphite powder sample



of 2 parts by weight of grease to 5 of graphite. The result is a thick plasticine-like consistency which can then be loaded into the capillaries without getting preferred orientation. This was tested by examining the (002) reflection. The addition of the grease puts up the background level of the film, and to make sure that there were no absorption edges anywhere near the lines being used, a sample of Apiezon grease was examined on a diffractometer. This showed a fairly uniform background in the area of importance.

#### 5.4.4 Choice of lines for analysis

As explained in section 5.3, in order to obtain the size of the layers and their thickness it is necessary to analyse three classes of lines; an (00 $l$ ) line to obtain the layer thickness, an (hk $l$ ) line to obtain the stacking factor, and an (hk0) line which gives the layer size after suitable correction for the stacking factor has been made. Optimum sensitivity is obtained when the instrumental broadening is as small as possible, and collimators and specimen sizes are kept low to aid this as already explained. However the line width for a given specimen size and collimator also depend on the Bragg angle and since this is a  $\cos 2\theta$  dependence the narrowest line width is obtained at high Bragg angles, Klug and Alexander<sup>97</sup> p.171. At very high Bragg angles a further source of broadening, due to the spectral line width of the incident radiation, begins to

become significant. This has a  $\tan \theta$  dependence<sup>98</sup> and so rises steeply at high angles. The optimum line width is thus obtained at high angles before the  $\tan \theta$  component has become significant and ideally the lines chosen for analysis should lie in this region.

In practice it turns out that there is very little choice for graphite. The first (hk0) line to appear is the (100) line but this cannot be used because the (101) line occurs so close to it that the tails overlap and the two cannot be properly separated. The (110) line, which is the only other line of this type with reasonable intensity, is therefore chosen. The (101) line must be rejected for the (hk $\ell$ ) line for the same reason and this leaves only the (112) line with reasonable intensity. The (110) and (112) lines are both fairly strong and lie in the same region, around  $80^\circ$  ( $2\theta$ ), and have similar intensities. The (00 $\ell$ ) line is chosen to fit in with the other two. The (002) line is rather broad because of the low Bragg angle of  $26^\circ$  ( $2\theta$ ) and in any case if the film is exposed to give a reasonable density for the (110) and (112) lines the (002) line is completely overexposed. The next line of this type, the (004) line, occurs at a high enough angle to bring the instrumental width down, but now its intensity is rather weak compared with the other two. It remains measurable, however, so it was the line chosen for analysis in this work.

The diamond line chosen to obtain the instrumental

broadening should lie in a similar region to the graphite lines being analysed. There are only five strong lines on the diamond film but fortunately the (220) line lies between the graphite (110) and (112) lines and is suitable for use as the standard.

#### 5.4.5 Film measurement

Line profiles were obtained from the films by measuring the density on a Hilger and Watts model L 451 microdensitometer. In this instrument light from a carefully controlled constant source is passed through the film on to a photocell. The output from this cell is thus inversely related to the film density. A slit which can be adjusted for both width and height controls the area of film illuminated and the optics are arranged to give a x 10 diminution of the slit size on the film. The film can be traversed across the light beam either by driving the lead screw by hand or by a synchronous motor working through a reduction gear box to give a very slow travel. The particular model which was available for use is primarily intended for examining spectrophotometer plates and so is not provided with a linear scale. However profiles could be obtained satisfactorily by using the motor drive and taking readings at timed intervals. The drive speed was measured and found to give a travel of 1 mm in 9.2 minutes, so that a reading taken every 15 seconds represent an interval of 0.028 mm which

is equivalent to  $0.028^\circ$  ( $2\theta$ ) for a 11.46 cm diameter camera. The slit length was the longest that could be used without getting errors due to line curvature. The optimum slit width depends on the resolution required. Highest resolution is obtained when the slit width is less than the scanning interval, but a very narrow slit gives a small output from the photocell. The good resolution of a narrow slit also shows up fluctuations due to film grain. These fluctuations can be smoothed by using slit widths greater than the scanning interval but with loss of resolution. A reasonable compromise between resolution and fluctuations was obtained with the slit width about half the scanning interval using a setting of 0.125 mm with a length of 16 mm.

Since the tail region of the lines is so important in the analysis it was necessary to start scanning the film well away from the line and to continue for an equivalent distance on the other side of the peak. This meant that it could take around 40 minutes to scan a fairly broad line. To keep conditions constant the lines were all scanned from the high  $\theta$  side to the low  $\theta$  side.

In practice it was found that the range of film densities that could be handled by the microdensitometer was fairly limited. This is because the narrow slit width used meant that if the film density was too high the photocell output became too low to use. It was necessary to arrange the film exposure time to

give the optimum maximum density for each sample, and as explained in section 5.4.1 this exposure varied with the degree of graphitisation. Because the optimum densities were fairly low it was assumed that they were in the linear region of the film response curve and a step-wedge calibration of the film response was therefore not carried out.

To allow for the logarithmic relation between film transmission and x-ray intensity the photocell output was plotted on logarithmic graph paper and subsequently measured up for analysis.

### 5.5 Method of analysis

The theory of the method of analysis of the lines using variance as a measure of line broadening has been described in sections 5.2 and 5.3. This section will consider how it was put into practice.

The readings from the microdensitometer are plotted on logarithmic graph paper and the best smooth curve is drawn through the points to average out the fluctuations due to film grain. Before any measurements can be made the background level must be drawn in. The background level on a Debye-Scherrer film is in general a curve with the level decreasing with increasing Bragg angle until the mid range of the film is reached and then increasing again in the back reflection region of the film. Langford and Wilson<sup>83</sup> showed that there is little

error introduced if over the width of the line the background is assumed to be linear, but not necessarily constant. The best straight line joining the extremes of the microdensitometer readings was thus taken as the background level.

The first stage of the analysis is to separate out the  $\alpha_1$  component of the line. Since the incident radiation, nickel filtered copper  $K_{\alpha}$  lines, consists of a doublet close together, each line obtained is also a doublet which is only resolved at high Bragg angles. Fortunately sufficient is known about the doublet to make the separation process relatively simple. The wavelengths of the two lines are known accurately, 1.54051 and 1.54433 Å<sup>99</sup>, so that the separation at any Bragg angle can be worked out. It is also known that the intensity of the  $\alpha_1$  component is almost exactly twice that of the  $\alpha_2$  component. Based on this Rachinger<sup>101</sup> devised an extremely simple geometrical method of separating the two components and this method was used. The curve is divided up into a suitable number of intervals and a second scale drawn which is displaced by an amount equal to the doublet separation. By working from the low  $\theta$  side of the curve and successively subtracting the  $\alpha_2$  component (which is half the  $\alpha_1$  component at a position one doublet separation earlier) the two components can be obtained from the original curve. Only the  $\alpha_1$  component is used for the subsequent analysis.

The next stage is to obtain the mean, variance and the

variance as a function of range. For this purpose the curve was divided into 30 or more numbered intervals and the intensity read off and tabulated. Columns of the values of  $nI$  and  $n^2I$  were constructed, where  $I$  is the intensity at the numbered interval  $n$ , and the columns summed.

The mean is then 
$$\frac{\sum nI}{\sum I}$$

and the variance is 
$$\frac{\sum n^2I}{\sum I} - \left( \frac{\sum nI}{\sum I} \right)^2$$

This is standard statistical computational procedure and can be carried out easily with the aid of a desk calculator. Although slightly tedious it was not thought necessary to programme it for the computer.

Langford and Wilson<sup>83</sup> showed that the variance-range analysis gave best results if the range used was symmetrical about the mean, so the value of the mean obtained was used to set the mid point for the range, and the variance as a function of range could be worked out by a method of successive subtraction using the values already tabulated. A plot of the variance versus range was almost invariably curved in the tail region, indicating that the background level had been drawn in incorrectly. Depending on the amount of the curvature an estimate of the background error was made and the variance recalculated until the optimum level with a linear tail region was obtained. With a little experience it was seldom necessary to do more than two recalculations before the optimum value was

found. The slopes and intercepts of the linear regions were then used as described in section 5.3 to find the stacking factor, layer size and thickness, and the strain.

## 5.6 Experimental results

Specimens were prepared and x-ray films taken of sections B, C, D, F, G and H of bar 22. Since only small quantities of material are necessary to prepare the specimens this was taken from the actual samples used for the mobility and thermal conductivity measurements. The (004), (110) and (112) lines on each film were measured up and analysed. To illustrate the process the complete results are given for one sample, 22 F, roughly in the middle of the range, and for the diamond standard. Figure 5.5 gives a plot of the microdensitometer readings for the 6  $\mu\text{m}$  diamond standard and shows the doublet separation. Figure 5.6 shows the variance of the  $\alpha$ , component of this line plotted as a function of the range of integration and shows how a linear tail region is obtained if the background level is optimised. A slope of  $0.0094^\circ$  ( $2\theta$ ) was obtained for the tail region with optimum background. Figures 5.7, 5.8 and 5.9 give the microdensitometer plots of the (004), (110) and (112) lines for graphite 22 F and figures 5.10, 5.11 and 5.12 the corresponding variance-range plots. Figure 5.11 also shows the line obtained when the point by point correction for the stacking faults has been made.

FIGURE 5.5

Microdensitometer readings of the 220 line from the 6  $\mu\text{m}$  diamond standard

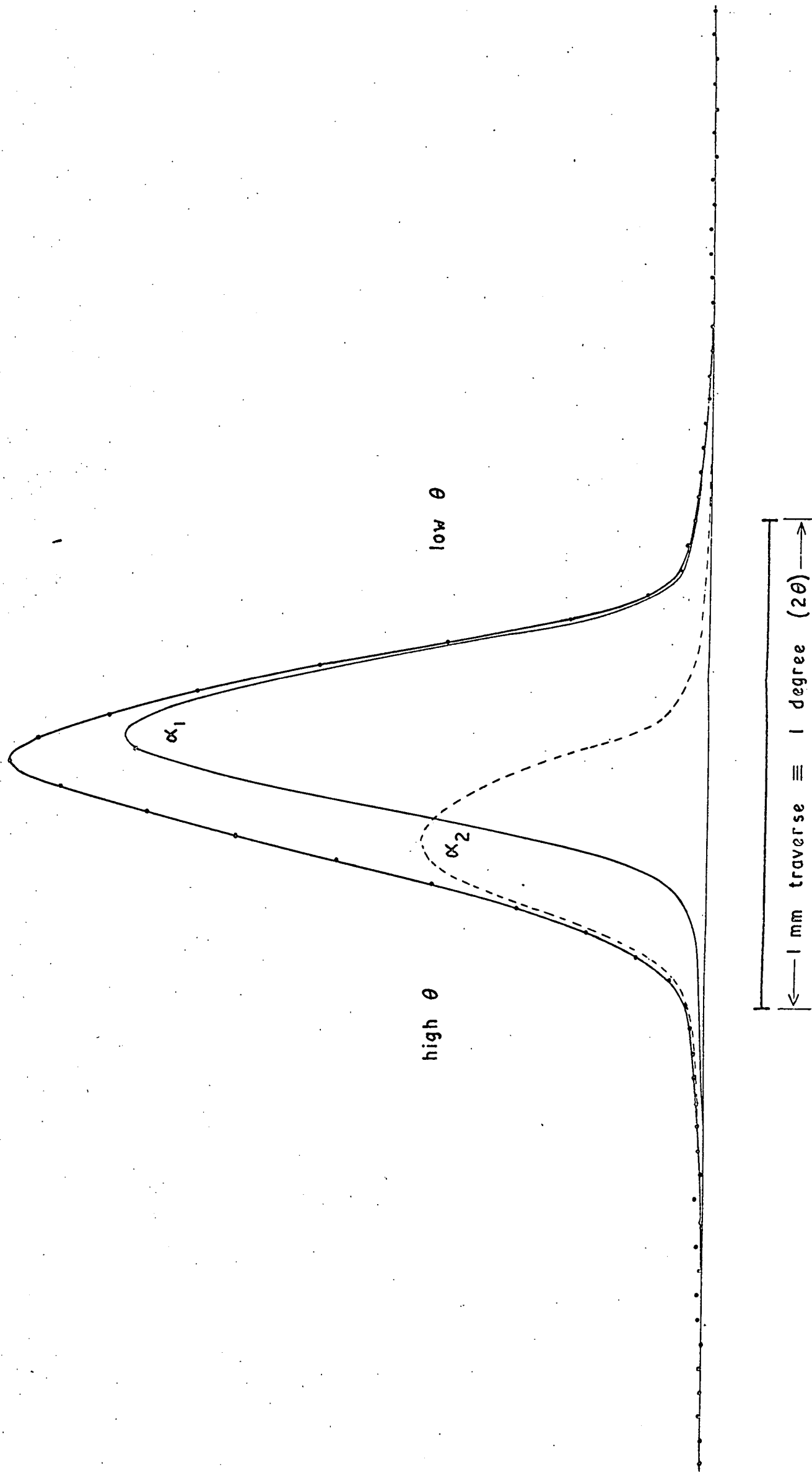


FIGURE 5.6

Variance-range plot of the 220 line from the 6 $\mu$ m diamond standard

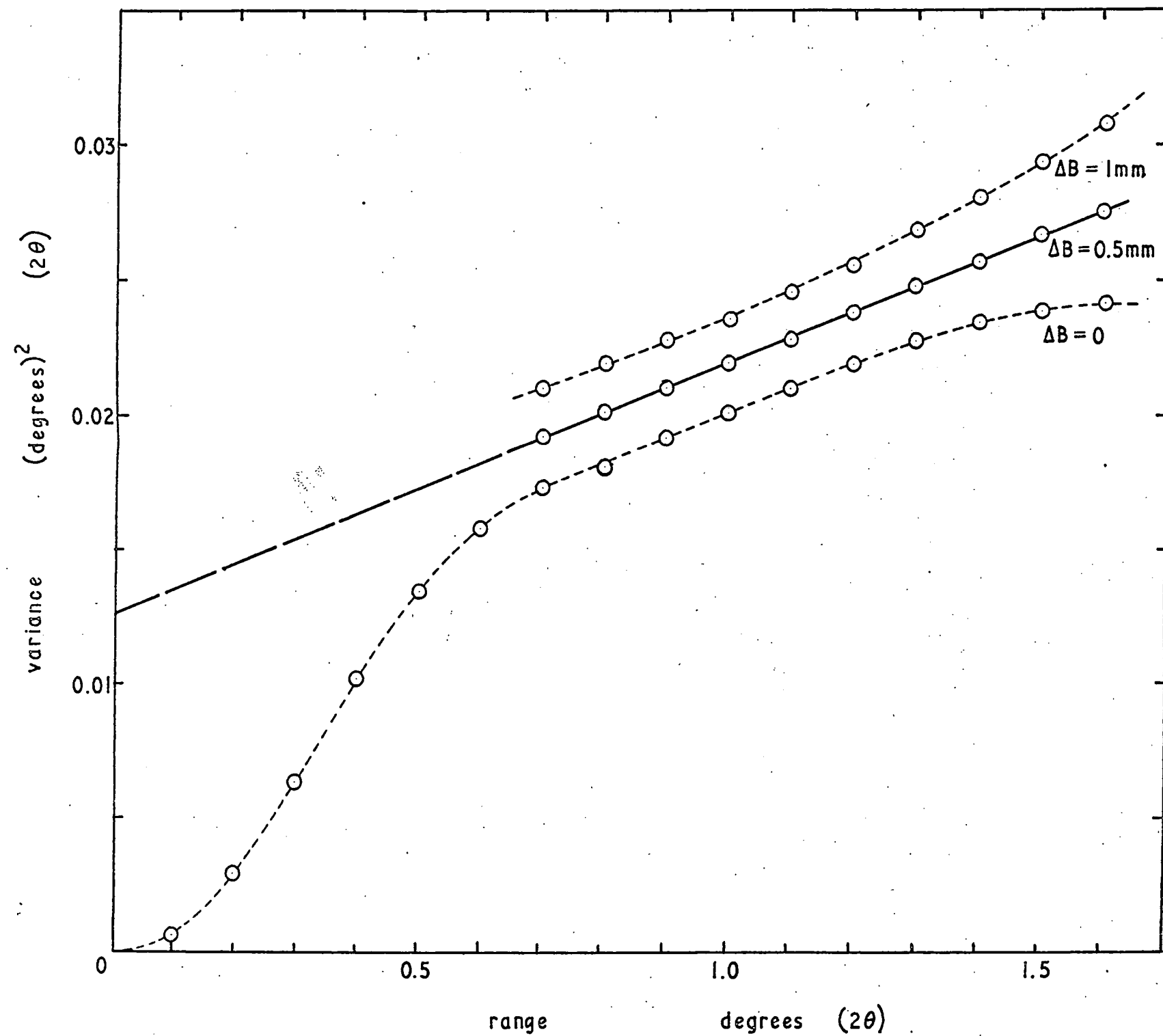


FIGURE 5.7

Microdensitometer readings of the 004 line from section 22 F

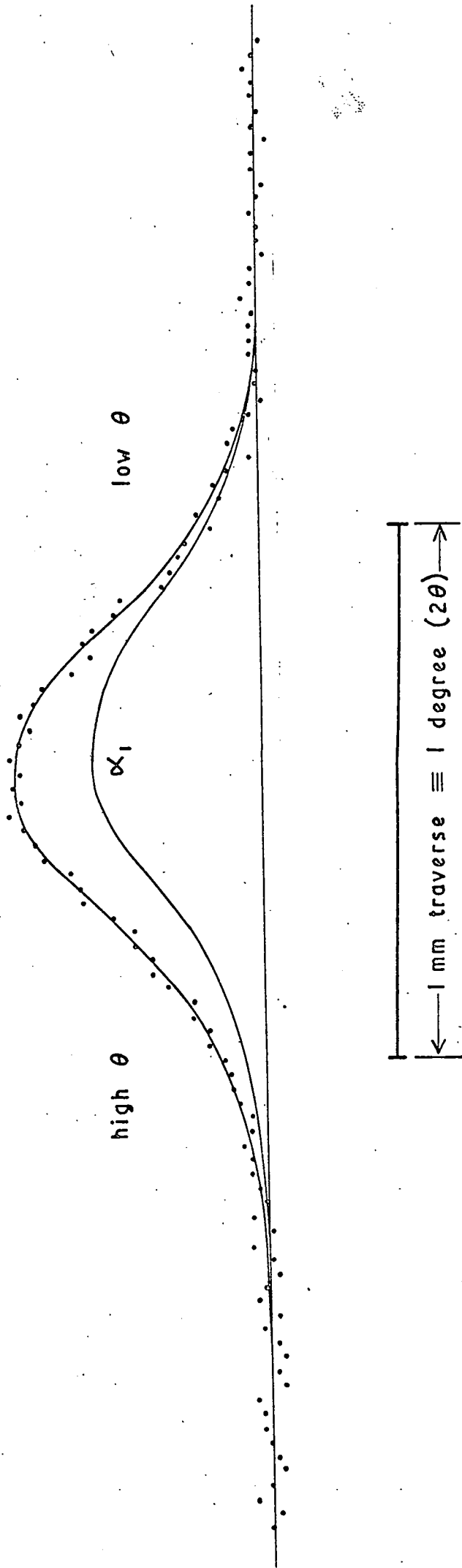


FIGURE 5.8

Microdensitometer readings of the 110 line from section 22 F

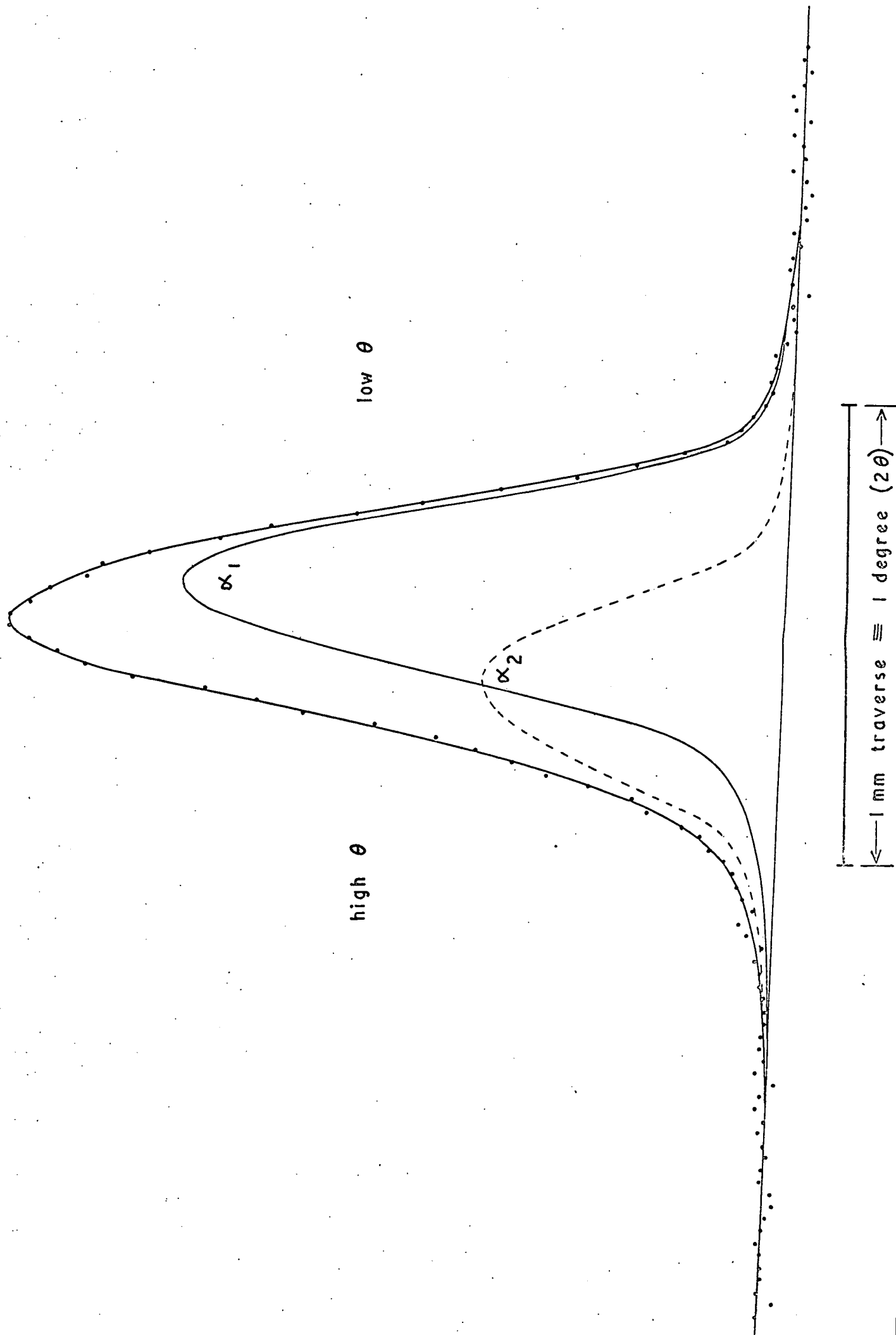


FIGURE 5.9

Microdensitometer readings of the 112 line from section 22F

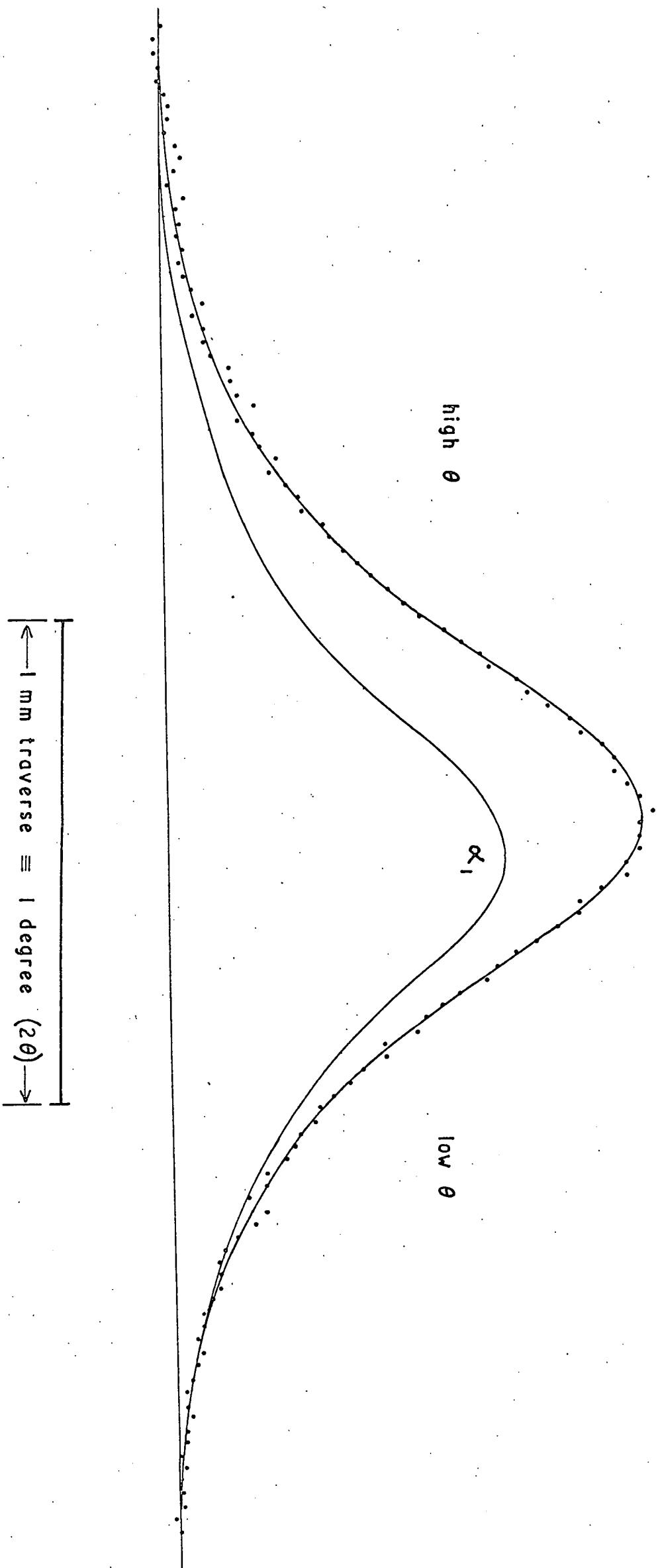


FIGURE 5.10

Variance-range plot of the 004 line from section 22 F

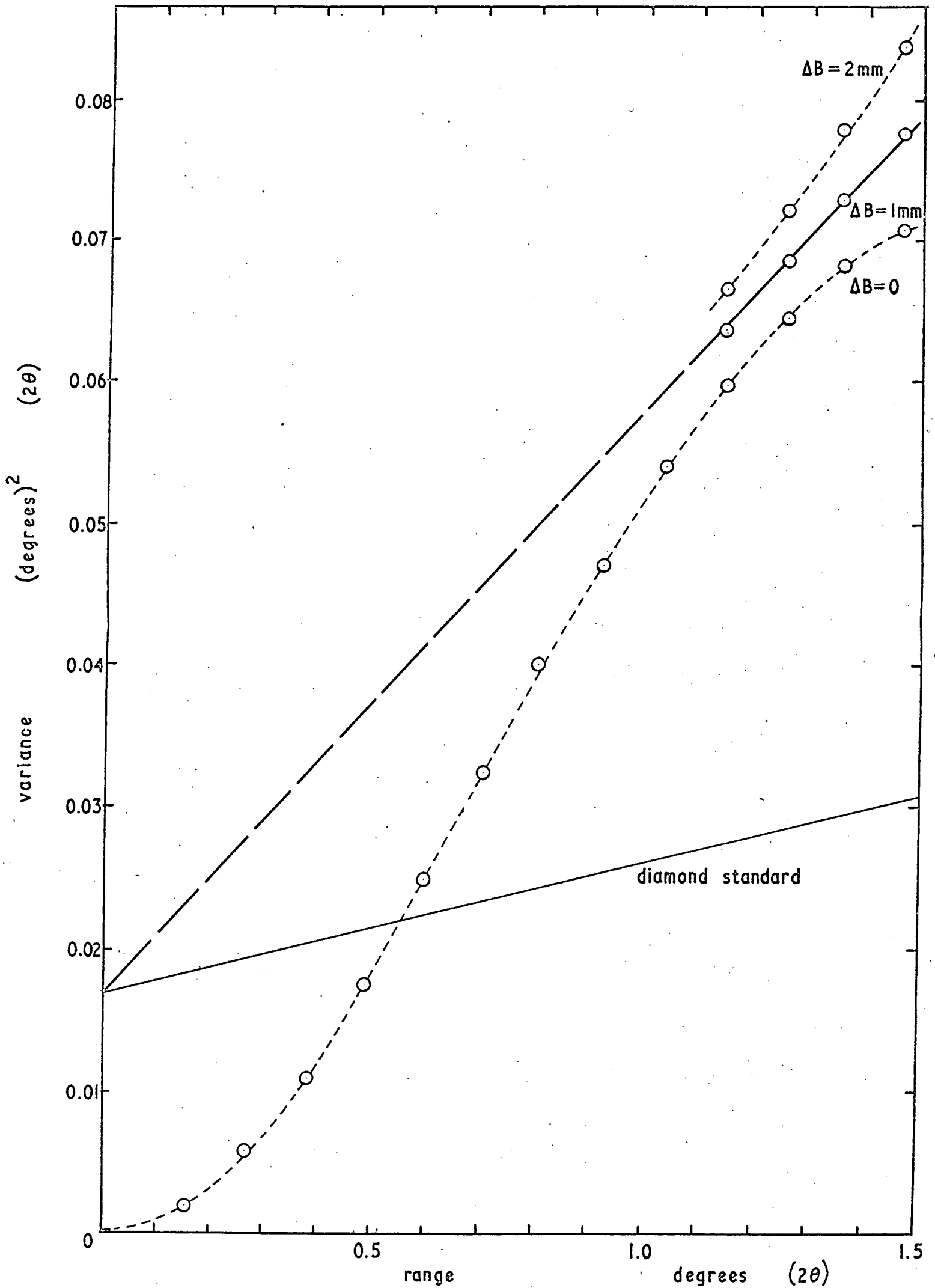


FIGURE 5.11

Variance-range plot of the 110 line from section 22F  
showing the stacking fault correction

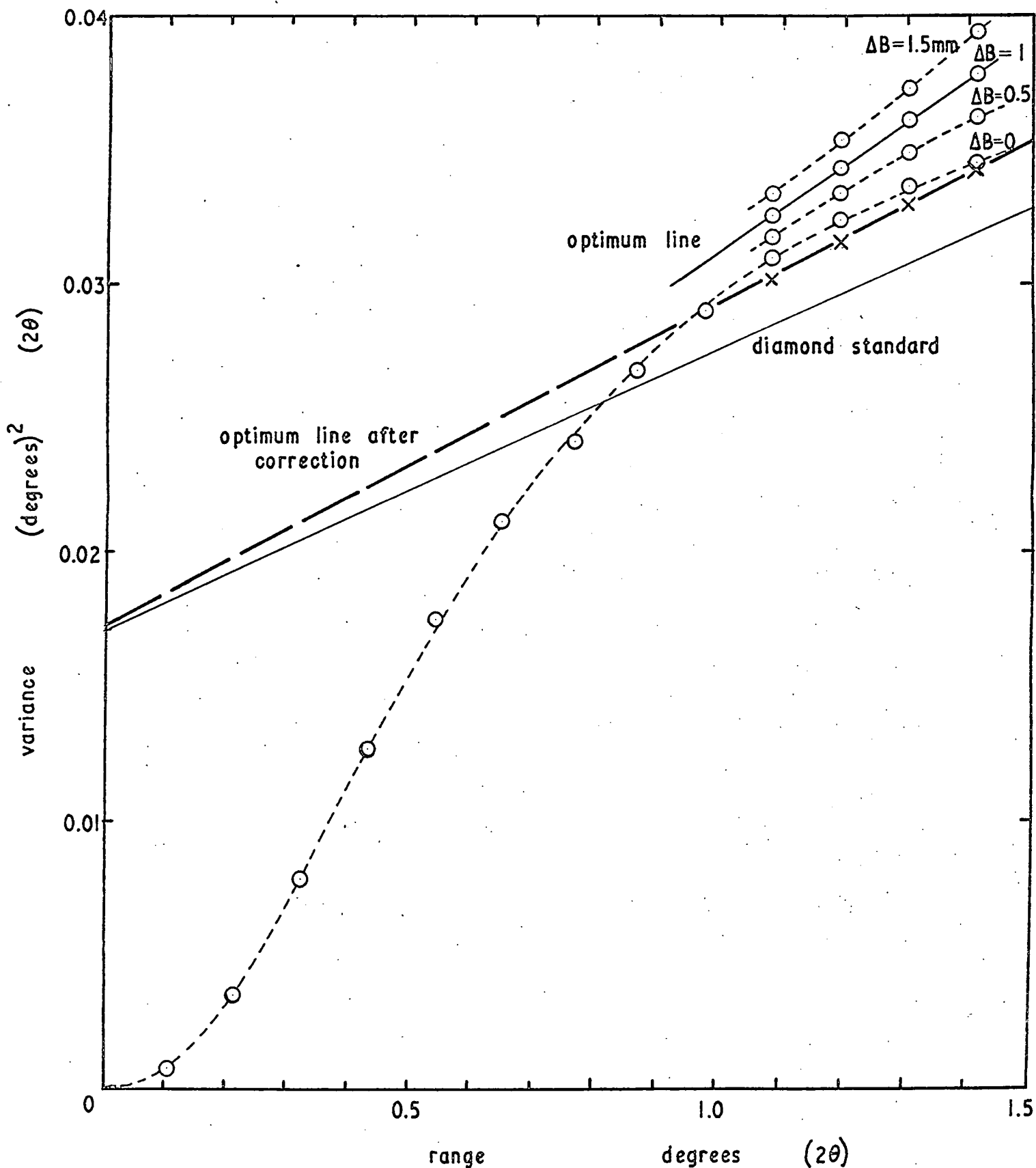
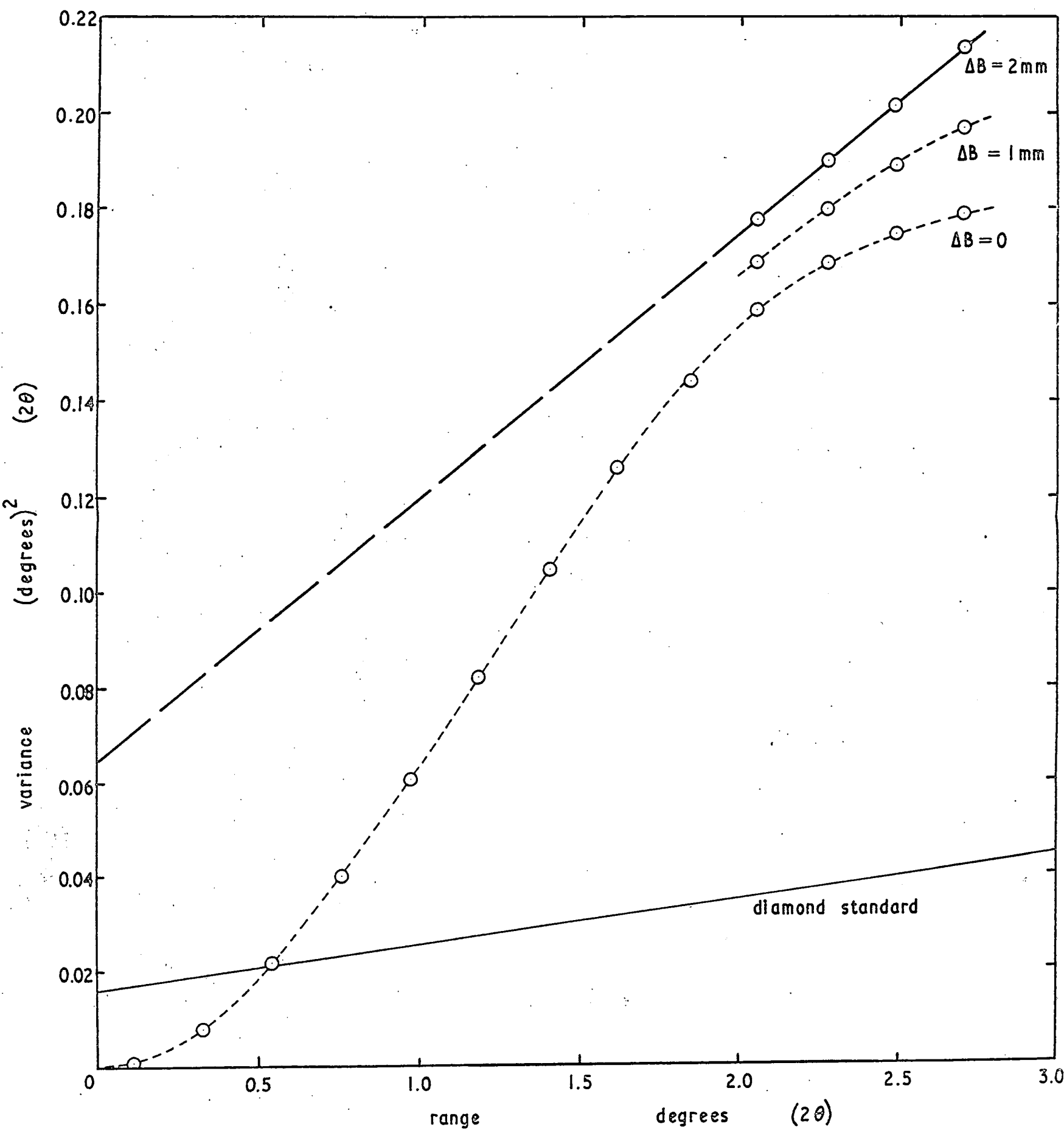


FIGURE 5.12

Variance-range plot of the 112 line from section 22F



### 5.6.1 Layer thickness

The thickness of the platelike crystallites in the c-direction was obtained by analysing the (004) lines from all the films and using the slope of the variance-range plot to give the crystallite size as described in sections 5.2 and 5.3. This analysis proved to be relatively straightforward since the range of crystallite sizes obtained was ideally suited to the method. The only slight difficulty was the rather low intensity for these lines on films that were exposed to give the optimum density for the (110) and (112) lines. The r.m.s. strain was obtained from the intercepts of the variance-range curves and these and the crystallite thicknesses are given in the table.

Section	Layer thickness $L_c$ Å	r.m.s. strain
B	1000	$1.9 \times 10^{-3}$
C	850	$1.9 \times 10^{-3}$
D	530	$1.8 \times 10^{-3}$
F	180	0
G	100	$2.6 \times 10^{-3}$
H	60	$3.4 \times 10^{-3}$

As expected, samples from the inside of the bar which have been heated to a higher temperature during deposition have larger crystallite thicknesses. The surface deposits have crystallites which are only 17 atomic layers thick compared with about 300 for the innermost deposits.

Sections B, C and D show little variation in strain but section F was found to be strain free. Since this section is next to the join (see figure 3.1) it must be presumed that the crack has served to relieve the strain in this section. The strain increases again in the surface layers which have had little annealing.

### 5.6.2 Stacking factor

The stacking factor,  $p$ , was obtained from the variance-range curves of the (112) lines as described in section 5.3. Results could not be obtained for section H, nearest to the surface of the bar, since this sample was so poorly graphitised that none of the 3-dimensional lattice lines appeared. Values for the stacking factor are as follows:-

Section	Stacking factor
B	0.0114
C	0.0123
D	0.0105
F	0.0186
G	0.080

These values were used to make the stacking fault correction to the (110) lines. Apart from section G which is clearly less well graphitised there is not a large variation, with a stacking fault only occurring about every 50 or 100 layers. Bacon<sup>100</sup>

showed that grinding graphite to a powder leads to an increase in defects so that the stacking factor obtained cannot be considered as an intrinsic property of the graphite. The apparently inconsistent low value for section D probably indicates only that a smaller amount of mechanical work was done in obtaining the powder specimen.

### 5.6.3 The a-direction layer size

The (110) lines for sections B, C, D, F and G were measured up, the profiles analysed to yield variance-range curves which were optimised. The stacking factors obtained from the (112) lines and given in the previous section were used to work out the Wilson stacking fault correction given in section 5.3. This correction was obtained as a function of range and was subtracted point by point from the variance values in the tail region of the profiles. The corrected values were then used to draw a new straight line whose slope and intercept were used to obtain the layer size and strain.

This analysis could not be carried out on the (110) line from section H since this sample was so poorly graphitised that the (110) line was strongly asymmetrical. Instead the layer size was worked out from the half width of the profile. The half width was first corrected for instrumental broadening using the Jones (b) correction curve and the layer size obtained using the random layer lattice Scherrer constant of 1.84.

(See sections 5.2 and 5.3.) Using this method no allowance can be made for the strain so an additional check was made by working out the layer size from the peak shift of the line. Since the two results are in very good agreement it can be concluded that the strain component did not contribute significantly to the width of the line. The results obtained for all the sections are given in the following table.

Section	Estimated formation temperature, °C	Layer size $L_a$ Å	r.m.s. strain
B	3020	31,000	$0.33 \times 10^{-3}$
C	2980	21,000	$0.79 \times 10^{-3}$
D	2910	19,000	$0.76 \times 10^{-3}$
F	2700	2,600	0
G	2550	1,200	$1.0 \times 10^{-3}$
H	2330	halfwidth 140 peak shift 130	-

The strain values are somewhat lower than those in the c-direction and section F is again strain free. The lower strain value in this direction is what would be expected from the layer structure of graphite since it is much easier to introduce c-direction strain by 'wrinkling' the layers than it is to distort the hexagon network in which the binding is so much tighter. Before correction the values for  $L_a$  ranged from 280 Å for section G to 4200 Å for section B.

#### 5.6.4 Accuracy

The accuracy which can be expected from x-ray determination

of crystallite sizes depends upon the range of sizes being examined. The method consists essentially of subtracting the known instrumental line width from the line width of the sample to yield the pure diffraction width. It follows that greater accuracy is obtained when the measured line is very broad compared with the instrumental line width, i.e. for the smaller crystallite sizes. Determination of the a-direction layer size of sections B, C and D in which the measured line was very little broader than the standard pushed the method right to its limit and it is unlikely that the accuracy of the determination was any better than  $\pm 50\%$  at this end of the size range.

The c-direction thickness, ranging between 60 and 1000 Å, is the size range most suitable for this method of determination and the results are probably accurate to  $\pm 10\%$ . Greater accuracy could probably have been achieved if a separate and even longer exposure had been made for the (004) line profile determination. As explained in section 5.4.4 the film was exposed for the (110) and (112) lines and consequently the (004) line was a little faint.

## 5.7 Discussion

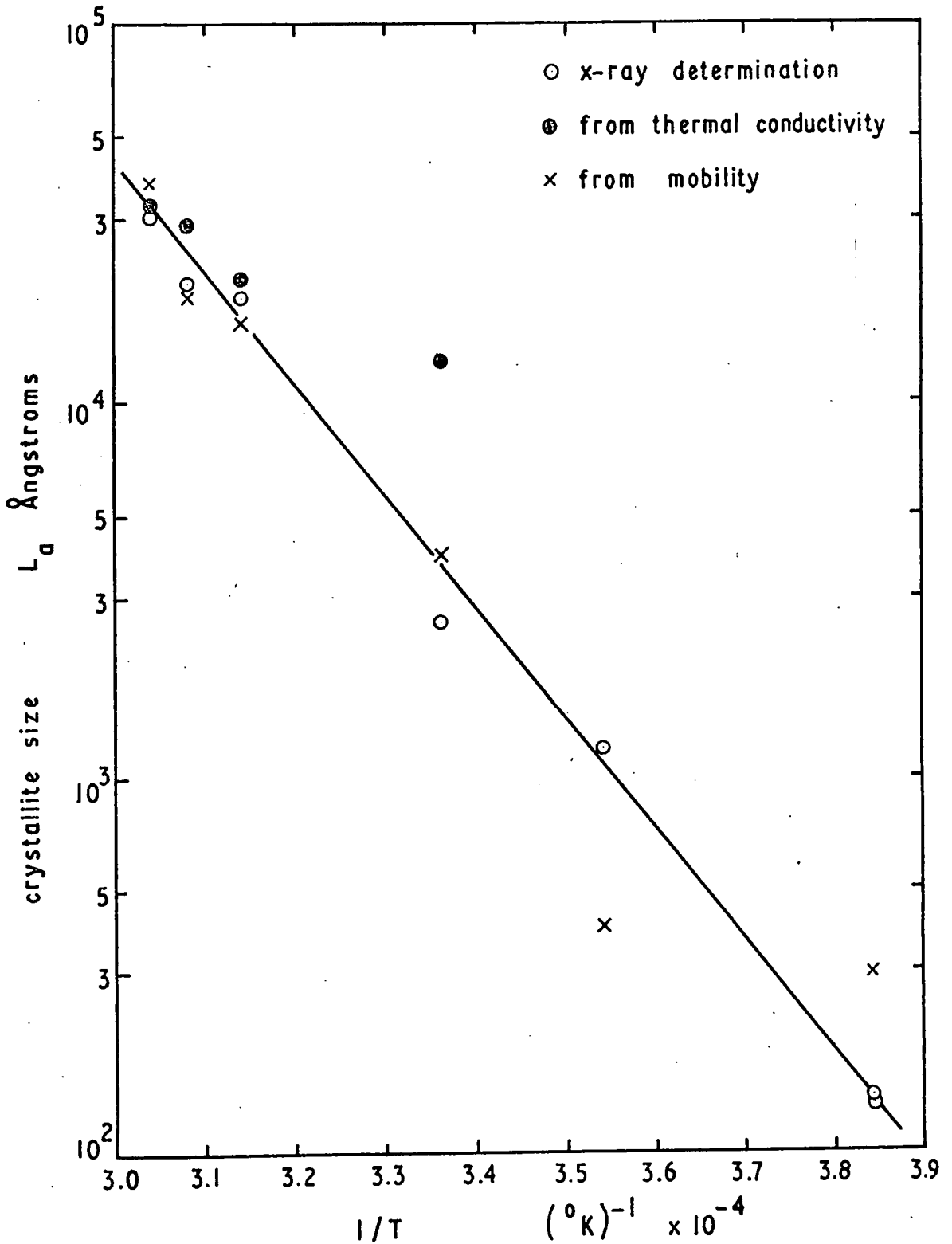
Using the stacking fault correction the a-direction layer sizes are in very good agreement with the crystallite sizes estimated from the mobility and thermal conductivity measurements.

(See section 4.4.) Without the stacking fault correction the layer sizes are nearly an order of magnitude lower. Such good agreement between the x-ray determination and indirect estimates of the crystallite sizes has not been reported anywhere previously and it shows that provided allowance is made for stacking faults, line broadening is a reliable method of obtaining the crystallite sizes. The need for complex mosaic theories of grain structure is removed.

Results from all three methods of determination are shown in figure 5.13 where the crystallite size is plotted on a log scale against the reciprocal of the estimated formation temperature. All the points lie reasonably about a straight line demonstrating the agreement between the methods. It should be noted that although the x-ray measurement becomes more accurate for smaller crystallite sizes the reverse is true for estimates from the mobility and thermal conductivity since both rely on using departure from single crystal temperature dependence. The mobility results become increasingly scattered about the line for the low formation temperature samples. As explained in chapter 4 the Smith and Rasor method works well when the thermal conductivity has the expected temperature dependence but section F departs from this and the crystallite size estimated in this way lies well away from the line in figure 5.13. From the slope of the line in this graph an activation energy for the crystallisation process can be obtained.

FIGURE 5.13

The a-direction crystallite size of sections from bar 22 as a function of formation temperature

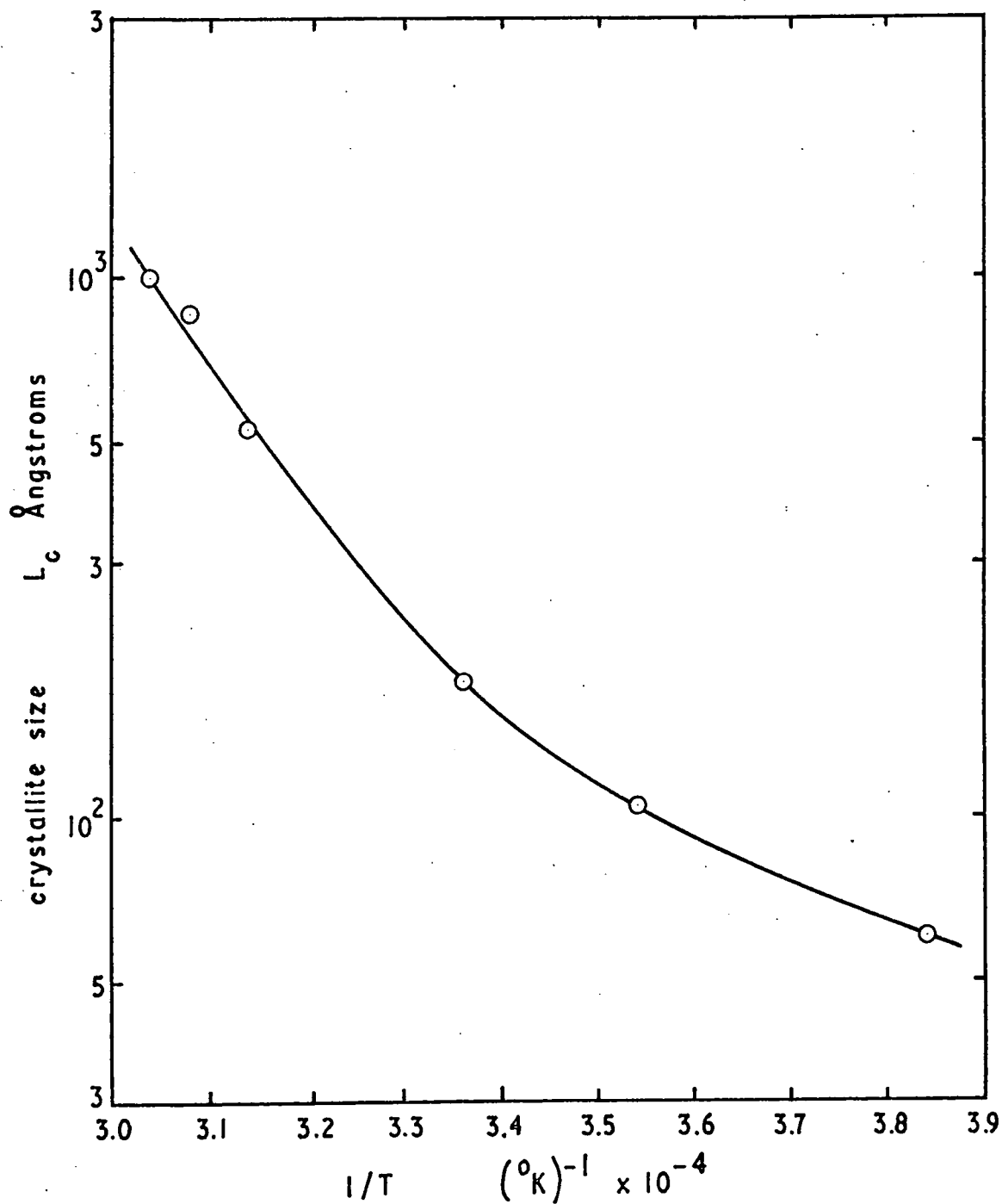


This is found to be 5.9 eV and the significance of this value will be discussed in the final chapter.

The c-direction layer thickness is shown plotted in a similar way in figure 5.14 and the points lie on a smooth curve. It is possible that the curve is approaching the 5.9 eV line which can be drawn through the values for sections B, C and D but results would be needed at higher formation temperatures to confirm this.

FIGURE 5.14

The c-direction crystallite size of sections from bar 22 as a function of formation temperature



## CHAPTER 6

### GENERAL DISCUSSION

This chapter is concerned with bringing together results from the previous four chapters and it divides naturally into two parts. The first part will discuss the Etingshausen cooling which might be expected from the graphite produced, compare the results with predictions and comment on the prospects of obtaining any worthwhile improvement. The second part will consider the relation between the deposition processes and the structure and properties of the resultant material.

#### 6.1 Etingshausen cooling

As shown in section 1.2, the figure of merit for Etingshausen cooling is

$$Z = \frac{Q^2 B^2 \sigma}{K}$$

which for high magnetic fields with  $\mu B \gg 1$  becomes

$$Z = \frac{Q^2}{\mu^2} \cdot \frac{\sigma_0}{K_L}$$

The values for  $Q$ ,  $\mu$  and  $\sigma$  obtained by Mills and given in section 1.5.1 can be used, together with the results for  $K$  from chapter 4, to obtain a value for  $Z$  in the temperature range down to  $70^\circ\text{K}$ , the lower limit of the measurements.

For sample 22 B which was prepared at the highest temperatures and is the specimen which most nearly approached the single crystal properties, the value of  $Z$  is  $9 \times 10^{-5} \text{ deg K}^{-1}$  at  $300^\circ\text{K}$  falling to a minimum of  $5 \times 10^{-5} \text{ deg K}^{-1}$  at  $145^\circ\text{K}$  and rising again to  $7 \times 10^{-5}$  at  $70^\circ\text{K}$ . These values of  $Z$  are much too low to give useful cooling since the corresponding values of  $\Delta T_{\text{max}}$  are only 4 deg K at room temperature falling to 0.2 deg K at  $70^\circ\text{K}$ . Clearly it is the extremely high value of the thermal conductivity in this temperature range which leads to such low values of  $Z$ . To examine whether there is any possibility of  $Z$  reaching useful values at low temperatures the next section will discuss the extrapolation, down to liquid helium temperatures, of the individual components of the high field figure of merit.

#### 6.1.1 Extrapolation to liquid helium temperatures

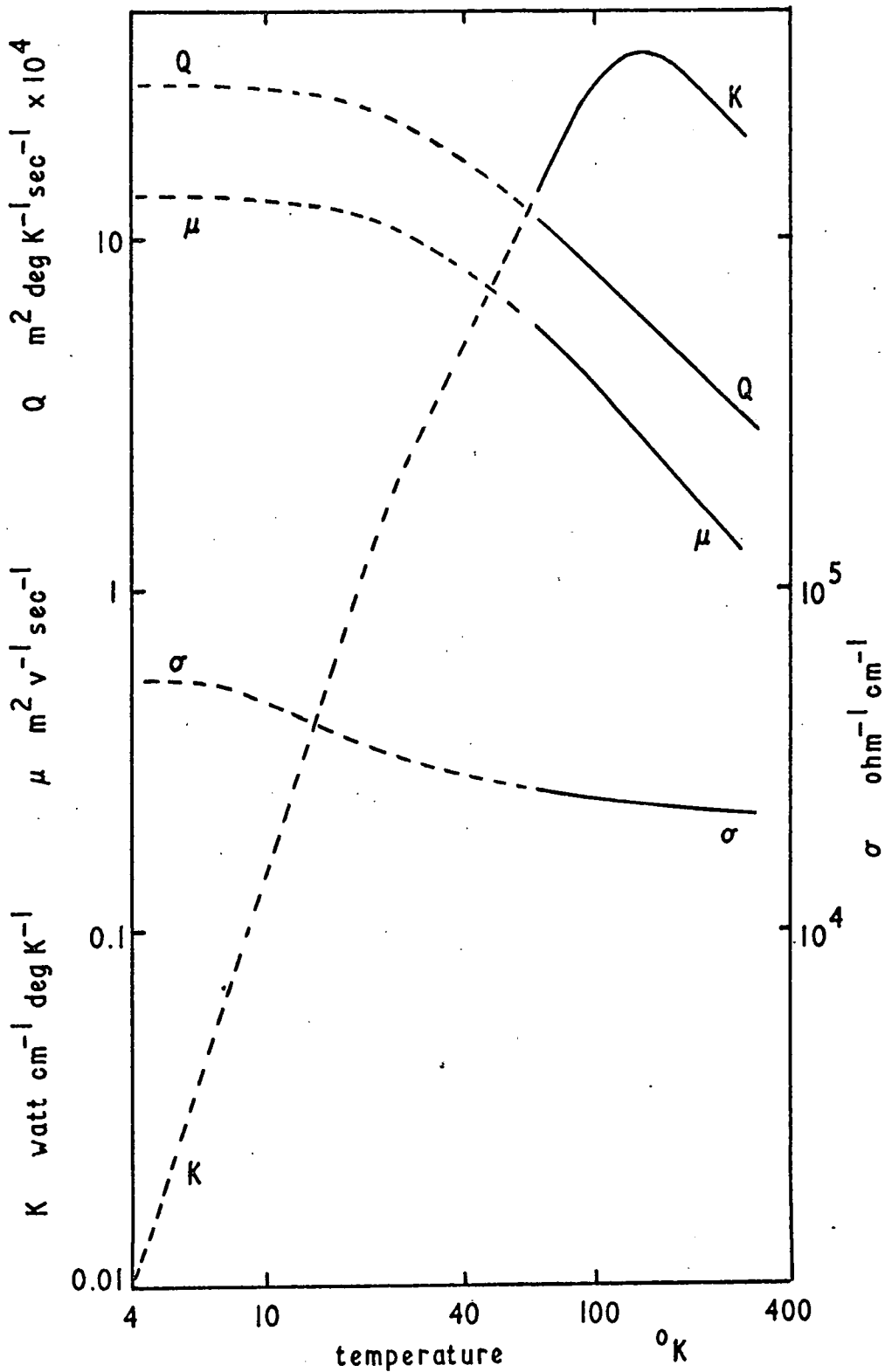
The expected behaviour of the low temperature thermal conductivity of pyrolytic graphite has already been discussed in chapter 4 where it was shown that on the low temperature side of the peak the thermal conductivity would fall as  $T^2$ , and at some lower temperature change to a steeper near  $T^3$  dependence. The transition would not occur in defective graphites and would occur at progressively higher temperatures with increasing perfection. This behaviour was confirmed by the measurements of Holland, Klein and Straub<sup>70</sup> on one sample

of pyrolytic graphite which had been heat treated at  $3250^{\circ}\text{C}$ . Since sample 22 B had a thermal conductivity approaching that of the sample measured by Holland, Klein and Straub it would seem reasonable to use their results as a basis for the extrapolation and in figure 6.1 the measured curve is shown together with the extrapolation. Holland, Klein and Straub also measured the electrical conductivity of the same graphite sample and again, since Mills' results for the electrical conductivity of sample 22 B, given in section 1.5.1, approach the values they obtained, their work can be used for the extrapolation and the measured and extrapolated curve is also shown in figure 6.1.

Mills' measurements of the carrier mobility of sample 22 B, shown in figure 1.4, are approaching the single crystal values at high temperatures but fall off at lower temperatures. It was assumed that this was due to the onset of crystallite boundary scattering so that an extrapolation to lower temperatures is obtained by supposing that the mobility will saturate at some constant value related to the crystallite size and this extrapolation is shown in figure 6.1. Measurements of the Nernst coefficient, displayed in figure 1.5, showed nearly the same temperature dependence as the carrier mobility, which is the behaviour to be expected from the expressions for the coefficient given in section 1.3. A similar extrapolation can thus be used for the Nernst

FIGURE 6.1

Measured values of the components of the Ettingshausen figure of merit of sample 22 B and their extrapolation to  $4^{\circ}\text{K}$



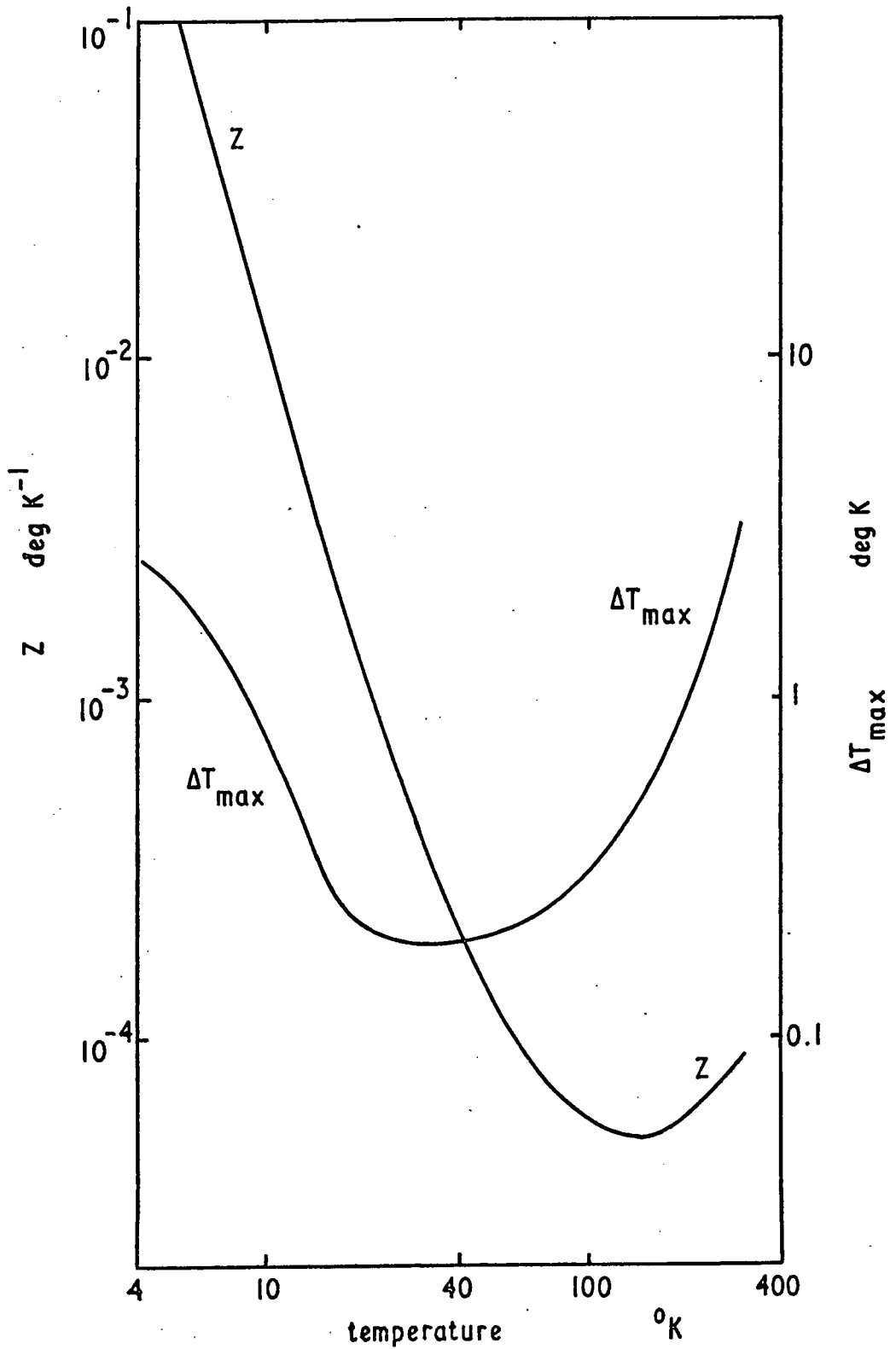
coefficient and a curve nearly parallel to the mobility curve is shown in figure 6.1.

Using the extrapolated curves for  $K$ ,  $\sigma$ ,  $\mu$ , and  $Q$  an estimated curve for the figure of merit,  $Z$ , is obtained and is shown in figure 6.2. The corresponding values of  $\Delta T_{\max}$  are also shown. Because of the rapid fall in the thermal conductivity,  $Z$  reaches values of a little over  $10^{-1}$  deg  $K^{-1}$  at  $4^{\circ}K$  which is nearing a useful value. However in the important mid-range of temperature between  $70^{\circ}$  and  $20^{\circ}K$  the value is still so low that the amount of cooling would be negligible.

The results of this extrapolation can be compared with a short research note reporting measurements of the thermomagnetic figure of merit of pyrolytic graphite at liquid helium temperatures. Goldsmid and Lacklison<sup>102</sup> attempted to measure the figure of merit of a sample of graphite, supplied by R.J. Diefendorf of the General Electric Company, United States, which had received a post deposition heat treatment at  $3500^{\circ}C$ . No experimental details are given but they obtained the figure of merit both by measuring the Etingshausen temperature difference directly and also by separately measuring the Nernst coefficient and thermal and electrical conductivities. Good agreement was obtained between the two methods which resulted in a maximum value for  $Z$  of  $9 \times 10^{-4}$  deg  $K^{-1}$  at a magnetic field of 500 G. This is some two orders of magnitude less

FIGURE 6.2

Predicted values of the Ettingshausen figure of merit  $Z$  and the maximum temperature difference  $\Delta T_{\max}$  for sample 22B



than the value predicted by extrapolation and it is worth examining their work a little closer to see if the source of the discrepancy can be found. They report values for the electrical conductivity and mobility of  $7.8 \times 10^5 \text{ ohm}^{-1} \text{ cm}^{-1}$  and more than  $10^6 \text{ cm}^2 \text{ V}^{-1} \text{ sec}^{-1}$  which are similar to the values obtained by Soule on single crystal specimens. Both values are approximately an order of magnitude larger than those predicted for sample 22 B at  $4.2^\circ \text{K}$ . The value of  $0.3 \text{ watt cm}^{-1} \text{ deg K}^{-1}$  for the lattice thermal conductivity is surprisingly high and does not entirely agree with the measurements of Holland, Klein and Straub even if allowance is made for the better quality of the material. It would have been helpful if the measurements had been made over a range of temperature so that the temperature dependence could have been examined. The resulting value of  $\sigma_0/K_L$  is about half that obtained by Holland, Klein and Straub. Using the reported values of the electrical conductivity, thermal conductivity, mobility and figure of merit it can be deduced that the value of the Nernst coefficient measured must have been  $18.6 \text{ cm}^2 \text{ deg K}^{-1} \text{ sec}^{-1}$ . This should be compared with the value of  $10.5 \text{ cm}^2 \text{ deg K}^{-1} \text{ sec}^{-1}$  for sample 22 B at  $80^\circ \text{K}$  and is obviously the major source of the discrepancy in the figure of merit. A much higher value of  $Q$ , corresponding to the high mobility, would have been expected, and again it would have been helpful if both  $Q$  and  $\mu$  had been measured as a function of temperature so that the relation between the two could have

been examined. Mills' measurements of  $Q/\mu$  agreed quite well with his theoretically obtained values so that it is surprising that the Nernst coefficient measured by Goldsmid and Lacklison is so low. Either the experimental results are in error or the simple theory of the Nernst effect breaks down in this material at low temperatures.

### 6.1.2 Phonon drag

In section 1.3 it was pointed out that a phonon drag contribution to the Nernst coefficient could possibly outweigh the disadvantage, as far as Etingshausen cooling is concerned, of the extremely high thermal conductivity of graphite. Such a contribution would be detected by examining the temperature dependence of the Nernst coefficient and the mobility. In the absence of phonon drag the Nernst coefficient would be expected approximately to follow the same temperature dependence as the mobility, except for a slight deviation due to the energy gap term in the expression for the Nernst coefficient of intrinsic material. Phonon drag would lead to enhanced values of  $Q$  over part of the temperature range. The measurements made by Mills of the Nernst coefficient of the samples did show a temperature dependence similar to that of the mobility, so on this reasoning it can be assumed that a phonon drag contribution is not obtained. However measurements of the thermoelectric power, reported in chapter 4 and discussed in section 4.3.2,

show the beginning of a peak which would occur at some temperature below  $70^{\circ}\text{K}$ . The experimental values are in agreement with other workers who suppose that the peak is due to phonon drag. There is thus conflicting evidence. In his comprehensive review of thermomagnetic effects Delves<sup>103</sup> discusses phonon drag and points out that the effect will only be found when the carriers are primarily scattered by acoustic phonons. Comparison of the theoretical and experimental part of Mills' work on the Nernst coefficient of these samples of graphite (see section 1.5.2) led to the conclusion that even at the highest temperatures measured lattice scattering did not predominate and better agreement was obtained if neutral impurity scattering was assumed. It is thus reasonable that no phonon drag component was seen in the Nernst coefficient and the peak in the thermoelectric power must be attributed to some other cause such as the variation in the ratios of carrier densities and mobilities proposed by Klein<sup>54</sup>. Presumably phonon drag will not be seen until the crystallite size can be made large enough, and defects within the crystallites reduced sufficiently, for lattice scattering to predominate.

### 6.1.3 Prospects for improving the figure of merit

The high field figure of merit depends upon two factors,  $Q/\mu$  and  $\sigma_0/K_L$ . All the reported measurements on pyrolytic graphites of varying degrees of perfection seem to indicate

that  $\sigma_0/K_L$  is roughly constant at any given temperature. That is to say an improvement in the structure of the material which results in an increase of the electrical conductivity also gives a corresponding increase in the lattice thermal conductivity. For example samples 22 B, C, D and F at 80°K are all around  $\sigma_0/K_L = 1.2 \times 10^3$  and this can be compared with Holland, Klein and Straub's value of  $1 \times 10^3$  for graphite prepared at 3250°C. Thus it can be argued that straightforwardly improving the quality of the graphite by increasing both crystallite size and internal perfection is unlikely to effect a large improvement in this factor. Delves has suggested that it might be possible to decrease the thermal conductivity without correspondingly affecting the electrical properties by using one of the many lamellar compounds of graphite in which elements such as bromine can be made to take up positions between the layers of the graphite lattice. This causes an expansion of the lattice in the c-direction to accommodate the extra sites, and usually results in a reduction of the anisotropy of the crystal. Most of the additives are either donors or acceptors so that although the resistivity of the compounds is lowered the essential intrinsic nature of the material is lost. Data would be required on the change of the thermal conductivity to know whether this would outweigh the loss of completely intrinsic properties. One possible reason for the apparent link between  $\sigma_0$  and  $K_L$  is that, as shown by Mills' results, the carriers show neutral impurity

scattering and at low temperatures the carrier mean free path becomes boundary limited. At low temperatures the phonon mean free path is also boundary limited and the agreement between the crystallite sizes calculated from the boundary limit of the mobility and from the thermal conductivity gives support to this view. If it becomes practicable to produce graphite of sufficiently large crystallite size and perfection for the carriers to be lattice scattered over the complete temperature range then it is possible that the link between  $\sigma_0$  and  $K_L$  might be broken.

Examining the factor  $Q/\mu$  to see how this depends on the perfection of the material leads to a similar argument. Although there is a small improvement in the value obtained for better material, order of magnitude increases are not likely so long as  $Q$  shows similar temperature dependence to  $\mu$ . However if the crystallite size and perfection could be increased sufficiently for lattice scattering to predominate and give the possibility of obtaining phonon drag effects then there could be a worthwhile improvement in  $Q/\mu$ . Heat treatment temperatures of  $3500^\circ\text{C}$  probably represent the practical limit and material has been prepared at this temperature by Diefendorf and was used in Goldsmid and Lacklison's measurements of the figure of merit at liquid helium temperatures. As already discussed, there are some aspects of their measurements which do not entirely agree with the present work, and before it can

be said with certainty that material heat treated at  $3500^{\circ}\text{C}$  does not give useful results, more must be known about its properties. For example the crystallite size and degree of preferred orientation, and the Nernst coefficient, thermal and electrical conductivities and mobility as a function of temperature should be known. The structure data would show whether the full potential of the heat treatment temperature was being realised and thus whether it is likely that any better quality material could be prepared. This aspect will be discussed further in the second part of this chapter. The electrical and thermal data would allow the discrepancies between Goldsmid and Lacklison's measurement and this work to be sorted out, but more particularly it should be examined to see whether, with the greatly improved mobility, lattice scattering is dominant, and if so whether there is any indication at all of phonon drag effects. Material prepared at these high temperatures requires extreme care in handling as it is soft and easily damaged and Goldsmid and Lacklison point out that the departure of the magnetoresistance from a  $B^2$  dependence at high fields may have been due to sample inhomogeneities. They also found that the Nernst coefficient was not field independent in this material but reached a maximum and then fell off with increasing field.

There is thus scope for further experimental work on material of higher quality than any used in this work and in

turn this could lead to further theoretical work if there were still large discrepancies in the results. However in spite of the possibility of effecting some improvement in performance it does not seem very likely that pyrolytic graphite will ever become a suitable material for a practical Etingshausen device.

## 6.2 Structure and properties

The two structural features of the pyrolytic deposits which were measured were the crystallite size and the preferred orientation. The properties of the material can be related to these parameters and to the deposition processes, and the next two sections will discuss the relationship. In the third section an attempt will be made to assess the quality of the material likely to be obtained when the pyrolytic process is refined and taken to its practical limit.

### 6.2.1 Preferred orientation

Chapter 3 has reported the measurements of the preferred orientation of the pyrolytic deposits and section 3.5 discussed the results in relation to the estimated formation temperature of the deposit. A linear relation between the angular misalignment and the formation temperature was obtained with all the results from bar 22 and results from other workers lying on two distinct lines; the outer layers of bar 22 and other people's 'as-deposited' results lying on one line and the

inner layers of bar 22 and other people's 'stress-annealed' results lying on the other line. Since the preferred orientation was measured because of its possible influence on the a-direction properties of the deposit, the break in bar 22 with the sharp change from poor to well oriented material should make it easier to detect any change of this nature. However examination of figure 2.4 which plots the resistivity and mobility of all the samples from bar 22 as a function of formation temperature, does not reveal the discontinuity between samples D and F that would be expected at around  $2800^{\circ}\text{C}$  if the crystallite misalignment strongly influenced the a-direction conductivity and mobility. The results lie on a smooth curve in spite of the sharp change of alignment. The thermal conductivity results shown in figure 4.2 again lead to much the same conclusion, since the difference in conductivity between samples C and D is much the same as that between samples D and F. However the rather different temperature dependence of the thermal conductivity of sample F may be the result of the poorer crystallite alignment in this case, but measurements from further samples over a wider temperature range would be needed to be sure of this.

The lack of correlation between crystallite alignment and the a-direction transport properties of pyrolytic graphite is at first sight rather surprising, but Stover<sup>104</sup> has proposed a model for pyrolytic graphite that accounts for this reasonably.

The angular misalignment of the crystallites measured by x-ray methods is an average over the whole sample and gives no information about the misalignment between neighbouring crystallites. Stover suggests that pyrolytic graphite could be considered as a 'wrinkled sheet' with a very low angular misalignment between neighbouring crystallites but that this misalignment can progressively add up to relatively large scale 'waves' in the sheet of crystallites. A low angle boundary of this nature could be a row of dislocations and there is some evidence from electron microscopy that these can occur<sup>105</sup>. Since the a-direction transport properties are much more likely to be affected by the boundaries between neighbouring crystallites rather than by the overall alignment this model accounts for the small effect of the average misalignment. As far as simply improving the a-direction transport properties is concerned there seems, therefore, little point in having extremely good crystallite alignment since the properties are almost completely controlled by the highest temperature reached during growth or subsequent annealing. However the next section will show that crystallite misalignment is important since it may be one of the factors limiting crystallite growth, so that it is worth discussing how material with good alignment might be obtained consistently.

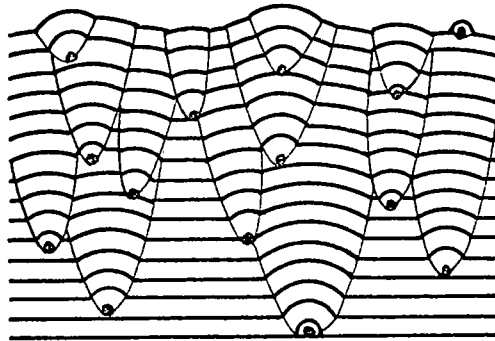
In section 2.3 it was pointed out that the growth rate was the one factor in the deposition process that apparently

could not be fully controlled since occasionally a much slower rate was obtained. It is probably significant that the well aligned inner layers of bar 22 were grown at this slower rate. Figure 3.1 also shows the variation in texture produced by the different rates of growth with a strong cone structure in the outer layers and very little indeed in the inner layers.

Harvey, Clark and Eastabrook<sup>35</sup> suggest that the cone structure is due to the random incorporation of soot particles during growth and figure 6.3 shows schematically how this model leads to the cone structure. Working from the measured preferred orientation their model gives a value of 5-10% by volume of incorporated particles at a deposition temperature of 1580°C, near the density minimum, in line with the theory of gas phase reactions proposed by Diefendorf<sup>32</sup>. The incorporated volume falls to less than 1% for a more highly oriented 2000°C deposit and presumably would be even less for a 2200°C deposit. It can be seen from figure 6.3 that this model is consistent with Stover's wrinkled sheet theory, since the waves are caused by the basal layers growing round the soot particles and thus leading to the high average misalignment. However as the basal layers remain nearly continuous the misalignment between neighbouring crystallites would be low. There would seem to be some evidence that growth on a fresh nucleus, such as a soot particle, is faster than on the remainder of the surface. If this is so a deposit incorporating soot particles would grow

FIGURE 6.3

Construction showing how the random  
incorporation of soot particles leads to  
the formation of growth cone structure



at a faster rate. Thus it appears that the slower growth rate of the inner layers of bar 22 coupled with the lack of cone structure and the much higher degree of crystallite alignment indicates that this part of the deposit was grown without the incorporation of soot particles. The probable reasons for this will now be discussed.

As has already been explained in section 2.4 growth was started at reduced propane pressure to prevent soot formation in the first few moments of growth, but this had become standard practice. Further examination of the experimental record of the growth of this bar, however, shows that the cleaning of the furnace was probably more thorough than usual and included changing the pump oils. Presumably the furnace had become contaminated again during the first part of the growth so that the second part included soot particles. Thus it would seem that a greater attention to cleanliness might lead to consistent production of material that was well aligned and did not include soot particles.

To achieve this extra cleanliness a fresh approach to the design of the furnace would be necessary and it would have to be upgraded from a small scale industrial prototype to a refined piece of laboratory equipment making use of modern techniques. For example an all stainless steel construction, used with a fully baffled pump system and liquid air traps, would be essential. Following the procedure used in the epitaxial growth of silicon

layers, a high gas flow would be needed. This would flush away any soot particles formed in the gas and so prevent deposits on the inside of the furnace. To aid this flushing process the geometry of the furnace would have to be changed to a tube rather than a pot with the growing bar mounted concentrically in the tube. It might be possible to use replaceable liners in the tube so that each growth run started with completely clean surfaces, though care would have to be taken to design them so that they did not get hot enough for the formation of low temperature pyrolytic deposits. Use of an improved furnace of this type could well lead to the consistent production of highly aligned soot-free deposits.

### 6.2.2 Crystallite growth

Electrical and thermal measurements on sections taken through the thickness of bar 22 have indicated that these properties depend upon the highest temperature reached during deposition or subsequent annealing. The measurements of the crystallite sizes in chapter 5 showed that the sizes obtained depended very strongly on temperature and since the previous section has demonstrated that the a-direction properties depend little on the relative misalignment of the crystallites, it would appear that it is the crystallite size that is the structural feature that is largely limiting the properties of the material. The saturation of the mobility and the thermal

conductivity measurements confirm the dependence on crystallite size. This section will therefore discuss some proposed mechanisms for crystallite growth to see how well the present results fit and also to provide a basis for estimating whether much improved material could be obtained.

Franklin<sup>106</sup> made an extensive study of the graphitisation at temperatures between 1000 and 3000°C of various forms of carbon. She found that they could be divided into two distinct classes which she designated 'graphitising' and 'non-graphitising'. In the graphitising carbons crystallite growth continues with increasing temperature but in the non-graphitising carbons crystallite sizes soon saturate at values of the order of 150 Å. As explained in section 5.3 the hexagon structure is present in carbon in the form of single layers of varying extent. Several of these layers may line up in parallel packets to form a random layer lattice. Franklin showed that the graphitising carbons have a fairly compact structure in which neighbouring packets have a tendency to lie in parallel orientation. In the non-graphitising carbons there is a strong system of cross-linking between the packets. This leads to random orientation of the packets and to a rigid and porous structure. Franklin goes on to suggest that crystallite growth probably takes place by the gradual displacement of whole layer planes and the initial orientation of the graphitising carbons facilitates this process. In the non-graphitising carbons the strong

cross links and the lack of orientation prevents crystallite growth. The extreme forms of non-graphitising carbon are the carbon blacks and soot in which the particles are spherical with the layer planes arranged tangentially. These particles do not graphitise at all readily. Mrozowski<sup>107</sup> suggested that the driving force for the movement of the layer planes could be provided by the thermal stress set up as a result of the anisotropy in the thermal expansion of the graphite crystal lattice. This force becomes ineffective for large angular misorientation of the layer planes. The general features of this theory have been confirmed and refined more recently<sup>108</sup> and Tsuzuku<sup>109</sup> has discussed the detailed mechanism for the relief of the thermal stress in terms of the generation and movement of dislocations.

The overall picture of crystallite growth is thus that it proceeds by gradual movement of the layer planes. Those with the least misorientation will graphitise first and the process will continue with increasing temperature until at some temperature crystallite growth saturates. The limiting value of the crystallite size will depend upon the structure of the starting material. Poorly oriented material with a large number of cross links will saturate at relatively low temperatures and well aligned material with no cross links will continue to graphitise with increasing temperature. Although, as discussed in the previous section, the a-direction properties of pyrolytic

deposits seem to depend little upon the crystallite misalignment the importance of obtaining well aligned deposits can now be seen, since misorientation may limit the growth of crystallites in any annealing process. Soot-free deposits are also required as not only does the inclusion of these particles give poorer orientation but their non-graphitizability must limit crystallite growth.

Although graphitisation and crystallite growth can be explained reasonably in terms of the gradual movement of the layer planes the detailed mechanisms involved in the movement have not been worked out with any certainty. There is no reason to suppose that a single mechanism will predominate over the complete range of annealing temperatures, and for the graphitisation of the various types of bonded commercial graphites many different thermal activation energies have been reported<sup>110,111</sup>. They vary from around 2.4 eV below 1500°C to around 6 eV at 3000°C. Fischbach<sup>112</sup> in his study of the kinetics of graphitisation in pyrolytic graphite suggested the somewhat higher value of 7.0 eV above 2500°C. However the Arrhenius plot of crystallite size shown in figure 5.13 gives a straight line over the whole temperature range and suggests that for this particular form of pyrolytic graphite a single process is largely responsible for the crystallite growth. The slope of the plot gives a value of 5.9 eV for the energy of the process. The study of radiation damage in graphite has led to estimates

of the activation energy of some specific processes that could be involved in crystallite growth. For example Hennig<sup>113</sup> obtained a value of 6.8 eV for the formation of a vacancy and values of 3.0 and 5.5 eV have been reported for the motion of a vacancy in the layer plane and perpendicular to it<sup>114</sup>. The energies of sublimation and self-diffusion are reported as 7.4 and 7.1 eV<sup>115,116</sup>. None of these values agree with the value of 5.9 eV obtained from figure 5.13. So far there have been no determinations of the energies associated with the generation and motion of dislocations of the type that Tsuzuku suggested could be involved in crystallite growth. Studies of the high temperature creep of graphite could possibly give further information. This is found to be a thermally activated process and is probably associated with the formation and motion of defects such as arrays of dislocations as well as the point defects mentioned previously. Again a range of activation energies is found for the bonded graphites, but Kotlensky<sup>117</sup> has reported a value of 6.7 eV for pyrolytic carbon which is somewhat lower than the 7.0 eV reported by Fischbach for crystallisation, though still higher than the value obtained here.

Up to this point this section has discussed crystallite growth only in terms of the layer plane growth, but growth is also taking place in the c-direction. An Arrhenius plot of the layer thickness was shown in figure 5.14 and the values do

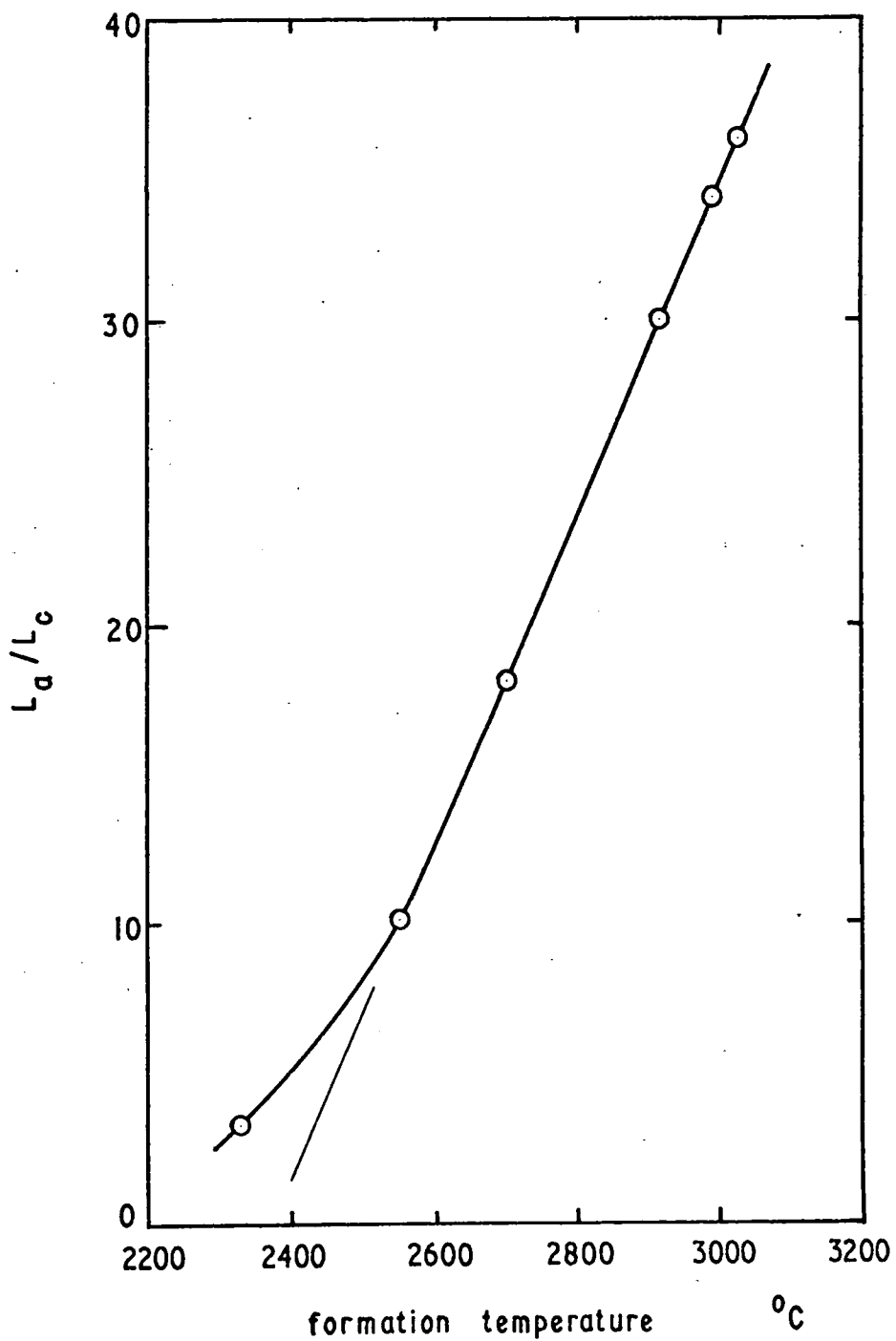
not seem to be associated with a definite activation energy, Growth in the c-direction proceeds more slowly at low temperatures. This is in line with many studies of graphitisation in very small crystallite size carbons in which it is found that growth first takes place by the two-dimensional growth of the layer planes and only after the planes have reached a critical size of around  $150 \text{ \AA}$  can c-direction growth take place. The values of  $L_a$  and  $L_c$  taken from the curves obtained by the best fit to the data of figures 5.13 and 5.14 can be used to give the ratio  $L_a/L_c$  as a function of formation temperature and this is shown in figure 6.4. Except at low temperatures when the two-dimensional limit described above is probably acting, it appears that the ratio  $L_a/L_c$  increases linearly with increasing temperature. Thus although c-direction growth is taking place the processes involved make a-direction growth increasingly easier as the temperature rises. By extrapolation the ratio  $L_a/L_c$  should be around 100 for annealing temperatures of  $3500^\circ\text{C}$ .

### 6.2.3 Prospects for obtaining improved quality graphite

All the measurements made so far on pyrolytic graphite indicate that the properties obtained depend almost entirely on the maximum temperature reached during deposition or subsequent annealing. The process induced by the high temperatures must take place relatively quickly since there is no evidence from bar 22 that the properties have been limited

FIGURE 6.4

The crystallite size ratio  $L_a/L_c$  as a function of formation temperature



by too short a treatment time. This has been found by other workers, and Fischbach<sup>112</sup> showed that the time to reach the new state was much less than 20 minutes for temperatures above 2700°C. However the previous section has shown that crystallite growth, and hence the related properties, may be limited at the highest temperatures by the initial degree of misalignment of the crystallites. It is thus important that the starting material is well aligned if the full potential of the highest treatment temperatures is to be achieved. Section 6.2.1 has shown that well aligned material can be obtained if soot-free deposits can be grown and has suggested conditions for achieving this. A second line of approach is the hot pressing method developed by Moore, Ubbelohde and Young<sup>39</sup>. This process results in material of better alignment than the inner layers of bar 22 and it can then be annealed at temperatures of up to 3640°C. However electron micrographs of the hot pressed material before annealing show soot particles and although these particles are partially recrystallised after annealing they are still visible as separate entities in the annealed material. This agrees with the theories of crystallite growth given in the previous section. The value of between 10 and 40  $\mu\text{m}$  quoted for the crystallite size of hot pressed and annealed material lies well under the crystallite growth line shown in figure 5.13 and confirms that the presence of soot particles is probably limiting the crystallite growth.

Goldsmid and Lacklison<sup>102</sup> also give an estimate of 20  $\mu\text{m}$  for material treated at 3500°C whereas the growth line predicts that 50  $\mu\text{m}$  ought to be possible at this temperature. It thus seems likely that better quality graphite than any measured so far could probably be prepared by annealing well aligned soot-free material at temperatures of 3500°C and above. Whether as-deposited soot-free material is well enough aligned for best results would have to be determined by experiment. It is possible that hot pressing the soot-free material before annealing might give some advantage.

Crystallite sizes of between 50 and 100  $\mu\text{m}$  probably represent the upper limit for graphite prepared by the pyrolytic process and its refinements. Measurements would show whether the properties of this material are still limited by the crystallite size and thus whether there was any prospect at all of obtaining useful cooling from pyrolytic graphite. If still larger crystallites were needed then alternative methods of material preparation would have to be investigated. For example it has recently been shown<sup>118</sup> that it is possible to produce graphite crystals some millimetres in size by growth from solution making use of the high solubility of carbon in either iron or nickel. This method is clearly capable of development since the work reported was in its early stages and it may well supersede pyrolytic graphite for those applications where single crystal properties are desirable.

### 6.3 Conclusions

The overall conclusions from this work may be listed as follows :-

- 1) The Brown and Watt method for the deposition of pyrolytic graphite has been developed successfully to give material of consistent properties.
- 2) The temperature profile developed across the deposit during growth was estimated. This allowed a bar to be cleaved into a number of sections having a range of effective formation temperatures.
- 3) Measurements of the thermal conductivity, together with the electrical and thermomagnetic measurements made by Mills, have shown that down to 70°K the best samples of pyrolytic graphite were not capable of giving useful Eттingshausen cooling. This is because of the high thermal conductivity and lack of phonon drag effects.
- 4) Extrapolation to liquid helium temperature shows that although an improved figure of merit should be obtained it is still not high enough to be useful in the absence of a significant phonon drag component.
- 5) The crystallite size was measured directly from x-ray line broadening and it was shown that good agreement with indirect methods was obtained if the proper correction for stacking faults was made. A thermal activation energy of 5.9 eV was obtained for

crystallite growth.

- 6) The processes involved in the deposition and annealing of the graphite are reasonably well understood qualitatively and it is shown that annealing well aligned soot-free deposits at  $3500^{\circ}\text{C}$  should give better quality material than any so far obtained.
- 7) An upper limit of  $100\ \mu\text{m}$  is proposed as the largest crystallite size likely to be obtained by the pyrolytic process.

APPENDIX I

PUBLISHED PAPERS ON WORK IN THIS THESIS

1. Thermomagnetic effects in pyrolytic graphite  
J.J. Mills, R.A. Morant and D.A. Wright  
British Journal of Applied Physics, 1965, vol. 16, pp. 479-85.
  
2. Some properties of resistance-grown pyrolytic graphite  
R.A. Morant  
British Journal of Applied Physics, 1966, vol. 17, pp. 75-9.
  
3. The crystallite size of pyrolytic graphite  
R.A. Morant  
Journal of Physics D: Applied Physics, 1970, vol. 3, pp. 1367-73.

<sup>3</sup>  
*Reprinted from*

*British Journal of  
Applied Physics*

The Institute of Physics and The Physical Society

Printed in Great Britain by Adlard & Son, Ltd., Dorking

# Thermomagnetic effects in pyrolytic graphite

J. J. MILLS, R. A. MORANT and D. A. WRIGHT

Department of Applied Physics, University of Durham

*MS. received 30th September 1964, in revised form 7th December 1964*

**Abstract.** The electrical conductivity, magnetoresistance, thermal conductivity and Nernst coefficient have been measured between 60 and 300°K for samples cut from a bar of pyrolytic graphite. The effective formation temperatures for the samples varied from 2300 to 3020°C. The experimental values of the Nernst coefficient  $Q$  agree quite well with theory, with a mean value  $Q = 2.7 (k/e) \mu$  at room temperature. This value, combined with the fact that  $Q$  is independent of  $\mu B$  over a wide range, indicates that boundary scattering is important compared with lattice scattering. The results indicate poor prospects for Etingshausen cooling.

## 1. Introduction

We have prepared pyrolytic graphite, and, as explained in §3, have obtained samples representing growth temperatures from 2100 to 3020°C. Several properties have been measured, including the Nernst coefficient, between 60 and 300°K. Measurements of the Nernst coefficient have not been reported previously. Comparison of the other results with those of other workers shows good agreement.

Other workers have made measurements on various types of pyrolytic graphite down to 4°K or below, and have observed systematic behaviour; it is therefore possible to extrapolate some of the present results to temperatures below 60°K. This makes it possible to make a further assessment of the feasibility of Etingshausen cooling (Wright 1963).

## 2. Preparation of pyrolytic graphite

Single crystal material is available only in the form of natural crystals 3 mm or less in size. These are soft and difficult to handle. Since graphite sublimes at 3600°C, growth from the melt is possible only under pressure. However the pyrolytic process is capable of producing material in which the crystallites are well oriented. The method used in the present work is that of Brown and Watt (1958), in which a rectangular bar of synthetic polycrystalline graphite is clamped between water cooled electrodes and heated electrically in hydrocarbon vapour. The hydrocarbon decomposes to form a graphite layer on the bar. During the growth the surface temperature is held constant. High density material with good crystallite orientation is obtained only at temperatures over 2000°C and most of our work has used a deposition temperature of 2200°C. Propane gas is used since this is readily obtainable in a fairly pure form, and the pressure is maintained at 50 torr. With these conditions a deposit of 2–3 mm can be grown in 3–5 hours. The deposit is polycrystalline with the crystallites approximately aligned with their basal planes parallel to each other and to the base material. The degree of alignment in the  $a$  direction improves with increase of annealing temperature (Guentert and Klein 1963). The directions adopted by the crystallites are randomly oriented about the  $c$  axis.

Like single crystal graphite, pyrolytic graphite produced in the above way is a semi-metal with overlapping conduction and valence bands. This leads to intrinsic properties, with equal electron and hole densities.

## 3. Measurements of electrical and thermal conductivity

The deposit was separated from the former and was readily cleaved into thin sections for measurement. The resistivity, magnetoresistance, Hall effect and thermal conductivity

The thermal conductivity was determined by observing the temperature gradient developed along the sample for a given power input to a heater attached at one end. To minimize heat losses there were no connections to the sample other than the 40 gauge wires necessary for the heater and thermocouples, and the container was evacuated. The thermocouples were attached along the length of the sample at approximately the same points 1 and 2 (figure 2) used for the Nernst measurements, but the edge contacts were replaced by contacts passing round the sample to ensure proper thermal contact.

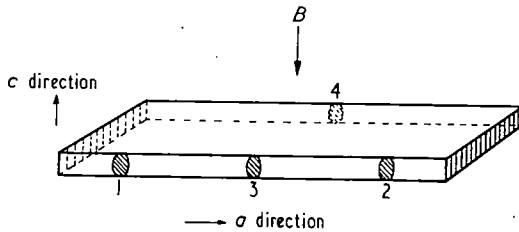


Figure 2. Experimental arrangement.

The thermal conductivity showed a  $T^{-1}$  variation at the higher temperature of measurement and  $T^2$  at the lower, the values increasing with formation temperature. The table shows the peak values and the temperature at which they occur, and the values at 80°K. The electrical conductivity varied little with temperature for the layers formed at low temperatures, but both the value and the slope increased with formation temperature. The table shows values at 300°K and at 80°K. The mobility rose with formation temperature as in the table and figure 1. Figure 1 shows also Soule's (1958) results for single crystals. He observed a  $T^{-1.2}$  dependence down to 20°K, and it can be seen that this slope is approached in the 3020°C curve at the high temperature end. The results fit well into the pattern of behaviour observed by other workers, and it appears that the growth temperatures determined as above account satisfactorily for the variation of properties through the bar. The mobility and thermal conductivity at low temperatures are limited by boundary scattering, and the methods used by Klein (1962) and by Smith and Rasor (1956) indicate that the crystallite size increases from about 0.1  $\mu\text{m}$  to 3 or 4  $\mu\text{m}$  as the formation temperature rises from 2300 to 3050°C.

Having established the pattern of behaviour of the sections studied, we can now consider the measurements of the Nernst coefficient.

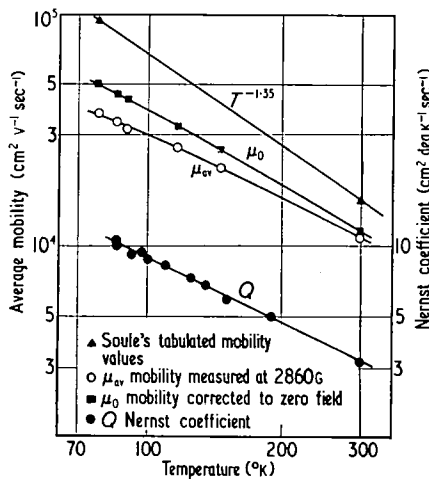


Figure 3. Comparison of the temperature dependence of the mobility and the Nernst coefficient.

results were substituted in the equations (cf. Tsidilkovskii 1962, equation (7.3)):

$$\left. \begin{aligned} I_{10} &= I_{102} + abI_{101} \\ I_{20} &= I_{202} - ab^2I_{201} \\ I_{11} &= I_{112} - abI_{111} + E_g I_{102} \\ I_{21} &= I_{212} + ab^2I_{211} + E_g I_{202} \end{aligned} \right\} \quad (2)$$

where  $a = n_e/n_h$  and  $b = \mu_e/\mu_h$ , and finally these results were used to determine the Nernst coefficient (cf. Tsidilkovskii 1962, equation 6.2):

$$Q_1 = \frac{Q_e I_{11} I_{20} - I_{10} I_{21}}{\mu_h k (I_{20}^2 + I_{10}^2)}. \quad (3)$$

The results are plotted in figure 4, curves 1 and 2.

The expressions for  $Q_1$  for intrinsic material take simpler forms for non-degeneracy ( $E_g > 2kT$ ) or for complete degeneracy ( $E_g < -8kT$ ). With acoustic mode lattice scattering ( $s = \frac{1}{2}$  in the relation  $\tau \propto E^{-s}$ ), and with  $a = n_e/n_h = 1$ ,  $b = \mu_e/\mu_h = 1$ , the non-degenerate result for low values of  $\mu B$  is:

$$Q_1 = \frac{3\pi}{16} \left( 3 + \frac{E_g}{kT} \right). \quad (4)$$

This is readily modified for the case  $b = 1.1$ , giving values which agree with those plotted in curve 1 to the right in figure 4 which were derived from the computer programme.

For full degeneracy in the low-field case with  $s = \frac{1}{2}$  it is necessary to use Putley's expression for mixed conduction (Putley 1960, table 3.4), and to substitute in it

$$\begin{aligned} Q_e = Q_h &= -\frac{\pi^2 k}{6 e} \mu \frac{kT}{E_f} \\ \alpha_e = -\alpha_h &= -\frac{\pi^2 k}{3 e} \mu \frac{kT}{E_f}. \end{aligned}$$

With  $b = 1$  this leads to

$$Q = \frac{\pi^2 k \mu kT}{6 e E_f} = \frac{\pi^2 k}{3 e} \mu \frac{kT}{E_g}. \quad (5)$$

Again this can easily be modified for  $b = 1.1$ , and the values agree with those to the extreme left of figure 4, curve 1.

If however the scattering is on uncharged defects, dislocations or grain boundaries,  $s = 0$  and (4) is modified to

$$Q_1 = \frac{1}{2} \left( 5 + \frac{E_g}{kT} \right). \quad (6)$$

For complete degeneracy (5) is modified to

$$Q_1 = \pi^2 \frac{kT}{E_g}. \quad (7)$$

We have not computed the intermediate range with  $s = 0$ , between  $E_g/kT = -8$  and  $E_g/kT = 2$ , but the expressions can be modified for  $b = 1.1$  and the form of the curve can be interpolated approximately as dotted in figure 4, giving curve 3.

Turning to the high-field case,  $\mu B \gg 1$ , we have from Tsidilkovskii for non-degeneracy,  $a = 1$ ,

$$Q = \frac{1}{c_r} \frac{k}{e} \frac{\mu_e \mu_h}{\mu_e + \mu_h} \left( 5 + \frac{E_g}{kT} \right). \quad (8)$$

For  $s = \frac{1}{2}$ ,  $c_r = 1.132$  and with  $b = 1.1$  the values of  $Q_1$  agree with those to the right in figure 4, curve 2. With  $s = 0$ ,  $c_r$  is 1.00, leading to the same result as equation (6), i.e.

No indications of phonon drag effects are given by the experimental values of  $Q$ , which is not surprising in view of the high carrier density and small crystallite size. It is still possible that such effects are present after deposition or annealing at 3500°C; this remains to be investigated.† Apart from this possibility, pyrolytic graphite will be useful for Ettingshausen cooling only if a means can be found for increasing phonon scattering without increasing that of electrons or holes.

### References

- BROWN, A. R. G., and WATT, W., 1958, *Proc. Conf. on Industrial Carbon and Graphite* (London: Society Chemical Industry), p. 86.
- GOLDSMID, H. J., and LACKLISON, D. E., 1965, *Brit. J. Appl. Phys.*, **16**, 573.
- GUENTERT, O. J., and KLEIN, C. A., 1963, *Appl. Phys. Letters*, **2**, 125.
- KLEIN, C. A., 1962, *J. Appl. Phys.*, **33**, 3338.
- 1964, *J. Appl. Phys.*, **35**, 2947.
- KLEIN, C. A., and HOLLAND, M. G., 1964, *Phys. Rev.*, **136A**, 575.
- MCCLURE, J. W., 1957, *Phys. Rev.*, **108**, 612.
- 1964, *I.B.M. J. Res. Dev.*, **8**, 255.
- MOORE, A. W., ÜBBELOHDE, A. R., and YOUNG, D. A., 1962, *Brit. J. Appl. Phys.*, **13**, 393.
- PUTLEY, E. H., 1960, *Hall Effect and Related Phenomena* (London: Butterworths).
- SLACK, G. A., 1962, *Phys. Rev.*, **127**, 694.
- SMITH, A. W., and RASOR, N. S., 1956, *Phys. Rev.*, **104**, 885.
- SOULE, D. E., 1958, *Phys. Rev.*, **112**, 698.
- TSIDILKOVSKII, I. M., 1962, *Thermomagnetic Effects in Semi-Conductors* (London: Infosearch).
- WRIGHT, D. A., 1963, *Brit. J. Appl. Phys.*, **14**, 329.

† The results published by Goldsmid and Lacklison in this issue indicate that such effects are not present in graphite annealed at 3500°C.

*Reprinted from*  
*British Journal of*  
*Applied Physics*

The Institute of Physics and The Physical Society

Printed in Great Britain by Adlard & Son, Ltd., Dorking

# Some properties of resistance-grown pyrolytic graphite

R. A. MORANT

Department of Applied Physics, University of Durham

*MS. received 5th July 1965, in revised form 4th October 1965*

**Abstract.** A bar of pyrolytic graphite, grown at a constant surface temperature of 2200°C by resistance heating of the substrate, was cleaved into a number of thin sections; crystallographic and *a*-direction thermal and electrical measurements were made as a function of distance through the deposit. These properties were found to vary in a systematic way consistent with the increased substrate temperature to be expected in this method of growth. The temperature profile through the deposit was estimated, yielding a substrate temperature of 3050°C for a deposit 2.4 mm thick. Comparison of the electrical properties with other workers' results on pyrolytic graphites annealed at known temperatures gives adequate confirmation of the estimated temperatures and shows that resistance-grown graphites may be used to measure *a*-direction properties of material effectively annealed at temperatures much in excess of the surface deposition temperature.

## 1. Introduction

In this laboratory pyrolytic graphite is deposited from propane by the resistance method of Brown and Watt (1958) in which a bar of synthetic graphite, acting as the substrate for the deposit, is heated by the passage of an electric current. The surface temperature is held constant during growth. Early x-ray examination of the bars showed variation of the structure through the deposit, with crystallinity increasing with the distance from the surface; similar non-uniformity was obtained in resistivity measurements. J. Harvey, D. Clark and J. N. Eastabrook (1962, R.A.E. Tech. Memo. Met. Phys. 361) pointed out that, because of the low *c*-axis thermal conductivity of the pyrolytic deposit, a considerable temperature difference could develop across the deposit during growth by this method, raising the substrate temperature above that of the surface. It was felt that the non-uniformity warranted further investigation and one bar of pyrolytic graphite was cleaved into thin sections and measurements of crystallite orientation, *a*-direction thermal conductivity, thermoelectric power, resistivity and mobility were made as functions of the distance through the deposit.

## 2. Growth conditions

The deposit, 2.4 mm thick, was grown at a surface temperature of 2200°C and a propane pressure of 50 torr. In this particular bar, growth was interrupted after about 1 mm thickness had been deposited and then continued for the remaining thickness. The growth rates, which apparently cannot be controlled, were  $1.3 \times 10^{-5}$  cm sec<sup>-1</sup> before the interruption and  $2.6 \times 10^{-5}$  cm sec<sup>-1</sup> after it. The difference this produced in texture can readily be seen in figure 1 (plate)† which shows a polished section through the bar. The figure also shows how the section was cleaved into 8 samples, each approximately 1.5 cm × 0.3 cm × 0.03 cm. No measurements were made on section E, which contained the join.

## 3. Structure

X-ray transmission photographs were taken with the x-ray beam both perpendicular and parallel to the layer planes and both showed progressive changes from the outside to the

† Plates at end of issue.

normal reflecting position and  $m$  is then taken as a measure of the preferred orientation. Values of  $m$  obtained for the sections are also given in the table and vary from 11 for the surface layer to 3000 for section B, comparing reasonably with Guentert and Klein's values of 8 for as-deposited material and 7000 for highly stress-annealed material.

#### 4. Thermal conductivity and thermoelectric power

Measurements of the  $a$ -direction thermal conductivity and thermoelectric power were made on four of the sections in the temperature range 65–360°K. The apparatus is shown schematically in figure 3. The sample was cemented directly to the small heater and the

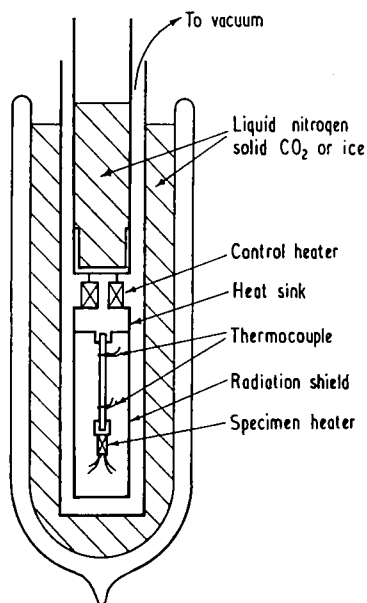


Figure 3. Sketch of the apparatus for measuring thermal conductivity and thermoelectric power.

heat sink with a silver dispersion and, because the material is so anisotropic, the dispersion was coated over the end faces and all sides for a short distance to ensure contact to all the layers. The temperature gradient was measured with copper-constantan thermocouples, and good thermal contact at these points was obtained by first twisting a fine-gauge copper wire around the specimen, completing contact with a thin fillet of silver dispersion and soldering the thermocouples to the wire. 40 s.w.g. wire was used for the thermocouples and heater leads which were kept apart and made as long as possible before being brought to a thermal anchorage point on the heat sink. The sample was surrounded by a radiation shield and the container evacuated. These precautions, and the limitation of the temperature gradient to about 1 degK along the sample, ensured that heat losses from the sample and its heater were minimized. The thermoelectric power relative to copper was obtained by measuring the voltage appearing between the copper leads of the thermocouples after the establishment of the temperature gradient, and was made in conjunction with the thermal conductivity measurements.

The results of the measurements are shown in figures 4 and 5. Experimental points are not given for the thermoelectric power but the scatter is comparable to that obtained in the thermal conductivity measurements. The thermal conductivities obtained are similar both in magnitude and temperature dependence to graphites prepared by hot pressing (Moore, Ubbelohde and Young 1964, Hooker, Ubbelohde and Young 1965) though those graphites were prepared at temperatures above those estimated for the present bar. Crystal-size can be estimated from the position of the peak in the thermal conductivity (Smith and Rasor 1956) and the results, given in the table, compare reasonably with those obtained

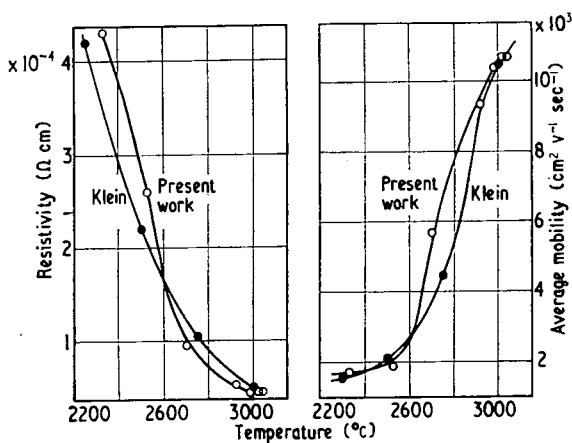


Figure 6. The effect of treatment temperature on the  $a$ -direction resistivity and average mobility measured at 300°K. Comparison of the estimated temperatures of this work and Klein's annealing studies.

temperatures. In figure 6 the room temperature mobilities and resistivities are shown plotted against annealing temperature for Klein's results and against the estimated temperature for the present results. The good agreement confirms the validity of the estimation of the temperatures developed during growth. It is not possible to get such a direct comparison with annealing studies for the remaining properties measured, but their variation through the bar is consistent with the estimated temperatures.

Graphite can also be prepared by heating the substrate in a tube furnace or inductively, and temperature gradients would not be expected in either method. Harvey, Clark and Eastbrook reported that a uniform deposit was obtained in a tube furnace; but there has, so far, been no report on this aspect of inductively grown deposits. Clearly, resistance-grown deposits would be unsuitable for many applications unless it were possible to use very thin sections or to anneal the bar at temperatures in excess of those reached by the innermost layers during growth. However, many  $a$ -direction measurements can be made on thin sections and can yield consistent information provided that the correct formation temperature is given. If a furnace that will reach temperatures well above 3000°C is not available, growth of a thick deposit is a convenient way of obtaining pyrolytic graphite specimens that have been effectively annealed at these high temperatures. When reporting work on pyrolytic graphite it is important to realize that it is not sufficient to characterize resistance-grown deposits by the surface temperature maintained during growth.

#### Acknowledgments

The author would like to thank Professor D. A. Wright for his encouragement and for the facilities of the department.

#### References

- BLACKMAN, L. C., SAUNDERS, G. and UBBELOHDE, A. R., 1961, *Proc. Roy. Soc. A*, **264**, 19–34.
- BROWN, A. R. G., and WATT, W., 1958, *Proc. Conf. on Industrial Carbon and Graphite* (London: Society of Chemical Industry), pp. 86–91.
- GUENTERT, O. J., 1962, *J. Chem. Phys.*, **37**, 884–91.
- GUENTERT, O. J., and KLEIN, C. A., 1963, *Phys. Rev. Letters*, **2**, 125–7.
- HOOKE, C. N., UBBELOHDE, A. R., and YOUNG, D. A., 1965, *Proc. Roy. Soc. A*, **284**, 17–31.
- KLEIN, C. A., 1962, *J. Appl. Phys.*, **33**, 3338–57.
- MILLS, J. J., MORANT, R. A., and WRIGHT, D. A., 1965, *Brit. J. Appl. Phys.*, **16**, 479–85.
- MOORE, A. W., UBBELOHDE, A. R., and YOUNG, D. A., 1962, *Brit. J. Appl. Phys.*, **13**, 393–8.
- 1964, *Proc. Roy. Soc. A*, **280**, 153–9.
- PLUNKETT, J. D., and KINGERY, W. D., 1960, *Proc. 4th Carbon Conf.* (London: Pergamon), pp. 457–72.
- RICHARDS, B. P., 1964, *J. Sci. Instrum.*, **41**, 649.
- SMITH, A. W., and RASOR, N. S., 1956, *Phys. Rev.*, **104**, 885–91.

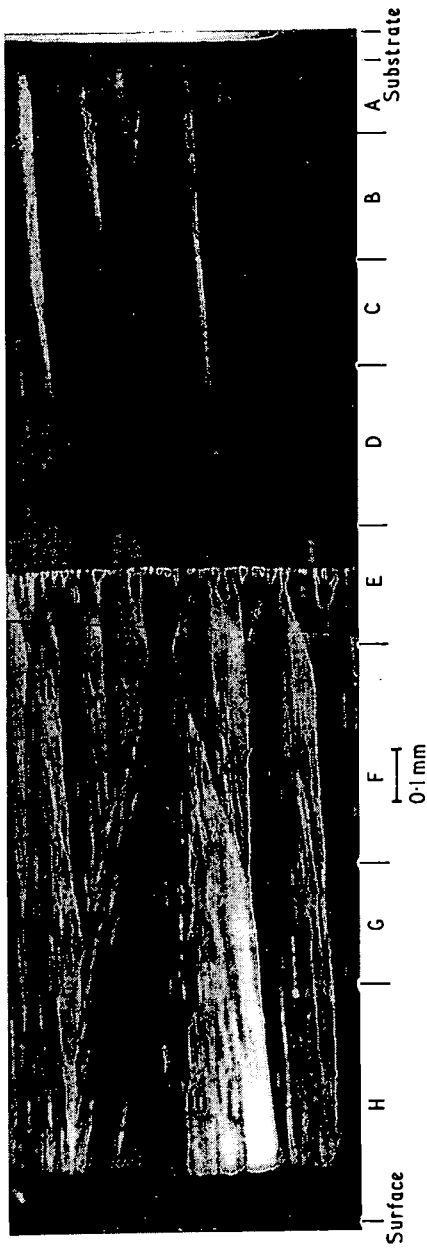


Figure 1. Polished section through the deposit showing the cleaved samples. Crossed polaroids.

# The crystallite size of pyrolytic graphite

R. A. MORANT

Department of Applied Physics and Electronics, University of Durham, Durham City

*MS. received 17th April 1970*

**Abstract.** x-ray line broadening techniques have been used to determine both *a*- and *c*-direction crystallite sizes for a range of pyrolytic graphite samples whose effective formation temperature lay between 2330 and 3020°C. x-ray line profiles were analysed using the variance method. It is shown that if the proper allowance is made for the stacking fault contribution to the 110 line, the x-ray determination gives results for the *a*-direction crystallite size in good agreement with estimates obtained from the mobility and thermal conductivity of the samples. The *a*-direction crystallite sizes ranged from 0.01 to 3 μm and gave a thermal activation energy of 5.9 eV for *a*-direction crystallite growth. The crystallite size ratio  $L_a/L_c$  increased linearly with formation temperature in the range 2500 to 3020°C reaching a value of 36 at 3020°C.

## 1. Introduction

In the Brown and Watt (1958) method of depositing pyrolytic graphite by resistance heating the substrate, temperature differences develop across the thickness of the deposit because of its very low *c*-axis thermal conductivity. Resistance-grown pyrolytic graphite is thus likely to have a gradation of properties through the deposit. The surface layers will have properties corresponding to the deposition temperature and the innermost layers will effectively be annealed at some higher temperature related to the thickness of the deposit. In a previous paper (Morant 1966) this gradation of properties was investigated and it was shown that the temperature profile across the deposit could be estimated accurately enough to assign an effective formation temperature to each of a series of thin samples cleaved from a single bar. One particular bar of graphite, deposited from propane at a surface temperature of 2200°C, yielded a series of samples effectively prepared in the temperature range 2200°C to 3020°C and *a*-direction resistivity, mobility, thermal conductivity and thermoelectric power were measured at temperatures from 300 K down to 70 K. The crystallite preferred orientation was also measured. As expected, the properties of the samples prepared at the highest temperatures approached nearest to those of single-crystal material. During growth of this bar deposition was interrupted and after resumption the growth took place at a much faster rate. This resulted in a large difference in texture between the inner and outer parts of the bar which could be seen in the preferred orientation measurements. At the join there was a sharp change from well oriented to poorly oriented material. However, the *a*-direction transport properties showed no discontinuity at this point so that these properties did not seem to be limited predominantly by the crystallite misalignment. The temperature controlled structural feature more likely to be limiting the *a*-direction properties was the crystallite size. From the low temperature saturation of the mobility an estimate of the *a*-direction crystallite size was made. A second estimate, in quite good agreement, was made from the position of the peak in the thermal conductivity curves. Kelly (1968) has also obtained crystallite sizes from this same thermal conductivity data using a less empirical procedure that yielded similar values. However, these are indirect estimates and it was thought desirable to measure the crystallite sizes of this series of samples directly by x-ray methods. This paper describes the use of x-ray line broadening techniques for determining both the *a*- and *c*-direction crystallite sizes of pyrolytic graphite.

### 3. Experimental techniques

Since only very small quantities of material were available from the cleaved samples a diffractometer could not be used and films were obtained using a Philips 11.46 cm diameter powder camera and nickel filtered copper radiation. To get maximum resolution in the film measurement Ilford Industrial CX fine grain film was used and the line profiles measured on a Hilger and Watts L 451 microdensitometer. Particular care was taken to obtain the tail regions of the profiles since the variance analysis depends upon the behaviour in the tail region.

Powder samples of a reproducible size were prepared by packing the material into selected thin walled Lindemann glass capillaries. The diameters of the specimens were all between 0.26 and 0.27 mm. Because of the platelike nature of graphite particles it is extremely difficult to pack the powder into a tube without getting preferred orientation, and Nelson and Riley (1945) showed that the effect of the orientation is to produce double-peaked profiles. This can be seen easily in the 002 line where the peaks are widely separated. For the 110 line the two peaks are nearly coincident and the result is a line profile that is narrower than that obtained from the standard material. Fitzer *et al.* (1966) showed that this problem can be overcome if the graphite powder is mixed in suitable proportions with a thick grease. The specimens were prepared by grinding the graphite and passing the powder through a number 120 sieve to remove any large particles. The powder was then mixed with Apiezon L grease in the proportion 2 parts by weight of grease to 5 of graphite. This produces material of a plasticine like consistency which can be loaded into the capillaries quite easily and the lack of preferred orientation was checked by examining the 002 line profile on the resultant film. The effect of the grease is to put up the background level on the film and a separate exposure confirmed that the increased background is uniform in the region of importance.

6  $\mu\text{m}$  particle size diamond was used as the standard material and the 220 line chosen to give the standard line profile since this line lies between the 110 and 112 lines in graphite. When analysed as described below the linear tail region of the variance-range plot for the 220 line profile had a slope of  $0.0094^\circ$  ( $2\theta$ ).

After obtaining the line profiles from the microdensitometer the variance analysis was carried out by first drawing in the best linear background level. The  $\alpha_1$  component of the line was then separated by the method proposed by Rachinger (1948). The variance of this profile was calculated as a function of the range of integration with the range set symmetrically about the centroid of the profile. The resultant plot of these values usually gave a curved tail region and the background level was then adjusted until a linear tail region was obtained. This analysis was carried out for the 004, 110 and 112 lines for each graphite sample.

Results from the analysis of the 004 line profile could be compared directly with the diamond 220 line profile to obtain the *c*-direction strain and crystallite size. The rms strain *e* is obtained from

$$e = \frac{1}{2}(W_{2\theta})^{1/2} \cot \theta$$

where  $W_{2\theta}$  is the range independent variance term given by the difference in the intercepts of the diamond and specimen tail region lines.

The crystallite size is obtained from the Scherrer equation modified for use with variance:

$$\frac{W_\theta}{\theta_2 - \theta_1} = \frac{K\lambda}{4\pi^2 L \cos \theta}$$

*L* is the crystallite size perpendicular to the crystal plane giving the reflection and  $W_\theta/(\theta_2 - \theta_1)$  is the difference in the slope of the diamond and specimen tail region lines.

The stacking factor, *p*, was determined from the slope of the linear tail region of the variance-range plot of the 112 line profile using the variance form of the expression given

*c*-direction of the graphite samples is well suited to the method, but the *a*-direction sizes, particularly those for the high temperature samples, give such narrow linewidths that very high accuracy cannot be expected. The mobility determination depends upon the departure from the single-crystal behaviour and this method becomes less reliable for the low temperature samples with smaller crystallite sizes. Estimation of the crystallite size from thermal conductivity measurements by Kelly's procedure or from the peak position seems to give results in agreement with values obtained from electronic properties provided that the material is highly oriented. However, when Kelly applied his method to thermal conductivity data from reactor-grade graphites of poor orientation the  $L_a$  values were always greater than those obtained from electronic properties. The sample prepared at 2700°C came from the poorly oriented part of the bar and  $L_a$  estimated from the thermal conductivity is also a comparable amount greater than that estimated from the mobility. The x-ray value of  $L_a$  for this sample is closer to the mobility value. Kelly suggested an accuracy of 10–20% for his estimates of  $L_a$  for well oriented material. For the high temperature samples the x-ray determination may not be as accurate as this, but within these limits it appears that the x-ray determination of  $L_a$  gives results in very reasonable agreement with the estimates from the mobility and thermal conductivity measurements.

## 5. Discussion

The *a*-direction crystallite sizes determined by all three methods are shown in figure 1 where  $\lg L_a$  is plotted against the reciprocal of the formation temperature. With the

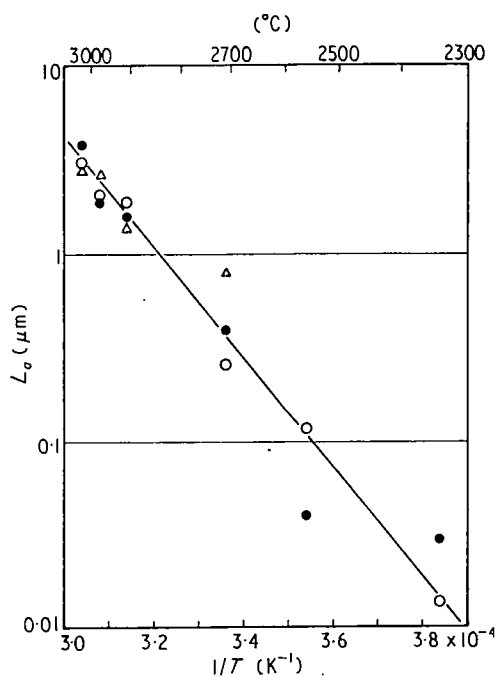


Figure 1. The *a*-direction crystallite size as a function of formation temperature. ○, x-ray determination; ● from mobility; △ from thermal conductivity.

exception of one thermal conductivity value, discussed in the previous section, the points lie reasonably about a straight line, though the mobility results become rather scattered at the low temperature end. A thermal activation energy for *a*-direction crystallite growth can be determined from the slope of this line and is found to be 5.9 eV. A similar plot for the *c*-direction crystallite sizes is shown in figure 2. Since a curve is obtained a single activation energy cannot be used to describe crystallite growth in this direction, though it is

Tsuzuku (1960) has suggested that this takes place by the formation and movement of arrays of dislocations. High temperature creep is also a thermally activated process which is explained in terms of the formation and movement of dislocations. The measurements of the high temperature creep of pyrolytic graphite made by Kotlensky (1966) yielded a thermal activation energy of 6.7 eV which although lower than Fischbach's value of 7.0 eV is still somewhat higher than the value obtained here for graphitization.

## 6. Conclusions

It has been shown that x-ray line broadening techniques can be used satisfactorily to obtain both *a*- and *c*-direction crystallite sizes for samples of pyrolytic graphite. The variance method of analysing the x-ray line profiles is found to be particularly suitable for graphite samples. In the *a*-direction good agreement between the x-ray determination and estimates obtained from the mobility and thermal conductivity of the samples is obtained if proper allowance for the stacking fault contribution to the 110 line is made. The results of the measurement of the crystallite size of a range of pyrolytic graphite samples prepared at temperatures from 2330 °C to 3020 °C yield a thermal activation energy for the *a*-direction crystallite growth of 5.9 eV. The crystallite size ratio  $L_a/L_c$  is found to increase linearly with formation temperature from 2500 °C to 3020 °C reaching a value of 36 at 3020 °C.

## Acknowledgments

The author would like to thank Professor A. J. C. Wilson for the use of the results of his calculations in advance of publication and for his comments on the paper, and also Professor D. A. Wright for his encouragement and the use of departmental facilities.

## References

- BACON, G. E., 1952, *Acta Cryst.*, **5**, 392.  
BROWN, A. R. G., and WATT, W., 1958, *Proc. Conf. on Industrial Carbon and Graphite* (London: Society of Chemical Industry), pp. 86–91.  
EELES, W. T., and WILSON, A. J. C., 1965, *Nature, Lond.*, **205**, 66.  
FISCHBACH, D. B., 1963, *Appl. Phys. Lett.*, **3**, 168–70.  
FITZER, E., FRITZ, W., and OVERHOFF, D., 1966, *Proc. 2nd Conf. on Industrial Carbon and Graphite* (London: Society of Chemical Industry), p. 144.  
JONES, F. W., 1938, *Proc. R. Soc. A*, **166**, 16.  
KELLY, B. T., 1968, *Carbon*, **6**, 485–96.  
KOTLENSKY, W. V., 1966, *Carbon*, **4**, 209–14.  
LANGFORD, J. I., and WILSON, A. J. C., 1963, *Crystallography and Crystal Perfection*, Ed. G. N. Ramachandran (London: Academic Press), 207–22.  
MIZUSHIMA, S., 1963, *Proc. 5th Carbon Conf.*, Vol. 2 (London: Pergamon Press), p. 439.  
MORANT, R. A., 1966, *Br. J. appl. Phys.*, **17**, 75–9.  
NELSON, J. B., and RILEY, D. P., 1945, *Phil. Mag.*, **36**, 711.  
RACHINGER, W. A., 1948, *J. Sci. Instrum.*, **25**, 254.  
TSUZUKU, T., 1960, *Proc. 4th Carbon Conf.* (London: Pergamon Press), p. 403.  
WARREN, B. E., and AVERBACH, B. L., 1950, *J. appl. Phys.*, **21**, 595.  
WILSON, A. J. C., 1962, *X-ray Optics* (London: Methuen), p. 87.  
— 1963, *Proc. Phys. Soc.*, **81**, 41.  
— 1970, *J. Phys. D: Appl. Phys.*, **3**, 403–4.

## APPENDIX II

### MORE RECENT PUBLISHED WORK ON GRAPHITE

Since the main body of this work was completed a number of papers relevant to it have been published, and these will be described briefly in this appendix.

In a series of papers<sup>119,120,121</sup> Kelly has theoretically examined the effects of defects on the thermal conductivity of graphite. In the first paper he investigated the effect of point defects and crystallite boundaries on the basal plane conductivity using Komatsu's two-dimensional approximation and also neglecting the effect of the shear elastic constant,  $c_{44}$ . The results show that vacancies are much more effective point scattering centres than isotopes, and that the effects of the natural isotope concentration can be neglected for graphites with crystallite sizes less than  $3 \mu\text{m}$ . In the second paper the two-dimensional approximation is removed and he considers both basal plane and c-direction thermal conductivities for highly oriented material with a finite crystallite size, and examines crystallite size ratios up to  $L_a/L_c = 10$ . He finds that a reasonable approximation is again obtained for basal plane conductivities if the shear interaction is neglected and derives an expression which allows  $L_a$  to be calculated from thermal conductivity data. This gives results in reasonable agreement with experiment. In the c-direction, however, it

is found that meaningful results cannot be obtained if the shear interaction is neglected. In the final paper the theory is refined to include the effects of the shear interaction,  $c_{44}$ , for both basal plane and c-direction thermal conductivities and the effect of this slightly raises the values of the crystallite sizes obtained from experimental data. As confirmation of his theoretical work Kelly has taken experimental measurements from a number of workers and used his expressions to derive the crystallite size. Among the results used were the thermal conductivity measurements of this work which have already been published (see Appendix I). This method of determining the crystallite size from thermal conductivity measurements is more satisfactory than the empirical method suggested by Smith and Rasor. However results from the two methods agree quite well. For comparison the crystallite sizes determined by all the different methods are shown in the table overleaf. If the new values of the crystallite sizes obtained from the thermal conductivity by Kelly are added to figure 5.13 they would not affect the position of the best straight line and hence the activation energy remains at 5.9 eV.

The value of crystallite size obtained for sample 22 F from thermal conductivity measurements is again higher than that obtained from the mobility and by x-ray methods. This may well be because the crystallites are not sufficiently highly oriented for Kelly's expressions to hold. When he applied the method

to the thermal conductivity results from polycrystalline bonded graphites of poor orientation he also found that the crystallite sizes were a comparable amount greater than ~~that~~ <sup>those</sup> deduced by other methods.

Sample	Crystallite size, $L_a$ $\mu\text{m}$			
	from mobility	from x-ray	from thermal conductivity	
			Smith and Rasor	Kelly
22 B	3.8	3.1	3.3	2.8
22 C	1.9	2.1	2.9	2.6
22 D	1.6	1.9	2.1	1.4
22 F	0.4	0.3	1.3	0.8

A paper has also recently been published on the thermoelectric power of single crystal graphite at low temperatures<sup>122</sup>. A crystal grown from solution was used and the thermoelectric power was measured from 300°K down to 7°K. A sharp negative peak was found at 35°K. The mobility ratio was also measured over the temperature range and the diffusion component of the thermoelectric power calculated. The values obtained fitted the experimental curve well at the higher temperatures and ~~was~~ <sup>were</sup> subtracted from the experimental curve at lower temperatures to separate out the peaked component. This component begins to become significant at about 100°K, rises to a peak of  $-17 \mu\text{V deg K}^{-1}$  at 35°K and falls sharply at lower temperatures. The authors attribute the peak to phonon drag effects.

## REFERENCES

1. Putley, E.H., 1960, The Hall Effect and Related Phenomena, (Butterworth) London.
2. O'Brian, B.J. and Wallace, C.S., 1958, J. Appl. Phys., 29, pp. 1010-2
3. El-Saden, M.R., 1962, J. Appl. Phys., 33, pp. 1800-3.
4. Norwood, M.H., 1962, J. Appl. Phys., 34, p.594.
5. Harman, T.C. and Honig, J.M., 1962, J. Appl. Phys., 33, p.3188.
6. Kooi et al., 1963, J. Appl. Phys., 34, p.1735.
7. Harman, T.C. and Honig, J.M., 1963, J. Appl. Phys., 34, p.239.
8. Honig, J.M. and Tarmy, B.M., 1964, J. Appl. Phys., 35, p.722.
9. Delves, R.T., 1964, Brit. J. Appl. Phys., 15, p.105.
10. Delves, R.T., 1962, Brit. J. Appl. Phys., 13, pp.440-5.
11. Harman, T.C., 1963, Appl. Phys. Letters, 2, p.13.
12. Harman et al., 1961, Phys. Rev. Letters, 7, p.
13. Goldsmid, H.J., 1963, Brit. J. Appl. Phys., 14, pp.271-4.
14. Cuff et al., 1963, Appl. Phys. Letters, 2, pp.145-6.
15. Cybriwsky, A., 1965, Rev. Sci. Instr., 36, pp.1153-5.
16. Soule, D.E., 1958, Phys. Rev., 112, pp.698-707.
17. Soule, D.E., McClure, J.W. and Smith, L.B., 1964, Phys. Rev., 134, pp. A 453-70.
18. McClure, J.W., I.B.M. J. Res. Dev., 8, p.255. 1964.
19. Geballe, T.H. and Hull, G.W., 1955, Phys. Rev., 98, p.940.
20. Goldsmid, H.J., Jenns, C.C. and Wright, D.A., 1959, Proc. Phys. Soc., 73, p.393.
21. MacDonald, D.K.C., 1962, Thermoelectricity, (John Wiley), New York.

22. Parrott, J.E., 1958, Proc. Phys. Soc., 71, p.82.
23. Wright, D.A., 1963, Brit. J. Appl. Phys., 14, pp.329-34.
24. Mills, J.J., 1965, Thermomagnetic properties in pyrolytic graphite, Ph.D. Thesis, University of Durham.
25. Berlincourt, T.C. and Steele, M.C., 1955, Phys. Rev., 98, p.956.
26. Bundy, F.P., Hall, T.P., Strong, H.M., and Wentorf, R.H., 1955, Nature, 176, p.151.
27. Grisdale, R.O., Pfeister, A.C. and von Roosbroeck, W., 1951, Bell Syst. Tech. J., 30, p.271.
28. Pirani, M. and Fehse, W., 1923, Z. Elektrochem., 29, p.168.
29. Nishiyama, Z., 1932, Sci. Rep. Tohoku Univ. (Ist Series), 21, p.171.
30. Brown, A.R.G. and Watt, W., 1958, Industrial Carbon and Graphite, (Society of Chemical Industry), p.86.
31. Brown, A.R.G., Clark, D. and Eastabrook, J., 1959, J. Less Common Metals, 1, p.94.
32. Diefendorf, R.J., 1960, J. de Chimie Physique, 57, p.815.
33. Plunkett, J.D. and Kingery, W.D., Proc. 4th Carbon Conf., 1960, (Pergamon) London, pp.457-72.
34. Blackman, L.C.F. and Ubbelohde, A.R., 1962, Proc. Roy. Soc., A 266, pp.20-32.
35. Harvey, J., Clark, D. and Eastabrook, J.N., 1962, R.A.E. Tech. Memo., Met. Phys. 361.
36. Moore, A.W., Ubbelohde, A.R. and Young, D.A., 1962, Brit. J. Appl. Phys., 13, pp.393-8.
37. Klein, C.A., 1962, J. Appl. Phys., 33, pp.3338-57.
38. Meers, J.T., 1962, Proc. 5th Carbon Conf., (Pergamon) London, pp. 461-465.
39. Moore, A.W., Ubbelohde, A.R. and Young, D.A., 1964, Proc. Roy. Soc., A 280, pp.153-69.
40. Guentert, O.J., 1962, J. Chem. Phys., 37, p.884.

41. Richards, B.P., 1964, J. Sci. Instr., 41, p.649.
42. Parry, G.S., 1965, Second Conf. on Industrial Carbon and Graphite, Society for Chemical Industry.
43. Stover, E.R., 1961, Proc. 5th Carbon Conf., (Pergamon) London.
44. Guentert, O.J. and Klein, C.A., 1963, Appl. Phys. Letters, 2, p.125.
45. Bragg, R.H. and Packer, C.M., 1962, Nature, 195, p.1080.
46. Fischbach, D.B., 1966, J. Appl. Phys., 37, p.2202.
47. Klein, C.A. and Holland, M.G., 1964, Phys. Rev., 136 A, p.575.
48. Shenker, H. et al., Reference Tables for Thermocouples, National Bureau of Standards, Circular No. 561.
49. Hooker, C.N., Ubbelohde, A.R. and Young, D.A., 1965, Proc. Roy. Soc., A 284, pp.17-31.
50. Smith, A.W., 1954, Phys. Rev., 95, pp. 1095-6.
51. Taylor, R., 1966, Phil. Mag., 13, pp.157-66.
52. Tyler, W.W. and Wilson, A.C. jnr., 1953, Phys. Rev., 89, p.870.
53. Blackman, L.C.F., Saunders, G. and Ubbelohde, A.R., 1961, Proc. Roy. Soc., A 264, pp.19-34.
54. Klein, C.A., 1964, J. Appl. Phys., 35, p.2947.
55. Mrozowski, S. and Chaberski, A., 1956, Phys. Rev., 104, pp.74-83.
56. Wallace, P.R., 1947, Phys. Rev., 71, p.622.
57. Drabble, J.R. and Goldsmid, H.J., 1961, Thermal Conduction in Semiconductors, (Pergamon), London.
58. Berman, R., 1952, Proc. Phys. Soc., 65 A, p.1029.
59. Slack, G.A., 1962, Phys. Rev., 127, pp.694-701.
60. Bowman, J.C. and Krumhansl, J.A., 1958, J. Phys. Chem. Solids, 6, pp.367-79.
61. Smith, A.W. and Rasor, N.S., 1956, Phys. Rev., 104, pp.885-91.

62. Hove, J.E. and Smith, A.W., 1956, Phys. Rev., 104, p.892.
63. Geballe, T.H. and Hull, G.W., 1958, Phys. Rev., 110, p.773.
64. Ziman, J.M., 1960, Electrons and Phonons, Oxford University Press, p.310.
65. Bergenlid, U., Hill, R.W., Webb, F.J. and Wilks, J., 1954, Phil. Mag., 45, p.851.
66. Keesom, P.H. and Pearlman, N., 1955, Phys. Rev., 99, p.1119.
67. De Sorbo, W. and Nichols, G.E., 1958, J. Phys. Chem. Solids, 6, p.352.
68. Komatsu, K., 1955, J. Phys. Soc. Japan, 10, p.346.
69. Komatsu, K., 1958, J. Phys. Chem. Solids, 6, pp.380-5.
70. Holland, M.G., Klein, C.A. and Straub, W.D., 1966, J. Phys. Chem. Solids, 27, pp.903-6.
71. Scherrer, P., 1918, Göttinger Nachrichten, 2, p.98.
72. Warren, B.E., 1941, J. Appl. Phys., 12, p.375.
73. Jones, F.W., 1938, Proc. Roy. Soc., A 166, p.16.
74. Stokes, A.R., 1948, Proc. Phys. Soc., 61, p.382.
75. Kochendörfer, A., 1944, Z. Krist., 105, p.393.
76. Warren, B.E. and Averbach, B.L., 1950, J. Appl. Phys., 21, p.595.
77. Wilson, A.J.C., 1962, X-ray Optics, (Methuen), London.
78. Warren, B.E., 1959, Prog. Metal Phys., 8, p.147.
79. Tournarie, M., 1956, C.R. Acad. Sci. Paris, 242, p.2016 and 2061.
80. Wilson, A.J.C., 1962, Nature, 193, p. 568.
81. Wilson, A.J.C., 1962, Proc. Phys. Soc., 80, p.286.
82. Wilson, A.J.C., 1963, Proc. Phys. Soc., 81, p.41.
83. Langford, J.I. and Wilson, A.J.C., 1963, Crystallography and Crystal Perfection, Ed. Ramachandran, G.N., (Academic Press) London, p.207.

84. Aqua, E.N., 1966, Acta Cryst, 20, p.560.
85. Lipson, H, and Stokes, A.R., 1942, Proc. Roy. Soc., A 181, p.101.
86. Warren, B.E., 1941, Phys. Rev., 59, p.693.
87. Wilson, A.J.C., 1949, Acta Cryst., 2, p.245.
88. Franklin, R.E., 1951, Acta Cryst., 4, p.253.
89. Bacon, G.E., 1951, Acta Cryst. 4, p.558.
90. Wilson, A.J.C., 1962, Norelco Reporter, 9, No.3.
91. Dawson, I.M. and Follett, E.A.C., 1959, Proc. Roy. Soc.,  
A 253, p.390.
92. Steward, E.G. and Cook, B.P., 1960, Nature, 186, p.797.
93. Eeles, W.T. and Wilson, A.J.C., 1965, Nature, 205, p.66.
94. Wilson, A.J.C., 1963, The Theory of X-ray Powder Diffractometry,  
(Philips Technical Library), Eindhoven.
95. Nelson, J.B. and Riley, D.P., 1945, Phil. Mag., 36, p.711.
96. Fitzer, E., Fritz, W. and Overhoff, D., 1966, Proc. 2nd  
Industrial Carbon and Graphite Conf., (Society  
of Chemical Industry), London, p.144.
97. Klug, H.P. and Alexander, L.E., X-ray Diffraction Procedures,  
(John Wiley), New York, p.171.
98. Ekstein and Siegel, 1949, Acta Cryst., 2, p.99.
99. Parrish, W. and Mack, M., 1963, Data for X-ray Analysis,  
(Philips Technical Library), Eindhoven, Vol. I.
100. Bacon, G.E., 1952, Acta Cryst., 5, p.392.
101. Rachinger, W.A., 1948, J. Sci. Instr., 25, p.254.
102. Goldsmid, H.J. and Lacklison, D.E., 1965, Brit. J. Appl. Phys.,  
16, pp. 573-5.
103. Delves, R.T., 1965, Reports on Progress in Physics, 28, pp.249-89.
104. Stover, E.R., 1963, Proc. 5th Carbon Conf., (Pergamon) London.

105. Roscoe, C. and Thomas, J.M., 1966, Carbon, 4, pp.383-90.
106. Franklin, R.E., 1951, Proc. Roy. Soc., A 209, p.196.
107. Mrozowski, S., 1956, Proc. Ist and 2nd Carbon Conf.,  
(Pergamon), London, p.31.
108. Bragg, R.H., Crooks, D.D., Fenn, R.W. jnr. and Hammond, M.L.,  
1964, Carbon, 1, pp.171-9.
109. Tsuzuku, T., 1960, Proc. 4th Carbon Conf., (Pergamon),  
London, p.403.
110. Fair, F.V. and Collins, F.M., 1963, Proc. 5th Carbon Conf.,  
Vol. I, (Pergamon) London, p.503.
111. Mizushima, S., 1963, Proc. 5th Carbon Conf., Vol.2,  
(Pergamon) London, p.439.
112. Fischbach, D.B., 1963, Appl. Phys. Letters, 3, pp.168-70.
113. Hennig, G., 1965, J. Appl. Phys., 36, p.1482.
114. Baker, C. and Kelly, A., 1965, Phil. Mag., 11, p.729.
115. Knight, R.T. and Rink, J.P., 1958, J. Chem. Phys., 29, p.449.
116. Kanter, M.A., 1957, Phys. Rev., 107, p.655.
117. Kotlensky, W.V., 1966, Carbon, 4, pp.209-14.
118. Austerman, S.B., Myron, S.M. and Wagner, J.W., Carbon, 1967,  
5, pp. 549-57.
119. Kelly, B.T., 1967, Carbon, 5, pp.247-60.
120. Kelly, B.T., 1968, Carbon, 6, pp.71-80.
121. Kelly, B.T., 1968, Carbon, 6, pp.485-96.
122. Takezawa, T, and Tsuzuku, T., Ono, A. and Hishiyama, Y.,  
1969, Phil. Mag., pp.623-8.
123. Wilson, A.J.C., 1970, J. Phys. D: Appl. Phys., 3, pp. 403-4.